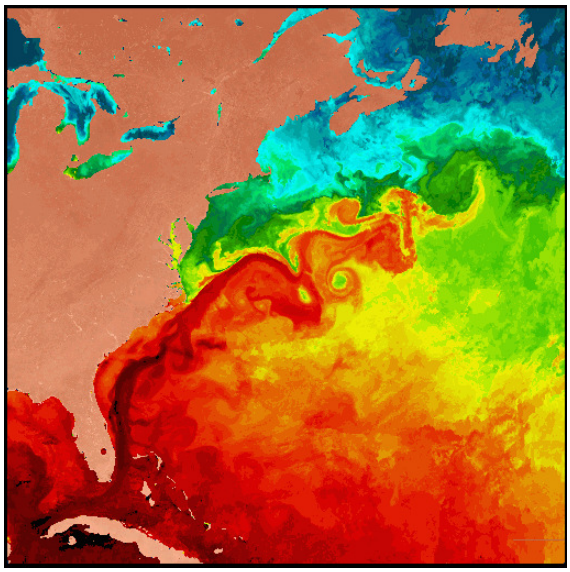

Large Scale Turbulence in the Atmosphere and Ocean

J. H. LaCasce

Dept. of Geosciences
University of Oslo
Oslo, Norway

LAST REVISED
March 16, 2023

Joe LaCasce
Department for Geosciences
University of Oslo
P.O. Box 1022 Blindern
0315 Oslo, Norway
j.h.lacasce@geo.uio.no

Contents

1 Equations

1.1 Basic equations

For what follows, we need to introduce the set of equations we'll be using, and the approximations we'll need. First are the momentum equations, written in vector form:

$$\frac{\partial}{\partial t}\vec{u} + \vec{u} \otimes \nabla\vec{u} + 2\vec{\Omega} \times \vec{u} = -\frac{1}{\rho}\nabla p - g\hat{k} + \frac{1}{\rho}\frac{\partial}{\partial z}\vec{\tau} \tag{1}$$

Here $\vec{u}$ is the velocity, ρ is the density, p is the pressure, g is gravity, $\vec{\tau}$ is the applied stress and $\vec{\Omega}$ is the rotation vector for the earth.

Note this equation actually represents three equations—one for each component of the velocity: u (x-direction), v (y-direction) and w (z-direction). The circle notation in the advective term signifies a *tensor product*. This represents 9 terms, 3 in each equation. For example, the x-component is:

$$\frac{\partial}{\partial t}u + \vec{u} \cdot \nabla u + \hat{i} \cdot (2\vec{\Omega} \times \vec{u}) = -\frac{1}{\rho}\frac{\partial}{\partial x}p + \frac{1}{\rho}\frac{\partial}{\partial z}\tau_x \tag{2}$$

where:

$$\vec{u} \cdot \nabla u = u\frac{\partial}{\partial x}u + v\frac{\partial}{\partial y}u + w\frac{\partial}{\partial z}u$$

We also have the continuity equation:

$$\frac{\partial}{\partial t}\rho + \vec{u} \cdot \nabla\rho + \rho(\nabla \cdot \vec{u}) = 0 \tag{3}$$

which expresses the conservation of mass. If the flux of density into a fixed volume is positive, the volume's mass will increase. Despite the simplicity of that idea, the equation is nonlinear and non-trivial.

But we can simplify this considerably if we make the *Boussinesq* approximation. This assumes that:

$$\rho = \rho_0 + \rho'(x, y, z, t) \tag{4}$$

where ρ_0 is a constant and that:

$$\rho_0 \gg |\rho'|$$

The density of water is nearly constant—it changes only slightly when heated (over a reasonable range). Under this assumption, the continuity equation to first order can be written:

$$\frac{\partial}{\partial t}\rho_0 + \vec{u} \cdot \nabla \rho_0 + \rho_0(\nabla \cdot \vec{u}) = 0 \tag{5}$$

which implies:

$$\nabla \cdot \vec{u} = 0 \tag{6}$$

Thus the Boussinesq fluid is *incompressible*; its volume is conserved.

The momentum equation is also simplified because the pressure term is now linear:

$$\frac{1}{\rho}\nabla p \quad \rightarrow \quad \frac{1}{\rho_0}\nabla p \tag{7}$$

The Boussinesq approximation is valid for the ocean and approximately so for the planetary boundary layer (the lowest 1 km) in the atmosphere. It is not accurate in the upper troposphere, due to the compressibility of air. But if one uses *pressure coordinates*, the pressure term is also linearized and the flow is incompressible, so the equations are similar to the Boussinesq ones we use hereafter.

We also require the stress term on the RHS of the momentum equation. We will write this as the sum of an (unspecified) forcing term and a diffusive damping term:

$$\frac{1}{\rho}\frac{\partial}{\partial z}\vec{\tau} = \mathcal{F} + \nu \nabla^2 \vec{u} \tag{8}$$

The forcing could be the wind acting on the ocean or convective motion forced by surface heating in the atmosphere. The diffusion term represents molecular dissipation, with $\nu \approx 10^{-5}\ m^2/sec$.

The momentum equation is often simpler to work with if we write the advective term in an alternate form:

$$\nabla \cdot (\vec{u}a) = \vec{u} \cdot \nabla a + a(\nabla \cdot \vec{u}) = \vec{u} \cdot \nabla a \tag{9}$$

The second term vanishes due to incompressibility. Also, we can write the gravity term as the gradient of the *geopotential*, gz. With these modifications, the momentum equation becomes:

$$\frac{\partial}{\partial t}\vec{u} + \nabla \cdot (\vec{u} \otimes \vec{u}) + 2\vec{\Omega} \times \vec{u} = -\nabla(\frac{p}{\rho_0} + gz) + \mathcal{F} + \nu\nabla^2\vec{u} \tag{10}$$

Notice the advective term is the only nonlinear one in the equation. This is *quadratically* nonlinear because it involves the product of the unknown velocities. Turbulence springs from these term, as we'll see shortly.

1.2 Scaling

Not all the terms in the momentum equation are equally important. To see this, we approximate each of the terms with "typical" values, i.e. U, L, P, etc. Neglecting external forcing, the x-momentum equation scales as:

$$\frac{\partial}{\partial t}u + \vec{u} \cdot \nabla u + \hat{i} \cdot (2\vec{\Omega} \times \vec{u}) = -\frac{1}{\rho_0}\frac{\partial}{\partial x}p + \nu\nabla^2 u$$

$$\frac{U}{T} \qquad \frac{U^2}{L} \qquad 2\Omega U \qquad \frac{P}{\rho_0 L} \qquad \frac{\nu U}{L^2} \tag{11}$$

We'll compare the size of each to that of the dissipation term. We do this by dividing by the last term, yielding:

$$\frac{L^2}{\nu T} \qquad \frac{UL}{\nu} \qquad \frac{2\Omega L^2}{\nu} \qquad \frac{PL}{\rho_0 \nu U} \qquad 1 \tag{12}$$

Thus the advection term is a factor of UL/ν times the size of the dissipation term. This is the **Reynold's number**, Re. How big is this? At the scale of weather systems in the atmosphere, we have:

$$Re = \frac{UL}{\nu} \approx \frac{(10\,m/sec)(10^6\,m)}{10^{-5}\,m^2/sec} = 10^{12}$$

So advection is *much* more important than molecular dissipation at these scales.

The second point concerns the time scale, T. We can write the first scaling term thus:

$$\frac{L^2}{\nu T} \equiv \frac{T_\nu}{T} \tag{13}$$

This is the ratio between the actual time scale of the motion, T, and the *dissipation time scale*, $T_\nu = L^2/\nu$. The latter represents the approximate time required for molecular friction to bring the motion at scale L to rest. How long is this? At the weather scales:

$$T_\nu = \frac{L^2}{\nu} \approx \frac{(10^6\,m)^2}{10^{-5}\,m^2/sec} = 10^{17}\ sec$$

This is roughly 10^{12} days, or about 3×10^9 years—or slightly less than the age of the earth! So we would have to wait for a *very* long time for molecular dissipation to halt a storm system. Storms spin down typically in less than a week or so, so something else is at work here.

The dissipation time scale is a strong function of the spatial scale. Consider a cup of coffee. You add milk to the coffee and stir it. How long do you have to wait for the coffee to cease moving? My cup is 7.5 cm across, so the dissipation time scale is:

$$T_\nu = \frac{L^2}{\nu} \approx \frac{(0.075\,m)^2}{10^{-5}\,m^2/sec} = 560\ sec$$

or about 9 minutes. But coffee settles down much faster, perhaps over 15 seconds. Again, there is something else at play.

Another important scaling is obtained if we instead divide through by $2\Omega U$, the size of the Coriolis term. Then we obtain:

$$\frac{\partial}{\partial t}u + \vec{u}\cdot\nabla u + \hat{i}\cdot(2\vec{\Omega}\times\vec{u}) = -\frac{1}{\rho_0}\frac{\partial}{\partial x}p + \nu\nabla^2 u$$

$$\frac{1}{2\Omega T} \qquad \frac{U}{2\Omega L} \qquad 1 \qquad \frac{P}{2\Omega U\rho_0 L} \qquad \frac{\nu}{2\Omega L^2} \tag{14}$$

The ratio of the advective term to the Coriolis term is $U/2\Omega L$, the **Rossby number**. This is usually small at large scales. At *synoptic scales* in the atmosphere (O|1000 km|), the Rossby number is:

$$\frac{U}{fL} \approx \frac{10\ m/sec}{10^{-4}\ sec^{-1}\ 10^{6}\ m} = 0.1$$

At the synoptic scales in the ocean (O|100 km|), the Rossby number is even less:

$$\frac{U}{fL} \approx \frac{0.1\ m/sec}{10^{-4}\ sec^{-1}\ 10^{5}\ m} = 0.01$$

Thus the Coriolis term is 10 and 100 times larger than the advective term respectively.

Scaling the other terms, we find the pressure gradient term is about the same size as the Coriolis term. So the dominant balance at weather scales is between the Coriolis and pressure gradient terms, known as the *geostrophic balance*. This is the reason that the winds circulate around a low pressure system, counterclockwise in the Northern Hemisphere.

Exercise: Other points

a) The time derivative term, $\frac{\partial}{\partial t}u$, is typically about the same size as the advective term at synoptic scales. Knowing this, discuss how you can deduce the scale of the pressure, P, above. What is P at the 1000 km scale in the atmosphere? How does this compare to observations from weather charts?

b) At what scale are advection and the Coriolis term of equal size in the atmosphere? What about in the ocean? What happens below this scale?

As we will see, this scale represents an important transition point in both systems.

2 Statistics in a nutshell

Turbulence often appears as "noise" in a signal. Consider the synthetic temperature time series $T(t)$ in the upper panel of Fig. (1). The temperature varies slowly in time but also has a high frequency component. If we *low-pass filter*[1] the time series, we get the signal in the middle panel. This has a smooth, even quasi-periodic variation. If we high-pass filter the time series instead, we get the signal in the lower panel. This appears to be "white noise", i.e. a random signal with no dominant frequencies. This looks completely unpredictable, i.e. we don't know from one instant to the next how it will behave. The low frequency motion could be the seasonal change in temperature, with warming in the summer and cooling in the winter. The high frequency motion on the other hand could be weather, which is unpredictable at scales beyond a few days.

Since turbulent signals are fundamentally unpredictable (we will demonstrate this in sec. 4), it often doesn't make sense to try and predict them. Rather than worrying about the exact values of the signal at any given time, we focus instead on *statistics*. In some cases, statistical aspects can be predicted.

We are most concerned about the range of possible values the signal can

[1] See for example `https://en.wikipedia.org/wiki/Low-pass_filter`.

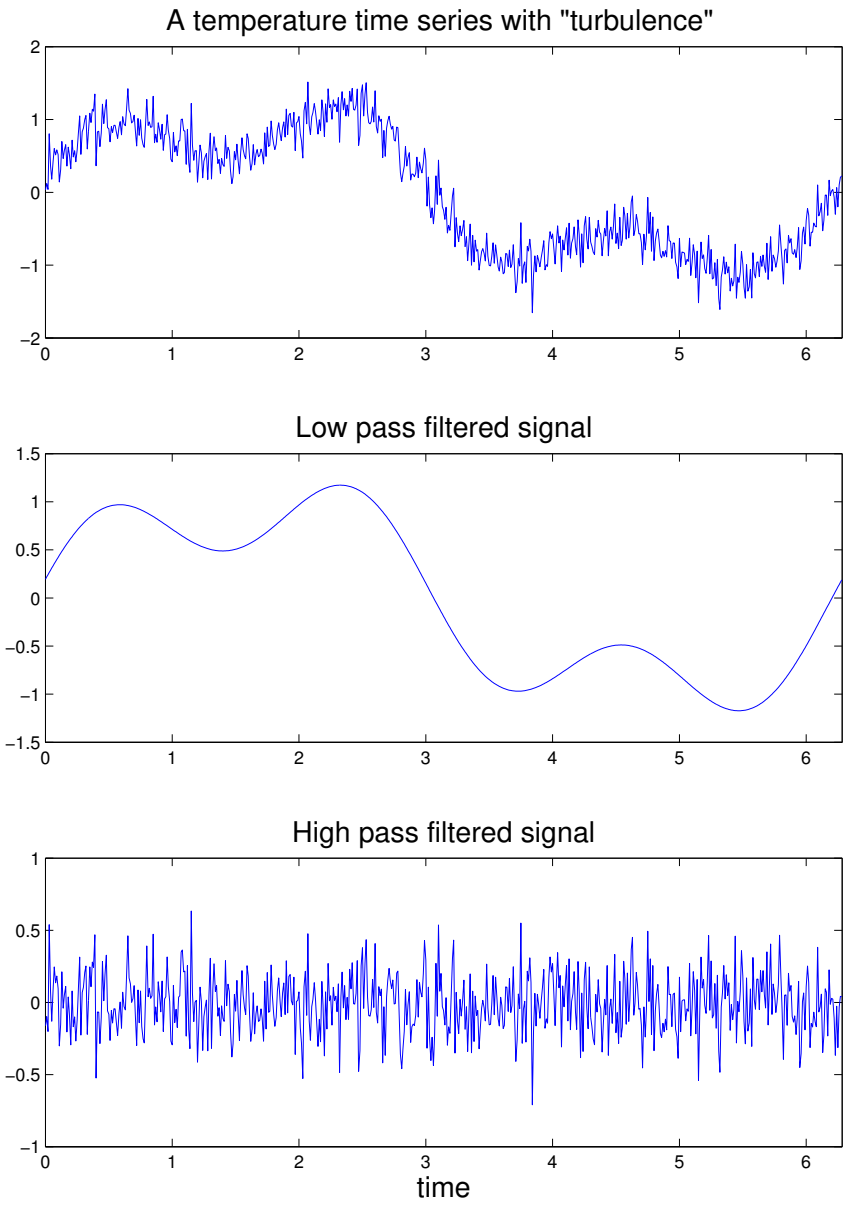

Figure 1: A time series of temperature measured over a certain period. The upper panel shows the whole time series, while the middle and lower panels show the low-pass and high-pass filtered time series.

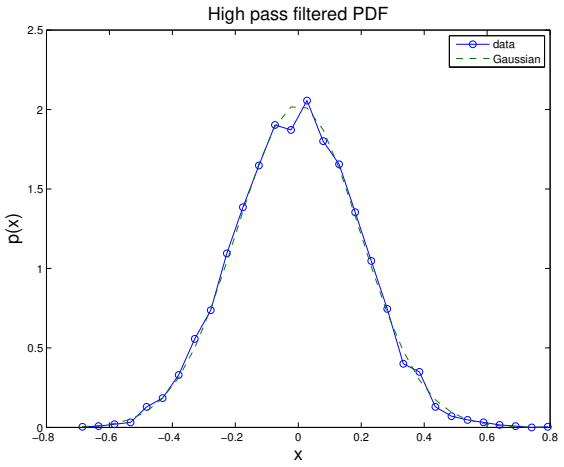

Figure 2: The probability density function (PDF) of the high-pass filtered time series in Fig. (1). The dashed curve is a Gaussian PDF.

have. We measure these with statistical *moments*—the mean, the variance, and so forth. The moments in turn can be derived from the *probability density function* (PDF) of the signal.

To obtain the PDF, we calculate a histogram of the signal. We do this by counting the number of times the temperature falls within a given range, e.g. between -0.2 and -0.1. Then we normalize the histogram so that:

$$\int_{-\infty}^{\infty} p(T)\, dT = 1 \tag{15}$$

The PDF indicates the probability of measuring particular values. The probability of getting any *exact* value, like $T = -0.15$, is effectively zero (since temperature is a continuous variable), but we can evaluate the probability it will have a value in a given range, for example from $T = -0.1$ to $T = 0.2$:

$$\int_{-0.1}^{0.2} p(T)\, dT \tag{16}$$

This indicates what fraction of time the temperature is found between these values.

Fig. (2) shows the PDF for the high-pass filtered time series in Fig. (1). The curve is centered around zero, but values as large as ± 0.6 C occasionally occur.

The dashed curve in Fig. (2) shows a *Gaussian* or "normal" distribution. The Gaussian is defined:

$$p(T) = \frac{1}{\sqrt{2\pi\delta^2}}\, exp(-\frac{(T- < T >)^2}{2\delta^2}) \tag{17}$$

The PDF from the high-pass filtered time series is very close to the normal distribution. This is useful to know, because the moments of a Gaussian can be derived analytically (see the exercises).

IT is often true that random signals exhibit a nearly Gaussian PDF. Indeed, there is an important result in statistics called the *Central Limit Theorem* which states that the sum of independent processes has a PDF which converges to a Gaussian. So if a time series is long enough, the PDF will eventually converge to a normal distribution.

Once we have the PDF, we can derive the statistical moments. The first moment is the *mean*:

$$< T >= \int_{-\infty}^{\infty} T\; p(T)\, dT \tag{18}$$

The mean is approximately where the PDF is centered. The mean for the distribution in Fig. (2) is -0.0022 C. This is close to zero, as we might have guessed.

The width of the PDF is determined by the second moment, the *variance*:

$$\begin{aligned} V &=< (T- < T >)^2 >=< T^2 > - < T >^2 \\ &= \int_{-\infty}^{\infty} T^2\, p(T)\, dT - (\int_{-\infty}^{\infty} T\; p(T)\, dT)^2 \end{aligned} \tag{19}$$

Notice that we subtract the mean prior to taking the square – otherwise the mean value itself would affect the answer. For our distribution, the variance is 0.0386 C^2.

The variance, being a square, is somewhat non-intuitive though. A better indicator of the width of the PDF is the *standard deviation*, which is the square root of the variance:

$$\delta = (< T^2 > - < T >^2)^{1/2} \tag{20}$$

This yields $\delta = 0.1965$ C. You can see that the PDF in Fig. (2) falls to roughly half its maximum value at ± 0.2 C. Thus the temperature in the high pass filtered time series is most often between -0.2 C and 0.2 C.

We can also calculate higher moments. The third order moment is the *skewness*. The skewness indicates how asymmetric about the mean the distribution is. A symmetric distribution has a skewness near zero. It is traditional to normalize the skewness by the cube of the standard deviation so that the result is a non-dimensional number:

$$S = \frac{\int_{-\infty}^{\infty} (T - < T >)^3 \, p(T) \, dT}{\delta^3} \tag{21}$$

In our case, S=0.0271, so the PDF is slightly skewed toward positive values.

The (normalized) fourth order moment is also useful:

$$K = \frac{\int_{-\infty}^{\infty} (T - < T >)^4 \, p(T) \, dT}{\delta^4} \tag{22}$$

This is the *kurtosis*. The kurtosis reflects the shape of the PDF. If the PDF has a sharp peak in the middle and long wings, the kurtosis is large, while if it is very flat, the kurtosis is small. In our case, k=2.9792. The kurtosis of a Gaussian distribution is exactly three. So our PDF is indeed close to normal.

Exercise: *Random examples*

In matlab, say: $x = 0.1$ + rand(1000,1); What is the mean of x? The standard deviation?

Use the histogram function to find out what kind of distribution x has. Explain why then that the mean of x is given by: $< x > \approx 0.1$ + 0.5

What is the probability that x lies in the range -0.1 to 0.1?

Now try: $x = 0.1$ + randn(1000,1);

Plot the PDF. What is the standard deviation? The kurtosis?

Exercise: *Gaussian distribution*

a) Show that the Gaussian distribution in (17) is normalized.

b) Show that all odd moments of the Gaussian are exactly zero.

c) Show that the kurtosis of a Gaussian is 3.0.

3 The Fourier transform

Another very useful operation we'll be using is the Fourier transform. The basic idea is that we project a function onto a basis of sinusoidal functions:

$$\phi(t) = \sum_{\omega} \hat{\phi}(\omega) e^{i\omega t} \tag{23}$$

Here $\phi(t)$ is a quantity which varies in time (such as temperature at a given location), and $\hat{\phi}(\omega)$ is the Fourier transform of ϕ. The sum goes over the range of ω, which is the *frequency*. Note that while $\phi(t)$ is usually a real function, the transform $\hat{\phi}(\omega)$ is complex, because the term $exp(i\omega t)$ is also complex.

By using the transform, we represent the signal, $\phi(t)$, by a series of

sinusoidal functions. Each wave has a *period*, which is given by:

$$T = \frac{2\pi}{\omega}$$

Long waves have large periods and small frequencies, while short waves have short periods and high frequencies. The transform variable, $\hat{\phi}(\omega)$, represents the *amplitude* of each wave.

Consider the temperature time series in Fig. (1). Taking the Fourier transform, the amplitude would be large for a few long (low frequency) waves – these would capture the low-pass filtered part of the signal. The amplitude would also be large for a number of high frequency waves, representing the high-pass signal. We would also expect a *spectral gap* in between, since there are few waves of intermediate scale. This is fairly unusual – most time series have a full continuum of waves.

Relation (23) shows us how to construct $\phi(t)$ if we know it's transform. But how do we obtain the transform in the first place? We can extract the component at a single frequency by integrating the equation, thus:

$$\frac{1}{\mathcal{T}} \int_0^{\mathcal{T}} \phi(t)\, e^{-i\omega' t}\, dt = \frac{1}{\mathcal{T}} \sum_{\omega} \int_0^{\mathcal{T}} \hat{\phi}(\omega) e^{i(\omega-\omega')t}\, dt \tag{24}$$

Here $\mathcal{T}$ is the length of the time series. Because $\mathcal{T}$ is finite, the frequencies have discrete values:

$$\omega = \frac{2\pi n}{\mathcal{T}} \quad \rightarrow \quad T = n\mathcal{T}$$

where n is an integer. This means there are an integral number of waves in the total record (the frequencies are *quantized*).

If $\omega \neq \omega'$, then the integral on the right hand side of (24) is exactly zero. If $\omega = \omega'$ though, then:

$$\frac{1}{\mathcal{T}} \int_0^{\mathcal{T}} \phi(t)\, e^{-i\omega t}\, dt = \frac{1}{\mathcal{T}} \int_0^{\mathcal{T}} \hat{\phi}(\omega) dt = \hat{\phi}(\omega) \tag{25}$$

So the integral extracts the amplitude at frequency ω. This is the Fourier transform of $\phi(t)$ in time.

The transform can be made in space as well. For instance, we can write:

$$\psi(x,y) = \sum_k \sum_l \hat{\psi}(k,l) e^{ikx+ily} \tag{26}$$

Here k and l are *wavenumbers*, which correspond to the frequency in space. The inverse of the wavenumber is the *wavelength*, which is the space version of the period. The wavelength in the x-direction is:

$$\lambda_x = \frac{2\pi}{k}$$

The corresponding transform is given by:

$$\hat{\psi}(k,l) = \frac{1}{LM} \int_0^M \int_0^L \psi(x,y) e^{-ikx-ily}\, dx\, dy \tag{27}$$

We've assumed a rectangular domain with sides of length L and M. Because these are finite dimensions, the wavenumbers are both quantized, as before.

An advantage of the Fourier transform is that it makes taking derivatives easy. Say that ψ is a 2D streamfunction, with the velocities given by:

$$u = -\frac{\partial}{\partial y}\psi, \quad v = \frac{\partial}{\partial x}\psi \tag{28}$$

Then:

$$\hat{u} = -il\hat{\psi}, \quad \hat{v} = ik\hat{\psi} \tag{29}$$

Another useful point concerns the energy. The total kinetic energy in the domain is:

$$E = \frac{1}{LM} \iint \frac{1}{2}(u^2 + v^2)\, dxdy \tag{30}$$

The Fourier version of this is:

$$E = \frac{1}{2} \sum_k \sum_l \ |\hat{u}|^2 + |\hat{v}|^2 \tag{31}$$

Thus the kinetic energy is the sum of the squares of the Fourier amplitudes (a result known as *Parseval's theorem*). Written in terms of the stream-function, the energy is:

$$E = \frac{1}{2} \sum_k \sum_l (k^2 + l^2) |\hat{\psi}|^2 \tag{32}$$

Very often, we'll talk about the energy *spectrum*. This is the argument of the sum above:

$$\mathcal{E}(k, l) = \frac{1}{2}(|\hat{u}|^2 + |\hat{v}|^2) = \frac{1}{2}(k^2 + l^2)|\hat{\psi}|^2 \tag{33}$$

Thus the total energy is the sum of the spectrum over all wavenumbers. The spectrum reveals the contribution to the energy by wavenumber (or frequency) and is a central quantity in turbulence theory.

Exercise:

Construct a time vector thus: $t = [0 : 999] * .001$. Let:

$x = sin(100\pi t) + sin(240\pi t)$

and:

$y = x + 2 * randn(size(t))$

Plot x and y vs. t. Then construct the power spectra of x and y, thus:

$N = 1000$

$X = fft(x, N)/N$

$Y = fft(y, N)/N$

$f = 0.001/2 * linspace(0, 1, N/2 + 1)$

$plot(f, 2 * abs(X(1 : N/2 + 1)), f, 2 * abs(Y(1 : N/2 + 1)))$

Here fft is the *fast Fourier transform*, an important numerical routine which calculates the transform.

What is the difference between x and y? Describe the spectra.

4 A chaotic example

As noted earlier, the "trouble" with the momentum equation stems from the quadratic nonlinearity on the LHS. We'll consider how this affects the solution in an idealized case.[2] The x-momentum equation is:

$$\frac{\partial}{\partial t}u + \vec{u} \cdot \nabla u + i \cdot (2\vec{\Omega} \times \vec{u}) = -\frac{1}{\rho_0}\frac{\partial}{\partial x}p + F_x + \nu\nabla^2 u \tag{34}$$

We represent this using a "toy" model:

$$\frac{d}{dt}u + ru^2 = 1 - u \tag{35}$$

This is an ODE with only a single dependent variable, $u(t)$. The terms on the RHS represent simple forcing and dissipation terms. The equation has a quadratic nonlinearity and that is multiplied by r, which is essentially the Reynolds number for the problem. If r is small, the flow is viscous and the equation is approximately linear. If r is order one or larger, the nonlinearity is important.

We will discretize the equation, using a simple Euler routine with a time step $dt = 1$:

$$\frac{u(t+1) - u(t)}{1} + ru(t)^2 = 1 - u(t) \tag{36}$$

We can rewrite this as:

$$u(t+1) = F(u(t)) = 1 - ru(t)^2 \tag{37}$$

This is a "map", in which a new value of u, at $t + 1$, is derived from the previous value. This particular map is a variant of the "logistic map".[3]

[2] This example is based on one given by Frisch [14].

[3] The logistic map was originally proposed by May [30]. His was an idealized model of a biological system where the growth rate of a population is proportional to the population itself. The paper became a landmark in the chaos literature.

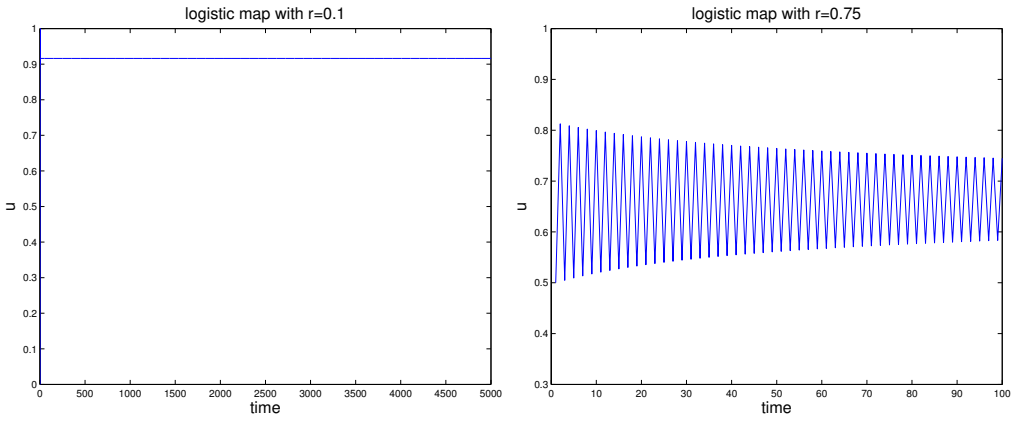

Figure 3: . Two solutions of the logistic map with u(0)=0. The solution at right has r=0.1 and the one on the right has r=0.75.

The behavior of the system depends entirely on the parameter, r. If $r = 0$, the solution goes immediately to $u = 1.0$. This is the viscous limit, when the forcing determines the solution.

If r is larger than zero, the solution approaches a smaller value. The value is known as a *fixed point*. This is defined as a point at which $u(t)$ will not change, i.e. where du/dt vanishes. If $u(t)$ starts on a fixed point, it will remain there. With $r \neq 0$, there are actually two fixed points, which we can find by solving:

$$\frac{d}{dt}u = -ru^2 + 1 - u = 0 \tag{38}$$

This quadratic equation has solutions:

$$u = -\frac{1}{2r} \pm \frac{\sqrt{1+4r}}{2r} \tag{39}$$

There are two roots, one positive and one negative. With $r = 0.1$, the roots are $u = 0.9161$ and $u = -10.9161$. Solving (37) numerically, we see the solution rapidly converges to the positive root (left panel of Fig. 3).

Only a single solution exists with $r = 0$, i.e. $u = 1$. When r is small but non-zero, there are two solutions, one near $u = 1$ and a second which

is large and negative, as above. This second root thus appears from $-\infty$ when r increases from zero.

Why does the numerical solution favor the positive root over the negative one? To see, we perform a *linear stability analysis*. Let's say the solution is near a fixed point, denoted u_a. The fixed point is such that:

$$F(u_a) = u_a \tag{40}$$

If we are near the fixed point, we can write:

$$u = u_a + \delta(t) \tag{41}$$

where δ is a small deviation. Putting this into (37), we have:

$$u(t+1) = u_a + \delta(t+1) = F(u_a + \delta(t)) \approx F(u_a) + F'(u_a)\delta(t) \tag{42}$$

after using a Taylor expansion. We keep only the first term, consistent with a "linear" analysis. Because $u_a = F(u_a)$, we get:

$$\delta(t+1) = F'(u_a)\delta(t) \tag{43}$$

Whether $|\delta_t|$ increases or decreases depends therefore on $F'(u_a)$. If we think in terms of iterations, we have that:

$$\delta_{n+1} = F'(u_a)\delta_n = (F'(u_a))^2\delta_{n-1} = (F'(u_a))^n\delta_1 \tag{44}$$

Thus if:

$$|F'(u_a)| < 1 \tag{45}$$

then δ will asymptote to zero. How it decays depends on the sign of $F'(u_a)$ (Fig. 4). If $0 < F'(u_a) < 1$, then δ decays monotonically to zero (upper left panel); if $-1 < F'(u_a) < 0$, then δ oscillates as it decays (upper right). On the other hand, if $F'(u_a) > 1$, δ increases monotonically (lower left)

and if $F'(u_a) < -1$, δ oscillates and increases (lower right). If δ decreases in time, we say that u_a is a *stable* fixed point; if δ increases, it is an unstable fixed point.

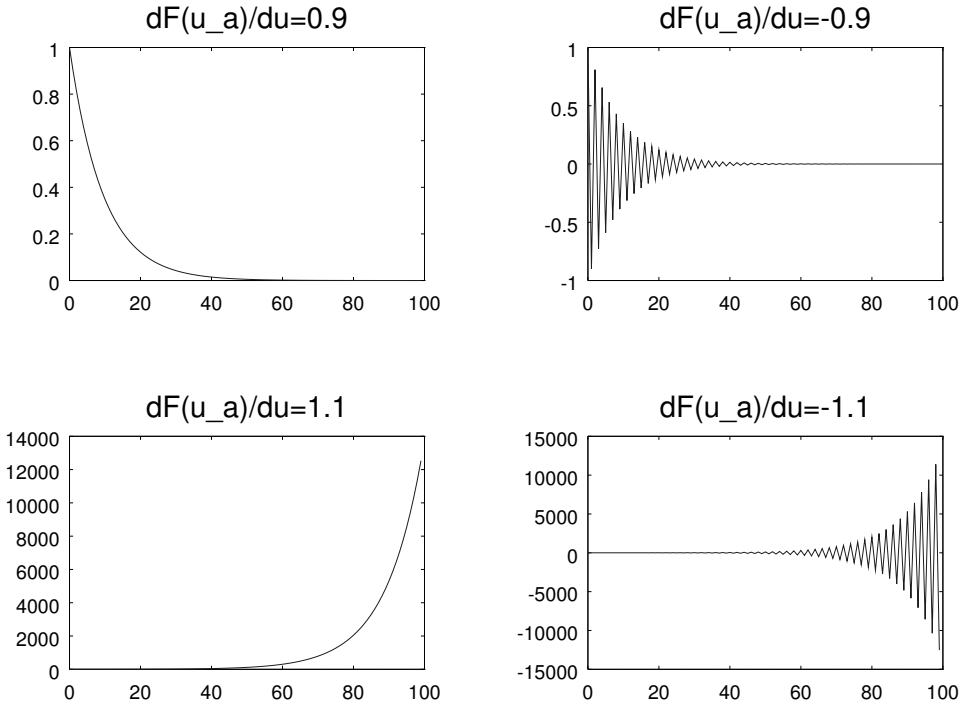

Figure 4: . The four different types of stability: monotonic decay (upper left), oscillating decay (upper right), monotonic growth (lower left) and oscillating growth (lower right).

We have that:

$$F'(u) = -2ru \tag{46}$$

With the positive root, $u_a = .9161$, so $F'(u_a) = -0.1832$, implying decaying oscillations. In fact there are oscillations in Fig. (3), but the decay is so rapid we don't see them. The other root, $u_a = -10.9161$ has $F'(u_a) = 2.1832$ and so is unstable. Thus the numerical solution converges to the positive root rather than the negative one.

Note the linear stability analysis only pertains for values of u *near the fixed points*. We can't say how the system will behave when it is far from the points. If we start at $u(0) = -11$, the solution becomes more and more negative, and so never approaches a steady state. Thus there is no guarantee the system will converge to the stable fixed point.

The oscillations are more noticeable when r is larger. An example, with $r = 0.75$, is shown in the right panel of Fig. (3). The roots in this case are $u = -2/3$ and $u = -2$. The solution again approaches the positive root. Note that $F'(-2/3) = -1$; so the linear stability analysis indicates we are on the border between stable and unstable solutions.

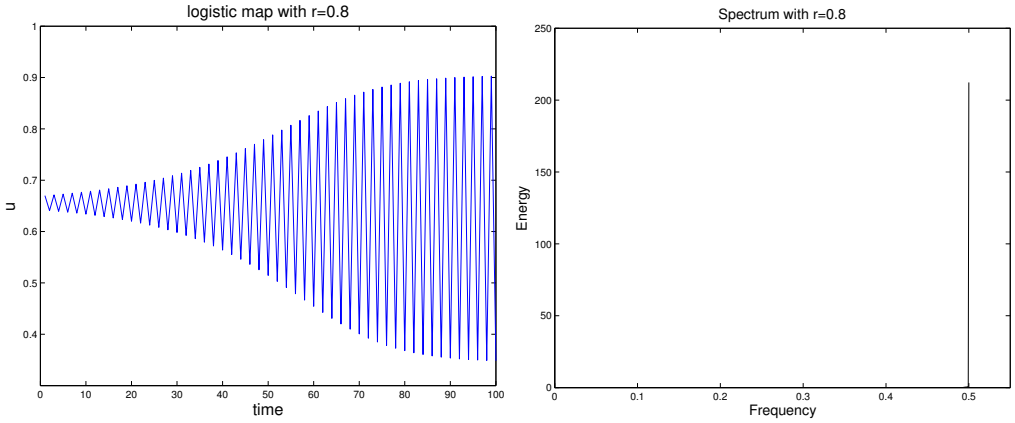

Figure 5: . The solution (left) and spectrum (right) with r=0.8.

Indeed, with a somewhat larger r the oscillations don't die out. Consider the case with $r = 0.8$ (left panel of Fig. 5). The fixed points are $u = 0.6559$ and $u = -1.9059$, and we see that u oscillates around the former. But the oscillation itself is stable. This is interesting, because linear stability suggests the point is unstable (since $F'(0.6559) = 1.05$. But the oscillations around the fixed point exhibit *finite amplitude stability*, as u remains in the neighborhood of the fixed point.

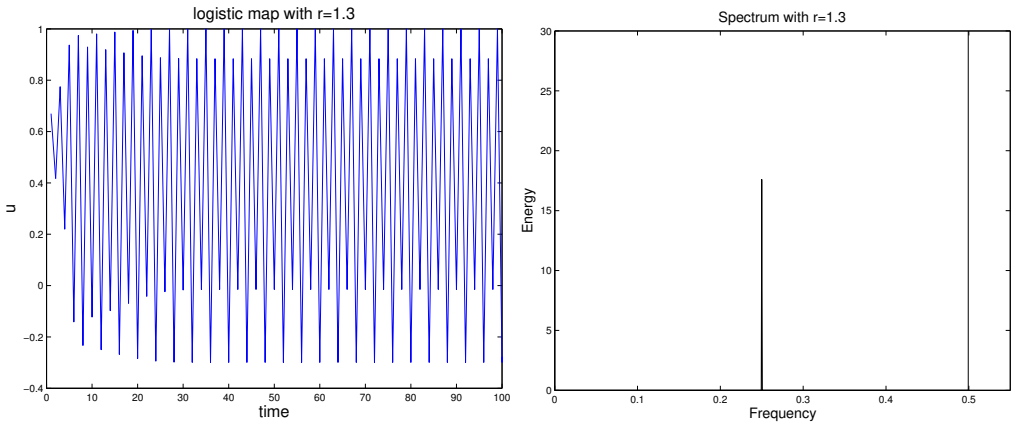

Figure 6: . The solution with r=1.3.

It is useful to consider the spectrum of u, as a function of the (non-dimensional) frequency, ω. This is shown in the right panel of Fig. (5). There is a single peak, at $\omega = 0.5$. This reflects the stable oscillation in the left panel.

Increasing r further, the behavior becomes more complex. The case with $r = 1.3$ is shown in Fig. (6). Now the fixed points are $u = 0.5731$ and $u = -1.3423$, and again u is oscillating about the positive root. But the oscillations are less regular. Looking at the spectrum, we see why: there are now *two* dominant frequencies; the solution is a superposition of these waves.

Increasing r further, the solution becomes even more complex as more and more frequencies appear. With $r = 2$ (Fig. 6), the solution is fully *chaotic*. The roots are $u = 0.5$ and $u = -1$, but u oscillates erratically between -1 and +1. Sometimes there are rapid changes and sometimes slower ones. In addition, the spectrum (right panel) is nearly "white" (flat), with contributions across the whole range of frequencies.

Chaotic signals are fundamentally unpredictable, because a chaotic sys-

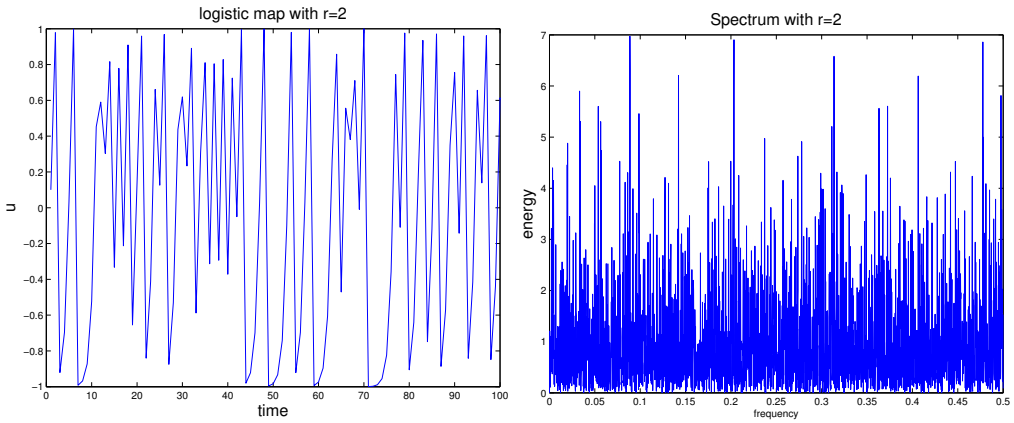

Figure 7: . The solution with r=2.

tem is *sensitively dependent on the initial conditions*. The initial value in Fig. (7) is $u(0) = 0.1$. Let's change that slightly, to $u(0) = 0.10001$. The two curves are plotted in Fig. (8). Initially the curves are together. But shortly after t=10, they begin to diverge. By t=20, the two are essentially independent of one another. If this were a temperature forecast, we would have two completely different values after about $t = 15$.

This is a central difficulty with chaotic systems: unless you know the initial conditions *exactly*, it's impossible to make a correct prediction—and there will always be some error in the initial conditions.[4]

Given that the motion is unpredictable, it doesn't make sense to worry about the exact value of u at any given time. Rather, we can focus on the statistics. The PDF of u is shown in Fig. (9) for both of the initial values used in Fig. (8). Despite that the two time series are different, the PDFs are almost identical. We see that u takes on all values in the range from [-1:1]. We also see that u is most frequently near the extremes, -1

[4]H. Poincaré noted in 1890 that the trajectories in systems with three interacting bodies—the minimum required to obtain chaos—depend sensitively on the initial conditions. In reference to the same effect, E. Lorenz remarked: "One meteorologist remarked that if the theory were correct, one flap of a seagull's wings could change the course of weather forever." The seagull was later changed to a "butterfly" and the dependence on initial conditions has become known as the "butterfly effect".

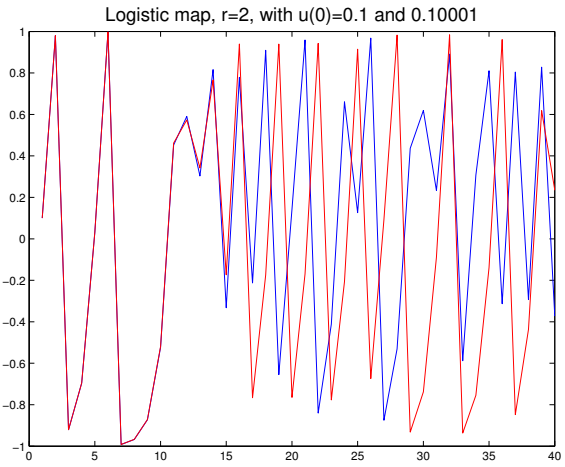

Figure 8: . The solution with r=2, with two initial values which are nearly the same.

and 1. These are the extremes of the oscillations, so u spends more time in their neighborhood (the same is true for a simple sinusoidal oscillation). Note too that unlike with our noise example earlier, this PDF isn't remotely Gaussian. The kurtosis is roughly 1.5, well below the Gaussian value of 3.

It's actually possible to predict the shape of the PDF. Making a suitable change of variables [14], one can convert this to a "tent map", which has a *uniform* (or flat) PDF. Then one can convert back again to u to predict the PDF. The solution is [14]:

$$p(u) = \frac{1}{\pi\sqrt{1-u^2}} \tag{47}$$

This is indicated by the red curve in Fig. (9).

There are several points here. One is that this system is *fully chaotic at* $r = 2$. If this is our Reynolds number, we see that the value is very low. With a Reynolds number of 10^{12}, as in the atmosphere, it isn't surprising the motion is chaotic.

Second, because u explores the entire range of values between -1 and 1, we say the motion is *ergodic*. Given (almost) any initial value, we can

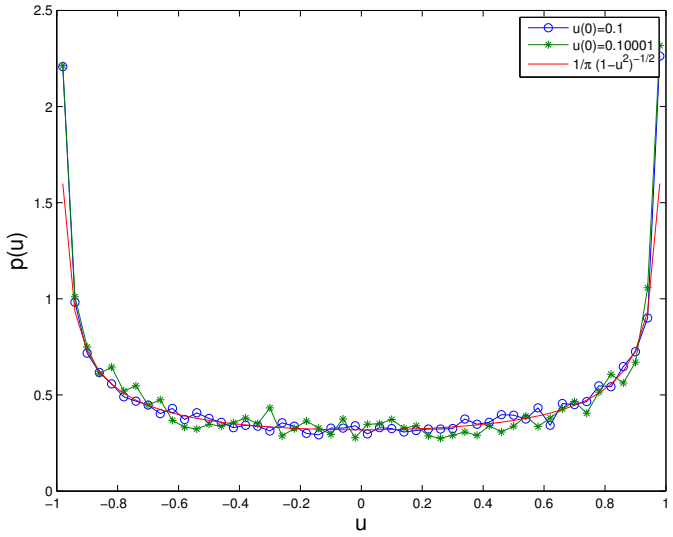

Figure 9: . The histogram of the logistic map with r=2 and 10,000 iterations. The red curve is the analytical prediction for this map, $p(u) = 1/(\pi\sqrt{1-u^2})$.

expect u to take on any other value in the range. Thus if we did an *ensemble* of experiments, measuring u at a point and then averaged all the values we obtained, we would get the same answer than if we had just averaged u in time.

However, we must be cautious about taking the logistic map too literally. The progression from stable fixed points, to more and more oscillations and then to chaos is typical of nonlinear systems with few degrees of freedom. In the atmosphere or ocean, where there are many, many degrees of freedom, the transition from stability to chaos is usually less clean. Nevertheless, the logistic map gives us a good idea of what a quadratic nonlinearity can do.

Exercise: *Another map*

Analyze the equation:

$$\frac{du}{dt} + ru^2 = (r-1)u \tag{48}$$

with $dt = 0.1$ (note!).

a) Write the equation as a map.

b) What are the fixed points?

c) Calculate the stability for each point. Notice that this depends not only on r, but on the time step, dt(!)

d) Write a code to solve the mapping. Check the solution for various values of r. How does the behavior compare to your expectations from the linear stability analysis?

e) Write a second code to calculate the spectrum of u. Check the spectra in the cases in (b).

f) What are the critical values of r where transitions occur? When are the solutions fully chaotic? Plot time series to show this.

5 Conservation laws

Central in much of the theory that follows are two *conservation laws*: one for energy and one for "enstrophy". These play a central role in the evolution of turbulent systems, allowing us to make basic deductions about the behavior.

Both the energy and enstrophy equations are derived from the momentum equation (10). The derivations are somewhat simpler using a modified version of the advective term, which comes from using a vector identity:

$$\vec{u} \cdot \nabla \vec{u} = \vec{\omega} \times \vec{u} + \nabla \frac{|\vec{u}|^2}{2}$$

Here $\vec{\omega}$ is the total *vorticity*, the curl of the velocity. Using this, we get:

$$\frac{\partial}{\partial t}\vec{u} + \omega_a \times \vec{u} = -\nabla(\frac{p}{\rho_0} + \frac{|\vec{u}^2|}{2} + gz) + \mathcal{F} + \nu\nabla^2\vec{u} \qquad (49)$$

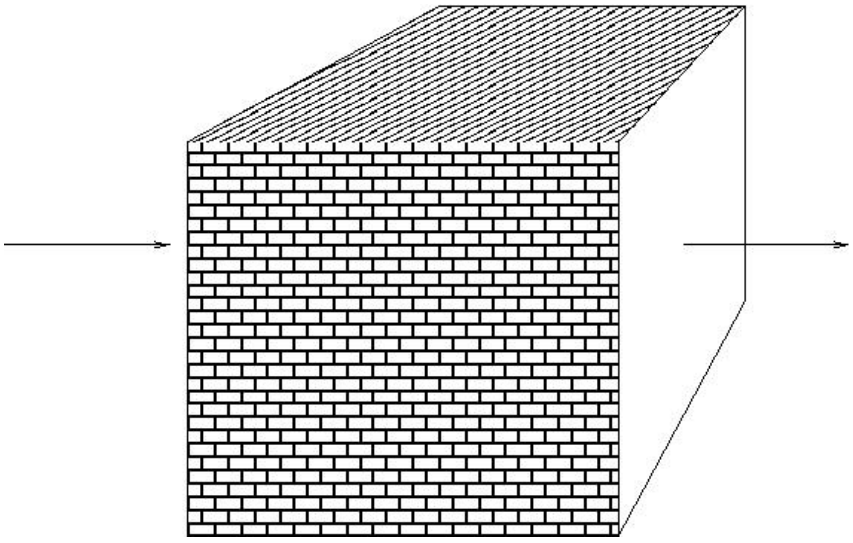

Figure 10: . A three dimensional volume. The boundaries are either solid or periodic.

The term:

$$\vec{\omega}_a = \vec{\omega} + 2\vec{\Omega}$$

is the *absolute vorticity*, the sum of the "relative vorticity", $\vec{\omega}$, and the "planetary vorticity", $2\vec{\Omega}$. Note how the two vorticities are essentially on equal footing here, showing how important the planetary rotation is.

The first term on the RHS of (49) is the gradient of the *Bernoulli function*, an important quantity in fluid mechanics.

5.1 Energy

If we take the dot product of equation (49) with the velocity, we get:

$$\frac{\partial}{\partial t}\frac{|\vec{u}^2|}{2} = -\nabla \cdot [\vec{u}(\frac{p}{\rho_0} + \frac{|\vec{u}^2|}{2} + gz)] + \vec{u} \cdot \mathcal{F} + \nu \vec{u} \cdot \nabla^2 \vec{u} \qquad (50)$$

We've used incompressibility to rewrite the Bernoulli term. Note too that the term with the absolute vorticity has vanished—this is because it is perpendicular to the velocity. So that term does not affect the total energy.

To obtain an equation for the total energy, we integrate (50) over a volume. For the volume, we'll assume either *solid* or *periodic* boundaries (Fig. 10). At solid walls, the normal component of the velocity vanishes. With periodic conditions, the velocity is the same on the opposite boundaries, so their difference is zero.[5]

Most oceans are bounded by solid walls on the sides and bottom. The sea surface is often considered as a solid boundary as well, because there are no currents flowing up into the atmosphere. The atmosphere can be modelled as having solid boundaries at the surface and at a chosen height (e.g. the tropopause). Often we specify solid boundaries at a northern and southern latitude, confining motion to the latitude band. But the longitudinal direction is periodic, as the flow can wrap all the way around the earth (such as the Jet Stream).

The main effect of these choices is on the integral of divergences. Consider the volume integral of the advection of some quantity, G:

$$\iiint \nabla \cdot (\vec{u}G)\, dV = \oiint G\vec{u} \cdot \hat{n}\, dS = 0 \tag{51}$$

By Gauss's theorem, the volume integral can be converted to a surface integral, as in the second term. This then vanishes with solid walls because the normal velocity is zero. It also vanishes with periodic boundary conditions. Consider the integral in the x direction:

$$\int_0^L \frac{\partial}{\partial x}(uG)\, dx = u(L)G(L) - u(0)G(0) = 0 \tag{52}$$

By periodicity, the two terms are equal so their difference is zero.

Thus, if we integrate (50) over the volume, the two divergence terms

[5]Boundaries can be important places, supporting boundary layers which are sometimes turbulent themselves. We purposely avoid such issues here.

vanish and we get:

$$\frac{d}{dt}E = \iiint \vec{u} \cdot \mathcal{F}\, dV + \nu \iiint \vec{u} \cdot \nabla^2 \vec{u}\, dV \tag{53}$$

Here:

$$E = \iiint \frac{1}{2}|\vec{u}^2|\, dV \tag{54}$$

is the total kinetic energy. Equation (53) implies the total energy changes only in response to forcing and dissipation. Advection doesn't change the total energy; it only redistributes energy in the domain.

Dissipation causes the energy to *decrease*. But this isn't obvious because the last term in (53) is positive. We can convert it though using another vector identity:

$$\nabla^2 \vec{u} = \nabla(\nabla \cdot \vec{u}) - \nabla \times (\nabla \times \vec{u}) = -\nabla \times \vec{\omega} \tag{55}$$

The second term vanishes by incompressibility. Taking the dot product with $\vec{u}$, we get:

$$\vec{u} \cdot \nabla^2 \vec{u} = -\vec{u} \cdot (\nabla \times \omega) = -\vec{\omega} \cdot (\nabla \times \vec{u}) + \nabla \cdot (\vec{\omega} \times \vec{u}) = -|\vec{\omega}|^2 + \nabla \cdot (\vec{\omega} \times \vec{u}) \tag{56}$$

using (yet) another vector identity. So we can write:

$$\nu \iiint \vec{u} \cdot \nabla^2 \vec{u}\, dV = -\nu \iiint |\vec{\omega}|^2\, dV + \nu \iiint \nabla \cdot (\vec{\omega} \times \vec{u})\, dV \tag{57}$$

The last term vanishes when integrated over space, because:

$$\iiint \nabla \cdot (\vec{\omega} \times \vec{u})\, dV = \oiint (\vec{\omega} \times \vec{u}) \cdot \hat{n}\, dS \tag{58}$$

This vanishes automatically for periodic boundary conditions. But it also vanishes with solid walls (see the exercise).

Thus the energy equation, without forcing, is:

$$\frac{d}{dt}E = -\nu \iiint |\vec{\omega}|^2\, dV \tag{59}$$

The energy dissipation is proportional to the integral of the squared vorticity, which is known as the *enstrophy*. Because the RHS is negative definite, the energy can only decrease in time.

An important question in turbulence theory is whether the energy is *conserved* when the viscosity goes to zero. This is relevant for the atmosphere and ocean, because the viscous damping term is so much smaller than the other terms in the momentum equation. It looks at first glance like energy should be conserved, because the RHS of (59) should go to zero with ν. But it could happen that the enstrophy *increases* as ν decreases. Say for example that:

$$\iiint |\vec{\omega}|^2 \, dV \propto \frac{C}{\nu} \tag{60}$$

in the limit of small viscosity. Then we would have

$$\frac{dE}{dt} = -C \tag{61}$$

Then the energy would decrease at a constant rate, regardless of how small ν was. For this to happen, there must be *production* of vorticity in the absence of forcing, so that the vorticity doesn't just decrease. To see whether or not this is the case, we must examine the vorticity equation.

Exercise: Why does the term on the RHS of eq. (58) vanish with solid walls?

5.2 Vorticity and enstrophy

We obtain the vorticity equation by taking the curl of equation (49):

$$\frac{\partial}{\partial t}\vec{\omega} + \vec{u} \cdot \nabla \vec{\omega}_a + \vec{\omega}_a(\nabla \cdot \vec{u}) - \vec{\omega}_a \cdot \nabla \vec{u} = \nabla \times \mathcal{F} + \nu \nabla^2 \vec{\omega} \tag{62}$$

We've used yet another vector identity to rewrite the advection term. Combining the second and third terms on the LHS, we get:

$$\frac{\partial}{\partial t}\vec{\omega} + \nabla \cdot (\vec{u} \otimes \vec{\omega}) = \vec{\omega}_a \cdot \nabla \vec{u} + \nabla \times \mathcal{F} + \nu \nabla^2 \vec{\omega} \tag{63}$$

Now, the question is whether the enstrophy, $|\vec{\omega}|^2$ is bounded if there is no forcing ($\mathcal{F} = 0$) and if the viscosity, ν, decreases toward zero. Taking the dot product with $\vec{\omega}$, we obtain:

$$\frac{1}{2}\frac{\partial}{\partial t}|\vec{\omega}|^2 + \nabla \cdot (\vec{u}\frac{|\vec{\omega}|^2}{2}) = \vec{\omega} \cdot (\vec{\omega}_a \cdot \nabla \vec{u}) + \nu \vec{\omega} \cdot \nabla^2 \vec{\omega} \tag{64}$$

Integrating this in space, and using the same vector identities that we did with the energy, we obtain:

$$\frac{d}{dt} \iiint \frac{1}{2}|\vec{\omega}|^2 \, dV = \iiint \vec{\omega} \cdot (\vec{\omega}_a \cdot \nabla \vec{u}) \, dV - \nu \iiint |\nabla \times \vec{\omega}|^2 \, dV \tag{65}$$

The last term is negative definite, causing a decay in the enstrophy. But the middle term has an undetermined sign. In fact, this can be positive, and as such, it can act as a source of enstrophy. Thus we can't say whether E is conserved in the limit of vanishing viscosity. Indeed, what happens in such high Reynolds number fluids is that the velocity gradients become very large at small scales and the enstrophy can be very large. And measurements of the total energy suggest it decreases in time, even when the viscosity is very small.

However, this isn't the case in *two* dimensions. Imagine a flow confined to a plane. This is not as unrealistic as it seems, because at large scales, atmospheric and oceanic motion is predominantly in the horizontal directions. Assuming the velocity is purely horizontal, we have:

$$\vec{u} = (u, v, 0) \tag{66}$$

The vorticity, which is perpendicular to the velocity, is then purely *vertical*:

$$\vec{\omega} = (0, 0, \frac{\partial}{\partial x}v - \frac{\partial}{\partial y}u) \equiv \zeta\hat{k} \tag{67}$$

It's possible to show that the important part of the planetary rotation vector is the one which is locally vertical [22]:

$$2\vec{\Omega} \approx 2\Omega sin(\theta)\hat{k} \equiv f\hat{k} \tag{68}$$

where θ is the central latitude.

Now, consider the enstrophy source term in eq. (65):

$$\omega_a \cdot \nabla\vec{u} = (\zeta + f)\hat{k} \cdot \nabla(u\hat{i} + v\hat{j}) = 0 \tag{69}$$

The term vanishes because the vorticity and the velocity are perpendicular. So the enstrophy source is *absent* in a 2-D flow, meaning the enstrophy can only decrease in time. Thus energy *is* conserved in the inviscid limit in 2-D:

$$lim_{\nu\to 0}\ \frac{dE}{dt} = 0 \tag{70}$$

This has an enormous effect on 2-D flows, as we will see.

But what about the enstrophy with vanishing viscosity? Without the production term, the RHS of equation (65) is negative definite. But it is not guaranteed that enstrophy is conserved unless we know that the curl of the vorticity is bounded in this limit. To see, we have to consider the next equation, for the *palinstrophy*. It turns out there is a source term for that as well. So we can't assume enstrophy is conserved in 2-D, just as we couldn't assume energy was conserved in 3-D. And numerical experiments show that the total enstrophy decreases in time, even when the viscosity is small, just as the energy decreases in 3D.

Thus in the limit $\nu \to 0$, energy in 2D isn't affected by the dissipation at very small scales. Why this is will become clear shortly.

Exercise: Show that the palinstrophy equation has a source term in 2D. This implies that enstrophy will decrease in 2D, even when $\nu \to 0$.

6 3-D turbulence

Now we return to the coffee cup. Why does it spin down so quickly? More specifically, how can dissipation, acting at molecular scales, affect the energy at the scale of the coffee cup? We'll see that this has to do with how energy is exchanged between scales.

6.1 Triad interactions

For this it is best to work in Fourier space. Imagine the forcing, $\mathcal{F}$, happens at large scales. This is the spoon stirring the coffee. The dissipation is at the molecular scale. Thus there is a range of *intermediate* scales where the forcing and dissipation aren't relevant. At these scales, it is advection which dominates the changes in the velocity.

We can illustrate how this works by focusing on just one of the advective terms, in the x-momentum equation:

$$\frac{\partial}{\partial t}u = -u\frac{\partial}{\partial x}u \tag{71}$$

We'll assume 1-D motion, in a periodic domain with a length L.

We first write the velocity on the LHS of (71) in terms of its Fourier transform:

$$u = \sum \hat{u}(k,t)\, e^{ikx} \tag{72}$$

Because the domain is periodic, k is quantized:

$$k = \frac{n\pi}{L}$$

Further, the time derivative of u is:

$$\frac{\partial}{\partial t}u = \sum \frac{\partial}{\partial t}\hat{u}(k,t)\, e^{ikx} \tag{73}$$

The RHS of (71) involves the product of two velocities. For this, we need two different transforms:

$$\begin{aligned} -u\frac{\partial}{\partial x}u &= -(\sum_l \hat{u}(l,t)e^{ilx})\,(\sum_m im\hat{u}(m,t)\, e^{imx}) \\ &= -\sum_l \sum_m im\hat{u}(l,t)\,\hat{u}(m,t)\, e^{i(l+m)x} \end{aligned} \tag{74}$$

Note the factor im comes from taking the x-derivative.

Now we isolate one Fourier component on the LHS of (71), to see how that is changing in time. We do that by Fourier transforming the whole equation, multiplying both sides by $exp(-ikx)$ and integrating over the domain. We get:

$$\frac{\partial}{\partial t}\hat{u}(k,t) = \frac{1}{L}\int_0^L im\hat{u}(l,t)\,\hat{u}(m,t)\, e^{i(l+m-k)x}\, dx \tag{75}$$

The wavenumbers l and m, like k, are quantized. So we can write:

$$l + m - k = \frac{(p+q-n)\pi}{L}$$

where n, p and q are all integers. Thus the sum $p + q - n = a$ is also an integer. Say this is different from zero. Then the integral above is:

$$\frac{1}{L}\frac{m}{a}\hat{u}(l,t)\,\hat{u}(m,t)e^{ia\pi x/L}|_0^L$$

But because the exponential is periodic, this vanishes. The only time the integral doesn't vanish is when $a = 0$, or:

$$k = l + m$$

Then the integral is one. Thus we have:

$$\frac{\partial}{\partial t}\hat{u}(k,t) = -\sum_l \sum_m im\,\hat{u}(l,t)\,\hat{u}(m,t)\,\delta(l+m-k) \tag{76}$$

where:

$$\delta(x) = \begin{cases} 1 & \text{if } x = 0 \\ 0 & \text{if } x \neq 0 \end{cases}$$

This means that wave interactions occur between groups of three waves, or *triads*, whose wavenumbers sum to zero.

If we consider the other advective terms, and three dimensional wavenumbers, the conclusion is the same. The only contributions come from triads of waves whose *vector* wavenumbers sum to zero:

$$\vec{l} + \vec{m} = \vec{k} \tag{77}$$

So, for instance, a Fourier mode with $\vec{k} = (3, 3, 0)$ will interact with waves with $(1, 2, 0)$ and $(2, 1, 0)$. This is known as a *local* interaction, because the wavenumbers for the triad are all similar. But the same mode will also be affected by the waves with $(-10, 2, 0)$ and $(13, 1, 0)$. These have a much smaller scale in the x-direction. This is a *non-local* interaction, as the components have very different sizes.

Consider Fig. (11), which shows a hypothetical energy spectrum, $\mathcal{E}$. We plot the spectrum as a function of the total wavenumber:

$$\kappa \equiv (k_x^2 + k_y^2 + k_z^2)^{1/2}$$

The wavenumber is on the x-axis. Note that increasing wavenumber implies *decreasing* size; so the large scales are on the left. Now the fluid is forced at a large scale, perhaps by the spoon in the cup. This produces an energy spectrum like that in dash-dot line—a spike at the forcing scale. Interactions between wavenumbers cause the spectrum to spread out, as the energy is transferred to other wavenumbers. Local interactions cause the energy to *cascade* to smaller scales (larger wavenumbers). At later times,

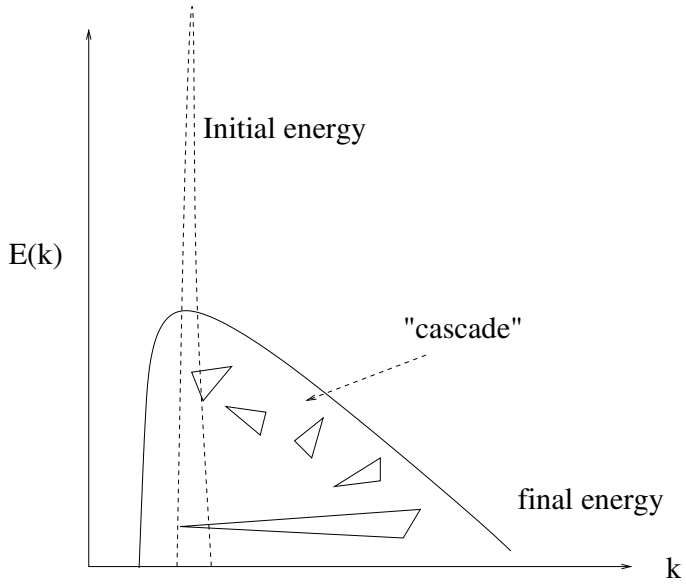

Figure 11: A hypothetical cascade of an initially narrow band energy spectrum to smaller scales. We imagine that energy is conserved during the cascade, so that the area under the curves is conserved (despite appearances).

there is energy across a range of wavenumbers. Then non-local interactions can occur, between large and small scale waves.

Eventually energy arrives at the smallest scales, where it is dissipated by molecular interactions. So this is how molecular dissipation can bring the coffee to rest: because *turbulence transfers energy down to the dissipation scales*.

6.2 Kolmogorov's inertial range

Forcing puts energy into the system and dissipation removes it. Energy is transferred via triad interactions from the large scales to the small. As the British scientist, Lewis Fry Richardson, put it:

Big whirls have little whirls,
that feed on their velocity.
And little whirls have littler whirls,

and so on to viscosity.

Kolmogorov proposed a theory for the energy transfer over the intermediate scales, which have become known as the *inertial range* [17]. The theory rests on several assumptions:

- The turbulence is in a statistically *steady state*. This means the energy, while fluctuating, isn't increasing or decreasing, and hence the spectrum retains its shape.
- The turbulence is *isotropic*—the same in all directions. So instead of using $E(k, l, m)$, we can focus on $E(\kappa)$, where κ is the magnitude of the wavenumber vector.
- The turbulence is *homogeneous*—the same at all locations in space. So we can talk about the dynamics in wavenumber space without worrying about variations from place to place.
- The triad interactions are *local* (the reason for this will become clearer later on).

As stated, the details of the forcing and dissipation don't matter in the inertial range. The only aspect which matters is the rate at which energy is transferred across scales. In a statistically steady state, this is a constant number. We denote this energy flux, ϵ.

It turns out that the energy spectrum has a characteristic power law slope in the inertial range, and this can be deduced solely from dimensional considerations. The spectrum, $E(\kappa)$, has dimensions of L^3/T^2. That's because energy has units of L^2/T^2, and the total energy is the sum over wavenumbers of the spectrum (recall wavenumbers have units of L^{-1}).

The energy flux on the other hand has units of L^2/T^3, as this is proportional to the time rate of change in the energy. Assuming that ϵ is the only important parameter, we must have:

$$E(\kappa) = C\epsilon^{2/3}\kappa^{-5/3} \tag{78}$$

where C is a constant.

The inertial range bridges the range of scales for the forcing down to the dissipation. The forcing scale is determined by the forcing itself (the size of the spoon). But at what scale does dissipation become important? This where the energy transfer rate due to turbulence is approximately the same as the dissipation rate.

We can deduce the scale by equating time scales. The dissipation time scale, discussed earlier, is:

$$T_\nu \propto \frac{L^2}{\nu} \propto \nu^{-1}\kappa^{-2} \tag{79}$$

The time scale in the inertial range can be deduced from the energy flux, again on dimensional grounds:

$$T_a \propto \epsilon^{-1/3}\kappa^{-2/3} \tag{80}$$

Notice that this varies across the range, with shorter time scales at smaller scales. In the dissipation range, the dissipation time scale is shorter than the cascade time scale, because energy decays before it is transferred. The opposite is true in the cascade range. At the transition between the cascade and the dissipation ranges, the two scales are equal. Equating them, we get:

$$\kappa_\nu = (\frac{\epsilon}{\nu^3})^{1/4} \tag{81}$$

The corresponding length scale is $L_\nu = (\nu^3/\epsilon)^{1/4}$, the *Kolmogorov scale*.

The Kolmogorov model is self-consistent with regards to dissipation. As noted in sec. (5), the energy dissipation is given by:

$$D = -\nu \iiint |\vec{\omega}|^2 \, dV$$

The term in the integral has a scale:

$$\frac{\nu U^2}{L^2} \propto \nu \kappa^2 U^2$$

U^2 varies as:

$$U^2 \propto \epsilon^{2/3} \kappa^{-2/3}$$

So the energy dissipation (per unit volume) scales as:

$$D \propto \nu \epsilon^{2/3} \kappa^{4/3}$$

At the dissipation wavenumber, κ_ν, this equals

$$\nu \, \epsilon^{2/3} \, \frac{\epsilon^{1/3}}{\nu} = \epsilon$$

Thus the dissipation rate is equal to the energy flux across the inertial range. The amount of energy put in by the forcing is removed by the dissipation.

But notice something—the dissipation rate is *independent of* ν! Imagine that we make ν smaller and smaller. Then the dissipation scale L_ν is smaller. But the dissipation *rate* is the same. The only difference is that the inertial range carries the energy to smaller scales.

This is a critical point. Because of the downscale cascade, energy will not be conserved in the fluid so long as there is even an infinitesimal amount of dissipation. Energy can only be conserved if there is identically *zero* dissipation.

The Kolmogorov picture can be illustrated as in Fig. (12). The energy is injected at wavenumber, κ_f, and at a rate ϵ. It then cascades downscale at

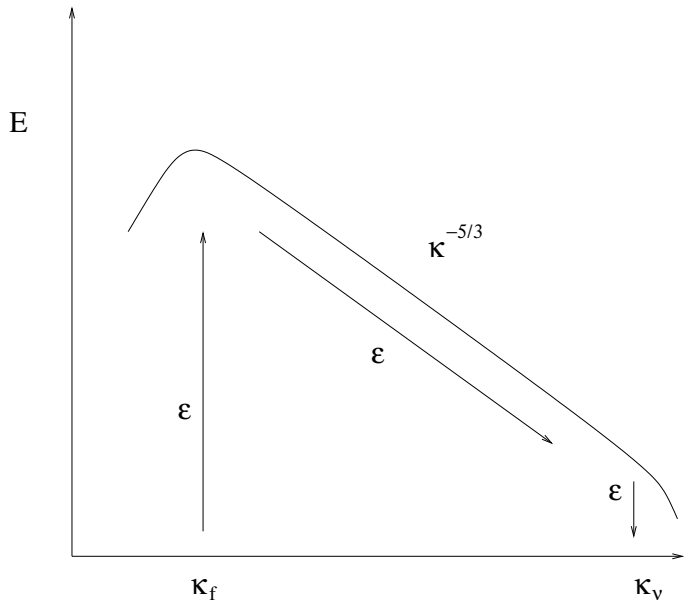

Figure 12: The Kolmogorov energy spectrum.

the same rate, ϵ, to the dissipation wavenumber, κ_ν, where it is dissipated at the same rate. In the inertial range, the only parameter which matters is ϵ, yielding the characteristic $\kappa^{-5/3}$ spectrum.

6.3 Shell models

A simple way to understand the Kolmogorov model is as follows. Imagine the turbulence involves energy transfer between discrete wavenumber bins (Fig. 13). In the figure, we have four bins, and so four different scales. Energy enters at the largest scale ($k = 1$) and is removed by dissipation at the smallest scale ($k = 8$).

In drawing the figure this way, we make the assumption that the wavenumber interactions are *local*; energy transfer occurs only between adjacent bins. The situation would be much more complicated if we allowed for transfer between all the bins.

The rate that energy is transferred from $k = 1$ to $k = 2$ is given by ϵ.

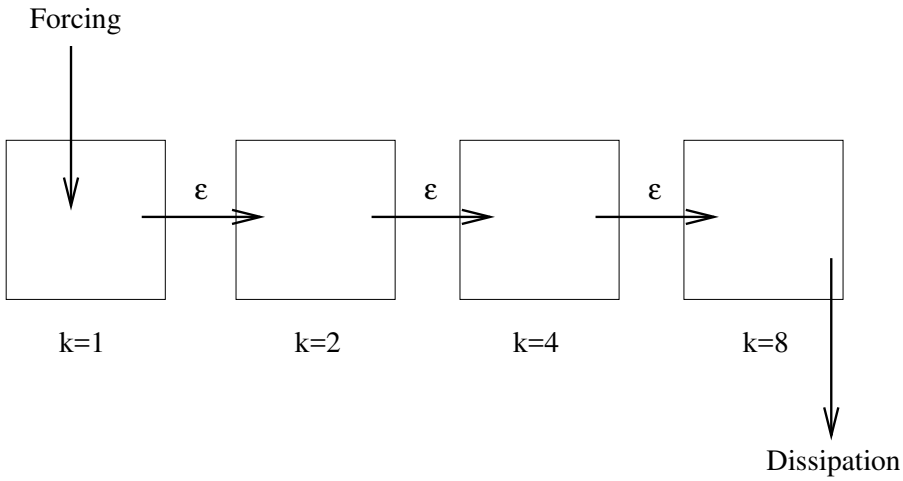

Figure 13: Energy transfer in the shell model. Energy is put in at the largest scale ($k = 1$) and removed at the smallest ($k = 8$).

This is the same rate as energy is transferred to $k = 4$. Imagine this were not so. Say the energy transfer from $k = 2$ to $k = 4$ was only $\epsilon/2$. Then the energy would be entering the $k = 2$ bin faster than it was leaving, and the energy in the bin would increase in time. The spectrum then would not be stationary in time. So the transfer rate must be the same between all bins.

Also notice that the rate that energy is removed from the last bin ($k = 8$) is also ϵ. So the dissipation rate is equal to the flux. Again, if this weren't so, the energy would pile up in the smallest bin.

In fact, this is a real possibility. In numerical models with too little dissipation, the energy cascades to the smallest scales faster than it's taken out. So the energy increases at the smallest scales and the model subsequently blows up. The shell model illustrates why this is so.

Exercise: *Structure functions*

Kolmogorov [17] didn't actually derive the form of the energy spectrum. Rather, he derived relations for the velocity *structure functions*.

These are powers of the velocity difference between two points. For example, the second order structure function is:

$$S_2(r) =< |u(\vec{x}+r) - u(\vec{x})|^2 > \tag{82}$$

The brackets indicate an *ensemble* average, i.e. an average over a number of observations. Use dimensional analysis to deduce how $S_2(r)$ varies with the separation, r. Compare this to the spectrum. Consider also the third order structure function, $S_3(r)$, which has a special significance in turbulence theory.

6.4 Observations

Observations support Kolmogorov's prediction for the energy spectrum. An example is shown in Fig. (14), from measurements in a jet in the laboratory [8]. The $k^{-5/3}$ dependence is seen clearly over roughly two decades (factors of 10) of the wavenumber.

Another well-known example is the observations of Grant et al. [15] in a tidally-mixed fjord on the west coast of the United States. This also yielded strong evidence of a $k^{-5/3}$ spectrum (Fig. 15).

There are numerous other examples as well, from the atmospheric boundary layer, in laboratory experiments and in numerical simulations. However, where the model is less successful is at predicting the *higher moments*. Energy, like the variance, is a second order statistic, being proportional to the velocity squared. But one can also look at higher powers, such as the skewness and the kurtosis. Or, one can look at velocity PDFs.

What is typically found is that the PDFs of velocity differences at separated points (the structure functions; see the exercise above) are not Gaussian. As shown in Fig. (16), the PDFs for velocity differences with large

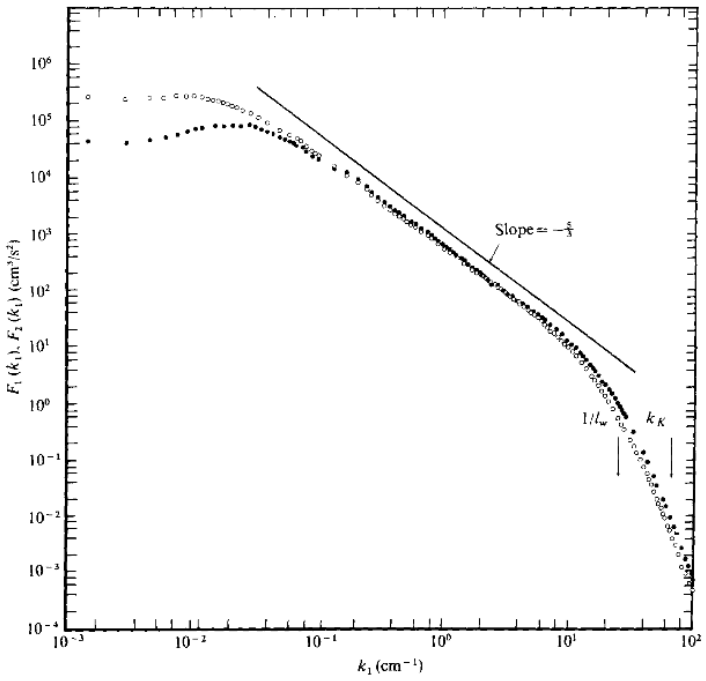

FIGURE 15. One-dimensional spectra of streamwise- and lateral-component velocity fluctuations for an axisymmetric jet; $Re = 3{\cdot}7 \times 10^6$, $x/d = 70$, $r/d = 0$. ○, $F_1(k_1)$; ●, $F_2(k_1)$.

Figure 14: The energy spectra for the stream-wise and transverse velocity components in a jet, with $Re = 626$. From [8].

separations are close to Gaussian. But as the separation, r, approaches the Kolmogorov scale, the wings of the PDFs become more and more extended. So the kurtosis increases to values exceeding 3.

While the velocities themselves have an approximately Gaussian distribution, the velocity *gradients* are not Gaussian. What one sees if one measures the gradients is that large values occasionally occur, much larger than would be expected for a Gaussian process. Such episodes appear as "bursts" in the time series. We say that the turbulence is "intermittent".

This can be taken into account in the shell model above, by stating that the turbulence fills only a fraction of the bins. This is the idea behind the "β-model". Such a model yields the same spectra as Kolmogorov, but predicts deviations in the higher moments, as observed. See for example

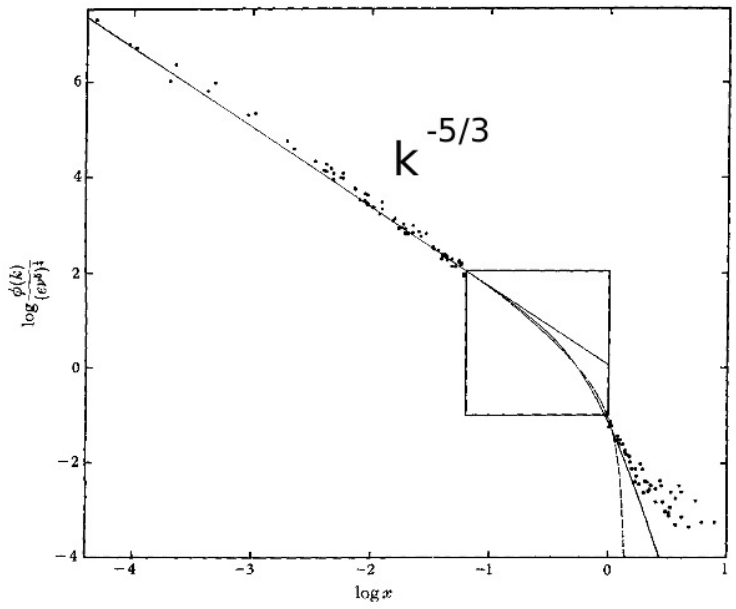

FIGURE 12. Seventeen spectra compared to the theories of Kolmogoroff, Heisenberg and Kovasznay. The straight line has a slope of $-\frac{5}{3}$, the curved solid line is Heisenberg's theory and the dashed line is Kovasznay's theory. Within the square, the observations are too crowded to display on this scale and they are shown in figure 13.

Figure 15: Energy spectrum from towed measurements in a tidal basin by Grant et al. [15]. The boxed region shows the region of transition to the dissipative range.

Frisch [14].

7 2-D turbulence

At synoptic or "weather" scales in the atmosphere and ocean, the motion is nearer two dimensional than three dimensional. This is because the vertical velocity, suppressed by rotation and stratification, is much smaller than the horizontal velocities. Turbulence in two dimensions is similar to that in 3-D, but also quite different.

Let's assume the velocities are purely two-dimensional:

$$\vec{u} = (u, v, 0) \tag{83}$$

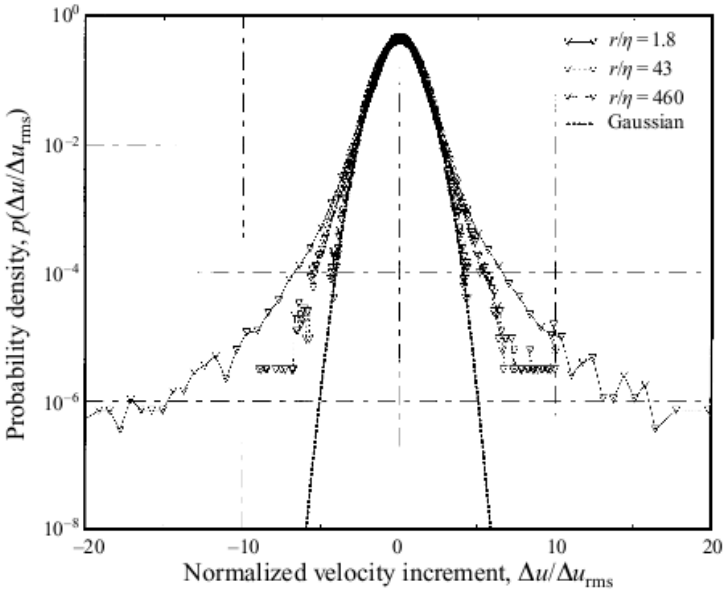

Figure 16: PDFs of the velocity differences for different separations, r. At the largest separations, near the forcing scale, the PDFs are nearly Gaussian. But approaching the Kolmogorov scale, the wings of the PDF become more and more extended.

Then the continuity equation is just:

$$\frac{\partial}{\partial x}u + \frac{\partial}{\partial y}v = 0 \tag{84}$$

This implies we can write the velocities in terms of a streamfunction, ψ:

$$u = -\frac{\partial}{\partial y}\psi, \quad v = \frac{\partial}{\partial x}\psi \tag{85}$$

The vorticity is perpendicular to the velocity, so it only has a vertical component:

$$\vec{\omega} = (\frac{\partial}{\partial x}v - \frac{\partial}{\partial y}u)\ \hat{k} = \nabla^2\psi\ \hat{k} \equiv \zeta\hat{k} \tag{86}$$

As shown, we define the 2-D relative vorticity ζ. The equation for the 2-D vorticity follows from (63):

$$\frac{\partial}{\partial t}\zeta + \vec{u}\cdot\nabla(\zeta + f) = \nabla\times\mathcal{F} + \nu\nabla^2\zeta \tag{87}$$

As noted earlier, the vorticity production term is absent because the vorticity and velocity are perpendicular.

Exercise: *2-D triads*

Triad interactions also occur in 2-D. Say that:

$$\psi = \sum_k \sum_l \hat{\psi}(k,l) e^{ik_x x + ik_y y} \tag{88}$$

Fourier transform the vorticity equation (87), without forcing or dissipation and assuming a domain with lengths 2π in each direction. Substitute in the expansions above and obtain an equation for $\frac{\partial}{\partial t}\hat{\psi}(\vec{k})$. Show the advective terms contribute in triads.

7.1 Conservation laws

Without forcing and dissipation, energy and enstrophy are conserved, as in 3-D. Both relations can be derived from the vorticity equation (87).

The enstrophy equation is the simplest. Multiplying (87) by ζ yields:

$$\frac{\partial}{\partial t}\frac{\zeta^2}{2} + \vec{u}\cdot\nabla\frac{\zeta^2}{2} = 0 \tag{89}$$

assuming $\mathcal{F} = 0$, $\nu = 0$ and $f = const.$ As the flow is incompressible, this is:

$$\frac{\partial}{\partial t}\frac{\zeta^2}{2} + \nabla\cdot\frac{\vec{u}\,\zeta^2}{2} = 0 \tag{90}$$

Integrating over the area:

$$\frac{d}{dt}\iint \frac{\zeta^2}{2}\,dx\,dy + \oint \frac{\zeta^2}{2}\vec{u}\cdot\hat{n}\,dl = 0 \tag{91}$$

The second term vanishes with either solid walls or periodic boundaries, so:

$$\frac{d}{dt}\iint \frac{\zeta^2}{2}\,dx\,dy \equiv \frac{d}{dt}Z = 0 \tag{92}$$

The total enstrophy is conserved in the absence of forcing and dissipation.

To obtain the energy equation, we multiply (87) by ψ and integrate over the area:

$$\iint \psi \frac{\partial}{\partial t}\zeta \, dxdy + \iint \psi \nabla \cdot (\vec{u}\zeta) \, dxdy = 0 \tag{93}$$

The first term can be written:

$$\iint \psi \frac{\partial}{\partial t}\nabla^2 \psi \, dxdy = -\frac{1}{2}\iint \frac{\partial}{\partial t}|\nabla \psi|^2 \, dxdy = -\frac{dE}{dt} \tag{94}$$

after integration by parts. For the second term, we use the following identity:

$$\nabla \cdot (\vec{u}\zeta\psi) = \psi \nabla \cdot (\vec{u}\zeta) + \zeta \vec{u} \cdot \nabla \psi \tag{95}$$

The last term is zero because $\vec{u}$ is parallel to the streamlines, so the dot product with the gradient is identically zero. So:

$$\iint \psi \nabla \cdot (\vec{u}\zeta) \, dxdy = \iint \nabla \cdot (\psi \vec{u}\zeta) \, dxdy = \oint \psi \zeta \vec{u} \cdot \hat{n} \, dl = 0 \tag{96}$$

again, for periodic conditions or a solid boundary. So:

$$\frac{dE}{dt} = 0 \tag{97}$$

in the absence of forcing.

Thus in the inviscid case, both energy and enstrophy are conserved. We exploit this in the following sections.

7.2 A triad interaction

The interesting aspect about 2-D turbulence is illustrated nicely by Fjørtoft [12].[6] We look at a triad interaction between three wavenumbers, as shown in the simple shell model in Fig. (17). Energy is initially in the center shell, at wavenumber k. The energy flows to the other two shells, one with a wavenumber $\kappa/2$ and the other with a wavenumber 2κ. The energy in the boxes is E_0, E_1 and E_2, going from left to right.

[6] A remarkable, short paper...with no references! Fjørtoft argues all his points on first principles.

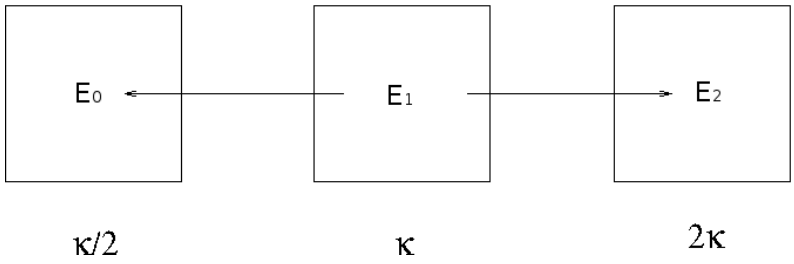

Figure 17: A triad in two dimensions. The energy is initially inthe center shell and flows to the other two. Each shell has a wavelength which is twice that of the shell to its right.

Assume $\nu = 0$, so that both the energy and enstrophy are conserved. This is a reasonable assumption in the inertial range, where dissipation is unimportant. Then:

$$E_0(t) + E_1(t) + E_2(t) = E_1(0) \tag{98}$$

and:

$$Z_0(t) + Z_1(t) + Z_2(t) = Z_1(0) \tag{99}$$

Now these two statements are related to each other, as follows. The energy in 2-D is:

$$E = \iint \frac{1}{2}(u^2 + v^2)\, dA = \frac{1}{2}\sum_k \sum_l (k^2 + l^2)|\hat{\psi}|^2 \tag{100}$$

from Parseval's theorem (sec. 3). The enstrophy on the other hand is:

$$Z = \iint \frac{1}{2}(\frac{\partial}{\partial x}v - \frac{\partial}{\partial y}u)^2\, dA = \frac{1}{2}\sum_k \sum_l (k^2+l^2)^2|\hat{\psi}|^2 = \sum_k \sum_l \kappa^2 E \tag{101}$$

So the enstrophy conservation statement for the boxes can be written:

$$\kappa_0^2 E_0(t) + \kappa_1^2 E_1(t) + \kappa_2^2 E_2(t) = \kappa_1^2 E_1(0) \tag{102}$$

Using our values for the wavenumbers, we have:

$$\frac{\kappa^2}{4} E_0(t) + \kappa^2 E_1(t) + 4\kappa^2 E_2(t) = \kappa^2 E_1(0) \tag{103}$$

or simply:

$$\frac{1}{4}E_0(t) + E_1(t) + 4E_2(t) = E_1(0) \tag{104}$$

Combining this with the energy equation (98), we get:

$$\frac{1}{4}E_0(t) = E_2(t) \tag{105}$$

so that:

$$E_0(t) = \frac{4}{5}\delta E_1, \quad E_2(t) = \frac{1}{5}\delta E_1 \tag{106}$$

where $\delta E_1 = E_1(0) - E_1(t)$ is the energy lost from the middle shell. Thus 80% of the energy goes to the *larger* scale wave. Energy is apparently going upscale rather than downscale! This is completely counter to expectations from 3D turbulence.

What about the enstrophy? We find that:

$$Z_0(t) = \frac{\kappa^2}{4}E_0(t) = \frac{\kappa^2}{4}\frac{4}{5}\delta E_1 = \frac{1}{5}\delta Z_1 \tag{107}$$

Similarly, we find:

$$Z_2(t) = \frac{4}{5}\delta Z_1 \tag{108}$$

So the situation is reversed: 80% of the enstrophy lost from the middle shell goes to the smaller wave. So contrary to the energy, enstrophy is shifting to smaller scales.

If you use different size waves, you will find different fractions of energy and enstrophy transfer. But if you look at the full range of possible triads, most act like the one above and transfer energy to larger scales.[34]

Exercise: *Another triad*

Consider the general case where $\kappa_0 = \kappa_1/n$ and $\kappa_2 = n\kappa_1$. What fraction of energy goes to the larger wavenumber and what fraction to the smaller. What about the enstrophy?

7.3 An integral argument

The transfer of energy to larger scales in 2D is known as the "inverse cascade", being in the opposite direction as in 3D. It was also noted by Batchelor [2], in the last few pages of his seminal book *Homogeneous Turbulence*, published in the same year as Fjørtoft's article.

Batchelor's argument goes like this. Imagine that we have a narrow energy spectrum initially, as in Fig. (11). The spectral peak will broaden in time, as energy is passed to other wavenumbers via triad interactions. We can express this as:

$$\frac{d}{dt}\int(\kappa-\kappa_i)^2\,E\,d\kappa>0 \tag{109}$$

where κ_i is the wavenumber peak of the initial spectrum. Expanding the LHS, we get:

$$\frac{d}{dt}[\int\kappa^2\,E\,d\kappa-2\kappa_i\int\kappa\,E\,d\kappa+\kappa_i^2\int E\,d\kappa]>0 \tag{110}$$

The first term is the total enstrophy and the last term is the total energy, both of which are constant. So we must have:

$$\frac{d}{dt}\int\kappa\,E\,d\kappa<0 \tag{111}$$

Written another way, this is:

$$\frac{d}{dt}(\frac{\int\kappa\,E\,d\kappa}{\int\,E\,d\kappa})=\frac{d}{dt}\kappa_m<0 \tag{112}$$

where κ_m is the mean wavenumber of the spectrum. This then is *decreasing in time*, implying the spectrum is shifting to the left, toward larger scales. Like Fjørtoft, Batchelor concluded that energy is moving upscale in 2-D.

We can use a similar argument to see what's happening to the enstrophy, following Salmon [43]. If the spectrum is spreading, we also can write:

$$\frac{d}{dt}\int(\kappa^2-\kappa_i^2)^2\,E\,d\kappa>0 \tag{113}$$

Expanding this, we get:

$$\frac{d}{dt}[\int\kappa^4\,E\,d\kappa-2\kappa_i^2\int\kappa^2\,E\,d\kappa+\kappa_i^4\int E\,d\kappa]>0 \tag{114}$$

The second term is proportional to the total enstrophy and the last term to the total energy. So we have:

$$\frac{d}{dt}\int\kappa^4\,E\,d\kappa=\frac{d}{dt}\int\kappa^2\,Z\,d\kappa>0 \tag{115}$$

So:

$$\frac{d}{dt}\frac{\int\kappa^2\,Z\,d\kappa}{\int\,Z\,d\kappa}>0 \tag{116}$$

Thus the mean square wavenumber for the enstrophy is *increasing* in time; the enstrophy spectrum is shifting to the right, toward small scales.

Thus *two* cascades are occurring simultaneously in 2-D: there is an energy cascade to larger scales, and an enstrophy cascade to smaller scales. That implies that there are two cascade ranges.

Exercise: *Batchelor, part 2*

Re-do Batchelor's arguments using the *mean* wavenumber instead of the initial wavenumber. Assume that the variance in wavenumber increases in time. Do you get the same results?

7.4 The two inertial ranges

That there are two inertial ranges in forced 2-D turbulence was realized by Kraichnan, Leith and Batchelor [19, 26, 3]. We assume the fluid is forced

and that the spectrum is stationary (not changing in time), just as in the Kolmogorov case in 3-D.

The first inertial range is the energy cascade range. We can determine the slope of this just as we did for the 3-D energy cascade. In fact, the slope is the same. The energy still cascades at a rate ϵ, and the spectrum has the form:

$$E(\kappa) = C\epsilon^{2/3}\kappa^{-5/3} \tag{117}$$

The only difference is the direction of transfer, which is now *upscale*. If the forcing were, say, at the 1 km scale, the energy cascade could conceivably produce eddies 1000 km large! This is truly remarkable.

But what happens to the energy when it gets to the large scales? After all, energy is normally dissipated at the other end of the spectrum, at the small scales; we have no means to remove energy at the large scales. So energy will just pile up there, and the spectrum will never reach a steady state.

To avoid this, we require additional dissipation which acts at large scales. A good candidate is *Ekman friction* [22]. This is drag due a frictional bottom boundary layer. Ekman layers occur at the surface in the atmosphere, and at the sea surface and the bottom of the ocean. We can include Ekman friction by adding a linear term in the vorticity equation. Specifically, we modify (87) thus:

$$\frac{\partial}{\partial t}\zeta + \vec{u}\cdot\nabla(\zeta + f) = \mathcal{F} - r\zeta + \nu\nabla^2\zeta \tag{118}$$

where:

$$r = \frac{f\delta_E}{2H}$$

is the inverse of the Ekman spin-down time. Here H is the depth of the fluid and δ_E is the thickness of the bottom Ekman layer.

Ekman friction acts equally at all scales. Consider the case without forcing or small scale dissipation, with $f = const.$ Then:

$$\frac{d}{dt}\zeta = -r\zeta \tag{119}$$

The solution to this is:

$$\zeta(t) = \zeta(0)e^{-rt} \tag{120}$$

So the vorticity decays exponentially, regardless of the scale.

Where does Ekman friction terminate the upscale cascade? To see, we equate time scales, as before. The Ekman damping time scale is just the e-folding time r^{-1} – independent of the scale of the motion. The advection time scale in the energy cascade is again:

$$\tau \propto \epsilon^{-1/3}\kappa^{-2/3}$$

Equating them, we can solve for the large scale dissipation wavenumber:

$$\kappa_r = (\frac{r^3}{\epsilon})^{1/2} \tag{121}$$

This is the boundary between the energy inertial range and the largest scales, which are dominated by Ekman friction. Note that with less friction (smaller r), the inverse cascade proceeds to larger scales.

Now to the other inertial range, where enstrophy cascades to smaller scales. In analogy to the energy range, we have an enstrophy cascade rate, η. This measures the rate of change of enstrophy, which itself has units of $1/T^2$. So the enstrophy transfer has units of $1/T^3$. On dimensional grounds, we infer the spectrum has a shape:

$$E(\kappa) = C\eta^{2/3}\kappa^{-3} \tag{122}$$

So this is *steeper* than the energy inertial range.

An interesting thing about the enstrophy cascade range is that, unlike with the energy inertial range, the advective time scale is *independent of the length scale*. We have simply that:

$$\tau \propto \eta^{-1/3} \tag{123}$$

This time scale is determined by the largest eddies in the cascade range. As such, the enstrophy cascade is "non-local"—the smaller scales are stirred by the eddies at the top of the inertial range.

Equating this time scale with the dissipation time at small scales, $\tau_d = (\nu\kappa^2)^{-1}$, we get the dissipation wavenumber:

$$\kappa_\nu = (\frac{\eta^{1/3}}{\nu})^{1/2} \tag{124}$$

This is where the enstrophy cascade terminates. As we did with the energy range in 3-D, we can calculate the rate at which enstrophy is dissipated, by scaling the enstrophy equation (65). At the dissipation scale, the RHS of (65) scales as:

$$\nu \left|\nabla \times \zeta\right|^2 \propto \nu \frac{U^2}{L^4} \propto \nu \frac{\eta^{2/3}\kappa_\nu^{-2}}{\kappa_\nu^{-4}} = \nu \frac{\eta^{2/3}\eta^{1/3}}{\nu} = \eta \tag{125}$$

So as with the energy in 3-D, the enstrophy dissipation is independent of the viscosity, ν. Even if ν is very small, enstrophy is transferred to the small scales and removed. Thus enstrophy is *not* conserved in 2-D turbulence, since it will always (eventually) be dissipated.

We summarize the cascades in Fig. (18). Energy and enstrophy are "injected" into the system at wavenumber κ_f. There are two inertial ranges: the $\kappa^{-5/3}$ range at larger scales and the κ^{-3} range at smaller scales. Energy cascades at a rate, ϵ, and enstrophy at a rate, η. Energy is removed at large scales by Ekman friction and at small scales by molecular dissipation.

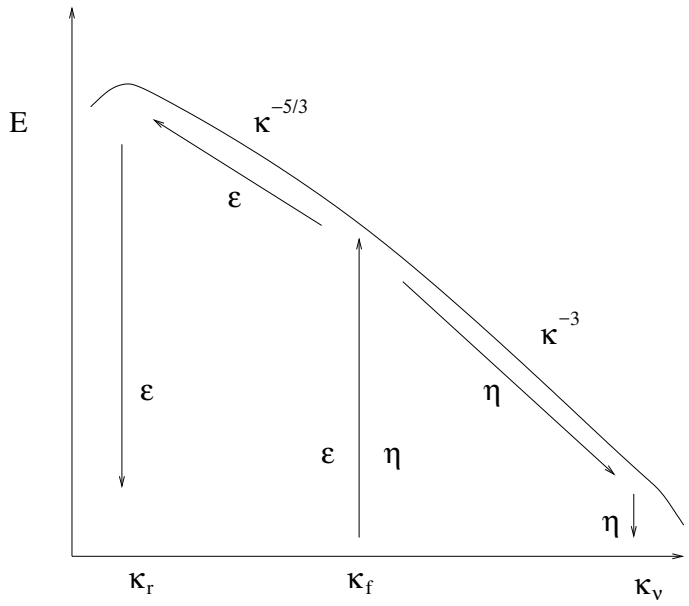

Figure 18: The energy spectrum for stationary 2-D turbulence, forced at wavenumber κ_f.

Exercise: *Energy dissipation rate*

Show that the energy lost to Ekman damping at the upper limit of the energy range is also equal to ϵ.

7.5 Physical interpretations

But what is enstrophy? How do we visualize these different cascades?

To see, it helps to understand the difference between the streamfunction and vorticity, and between energy and enstrophy. The vorticity is:

$$\zeta = \nabla^2 \psi$$

In terms of Fourier-transformed variables, we have:

$$\hat{\zeta} = -\kappa^2 \hat{\psi}$$

So the vorticity is multiplied by the wavenumber squared. As such, vorticity is like a *high-pass filtered* version of the streamfunction. We "see" the

smaller scales better with vorticity than with the streamfunction.

Shown in Fig. (19) is the streamfunction obtained from a 2-D turbulence simulation (run without forcing, from random initial conditions). The field is fairly smooth, with high and low pressure regions side by side. Shown in the right panel is the vorticity at the same time. This has much more small scale structure. There are vortices, but also many small filaments between the vortices. We could hardly have guessed these structures existed, looking at the streamfunction.

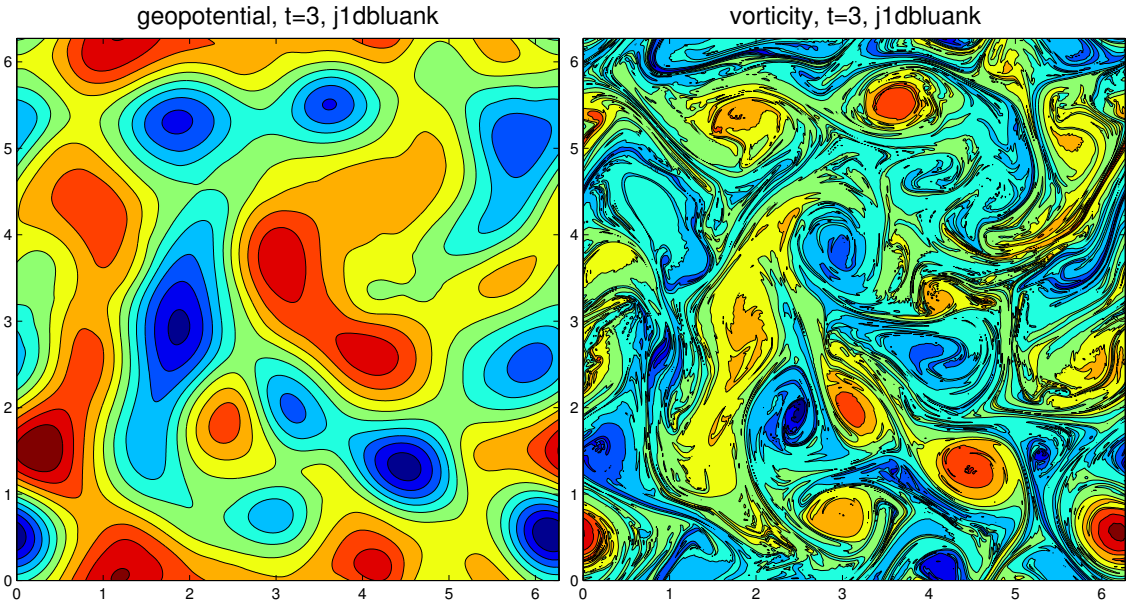

Figure 19: A snapshot of the streamfunction (left) and vorticity (right) from a 2-D turbulence simulation. Note the vorticity has much more small scale structure.

Another important difference between the streamfunction and the vorticity is that only the latter is conserved in the absence of forcing and dissipation; the streamfunction can change regardless. Watching an animation of the streamfunction, you see high and low pressure regions appear and disappear. But watching the vorticity, you can track single vortices; these only disappear when they collide with other vortices.

The energy essentially reflects the streamfunction, while the enstrophy reflects the vorticity. From before, we showed that:

$$Z(\kappa) = \kappa^2 E \tag{126}$$

So the enstrophy is like a high-pass version of the energy. While the energy gauges the large scale structures, the high and low pressures in Fig. (19), the enstrophy is more affected by the small scale filaments being strained out *between* the pressure systems. It is these filaments which are being dissipated by the small scale damping.

Another question is what is the difference between a local spectrum and a non-local one? The energy range is local, having a slope of $\kappa^{-5/3}$ and the enstrophy range with a slope of κ^{-3} is non-local. In fact, κ^{-3} is the shallowest non-local spectrum—anything steeper is non-local.

In a local spectrum, there is more energy at the smaller scales relative to the larger scales. Because the spectrum falls off faster in the non-local case, the smaller scales are much less energetic, and this has consequences for mixing. In the local regime, the eddies which are most important for structures of size L have the same size. This produces a "chunky" look, for example to smoke blowing away from a chimney. But in the non-local case, the most important eddies are at the top of the spectral range. In the ocean, this might be the deformation scale. Thus structures below that scale get strained out into filaments, much like the vorticity in between the vortex structures in Fig. (19). We'll see more examples of the differences hereafter.

7.6 The vortex view

The tradition view of 2-D turbulence, following Kraichnan [19], is in terms of the Fourier components. Like Kolmogorov [17], we have assumed the turbulence is homogeneous and isotropic. But as with the velocity gradients in 3-D turbulence, 2-D turbulence exhibits intermittency. And this intermittency is hard to miss— if one looks at the vorticity field.

Beginning in the 1980s, the computer power was sufficient to simulate 2-D turbulence at reasonably large Reynolds numbers. What researchers began to see was that the vorticity is dominated by long lived or "coherent" vortices. These are essentially the cyclones (and anticyclones) which are familiar in the weather. Atmospheric vortices also persist for long periods of time—it is possible to track storms from their origin in the western Atlantic to their demise in the Nordic Seas.

Vortices also account for *extreme* velocities. An observer at a fixed location will notice the velocities rise and fall, then a vortex will strike and the velocities will be very large, as with a hurricane. Having vortices also mean the flow is no longer homogeneous—the vortex parts of the flow are distinct from other locations.

In numerical simulations, freely-evolving (unforced) turbulence quickly evolves to a state where the vortices dominate the flow, as the vorticity between vortices is strained out and dissipated [31, 32]. Thereafter, the evolution is primarily a process of *mergers* between vortices. Positive vortices (cyclones) merge with other cyclones and negative vortices (anticyclones) merge with other anticyclones. The merged vortices are larger than the vortices which joined to make them. In this way, energy is shifted toward larger scales—the flow is dominated by fewer, larger vortices.

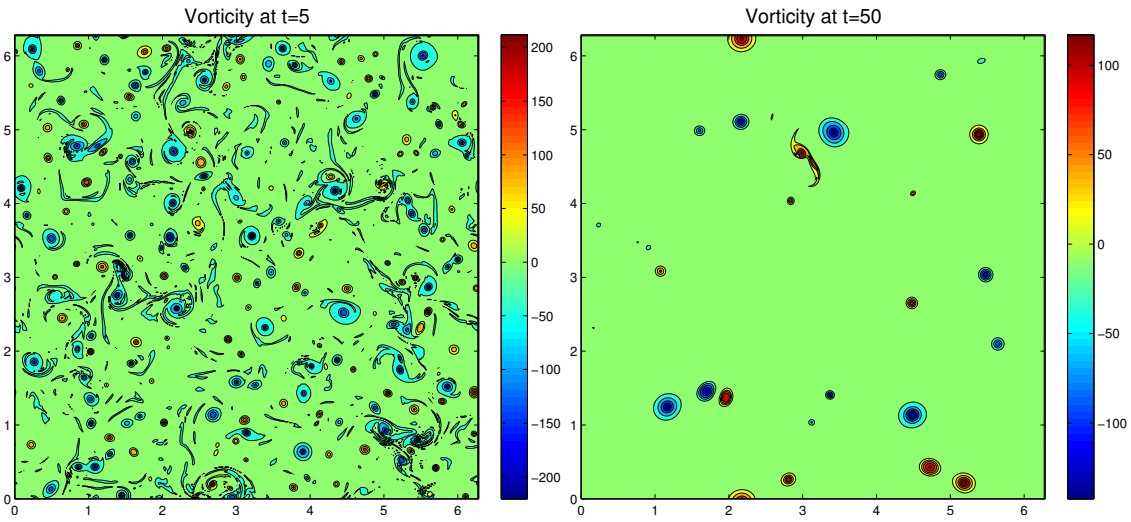

Figure 20: Snapshots of the vorticity from a 2-D turbulence simulation. The panel at left is at an earlier time, and the one at right at a later time.

This is illustrated in Figs. (20). The left panel shows the vorticity from a simulation begun with random initial conditions. After a short period, vortices emerge, with both signs (cyclones and anticyclones). As time goes by, the vortices merge, so there are fewer at later times (right panel). Left to itself, the system would eventually evolve to a dipole—one cyclone and one anticyclone.

McWilliams [32] studied the statistics of the vortices. He found that the number of vortices decays as a *power law* (Fig. 21), i.e.:

$$N_v \propto t^{-\alpha} \tag{127}$$

where $\alpha \approx 0.7$. The finding was supported in a subsequent calculations using "point vortices" (right panel of Fig. 21).

The vortices are important for the flow. Carnevale et al. [7] showed that all the important measures in these simulations could be explained in terms of the vortex statistics. Theirs is a "mean field theory", and it goes as follows. Assume that the vortices are *patches* of uniform vorticity, positive

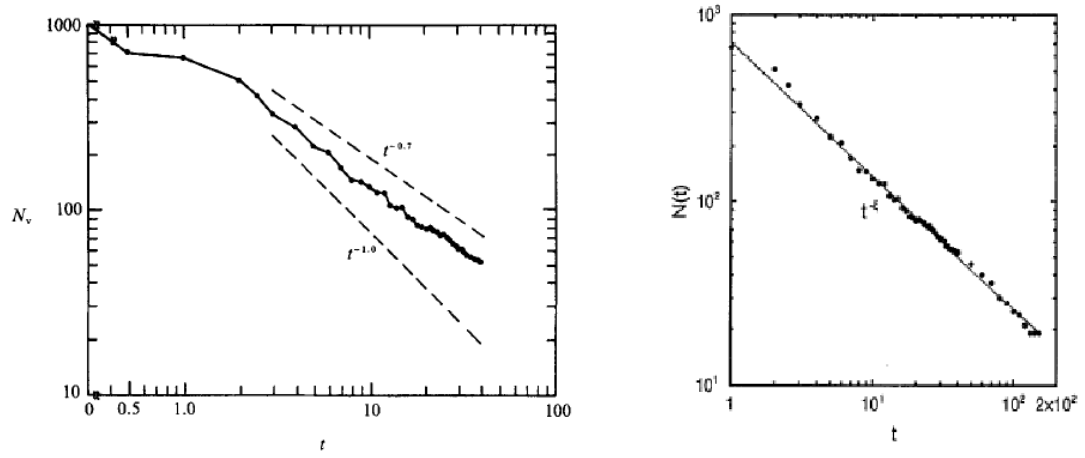

Figure 21: The number of vortices as a function of time for a freely-evolving turbulence simulation (left panel); from McWilliams [32]. The number of vortices in a "point vortex" simulation (right panel); from Weiss and McWilliams [49].

or negative. Thus the vorticity of a vortex can be written:

$$\zeta = \begin{cases} \zeta_c & \text{if } r \leq b \\ 0 & \text{if } r > b \end{cases}$$

Here b is the radius of the vortex patch.

The patch also has a velocity field. Using cylindrical coordinates and assuming no radial flow, we have:

$$\zeta = \frac{1}{r}\frac{\partial}{\partial r}(rv) \tag{128}$$

So:

$$v = \frac{1}{r}\int_0^r \zeta r \, dr \tag{129}$$

Thus for the patch:

$$v = \begin{cases} \zeta_c r/2 & \text{if } r \leq b \\ \zeta_c b^2/(2r) & \text{if } r > b \end{cases}$$

Using this, we can calculate the energy of the vortex. Integrating over the domain (which we assume is larger than the vortex radius, b), we get:

$$E = \frac{1}{L^2}\int_0^L \frac{v^2}{2} r \, dr = C\zeta_c^2 b^4 \tag{130}$$

where C is a constant which depends on the domain scale, L (we've assumed a square domain here, for simplicity).

If there is more than one vortex, the total energy is the sum of the contributions from all the vortex patches:

$$E = \sum_i E_i \tag{131}$$

We will neglect the energy associated with the integrations between the vortices. To write this sum, we make a mean field approximation; we have replace the sum above with N times the average vortex quantities, if N is the total number of vortices. Thus we have:

$$E \propto \frac{1}{L^2} NC\, \zeta_c^2\, b^4 \propto \rho\, \zeta_c^2\, b^4 \tag{132}$$

where ρ is the vortex density in the domain, N/L^2.

Now, we demand that energy be conserved in this system—so E =const. Thus:

$$\rho\, \zeta_c^2\, b^4 = const. \tag{133}$$

We know that:

$$\rho \propto t^{-\alpha} \tag{134}$$

with $\alpha \approx 0.7$. Thus the product of $\zeta_c^2\, b^4$ must *increase* at the same rate.

Carnevale et al. [7] make one further assumption—that the vortex amplitude is also conserved in mergers. If we take two patches and combine them, the amplitude won't change. That implies that the mean amplitude is also constant. So:

$$b \propto t^{\alpha/4} \tag{135}$$

The mean vortex radius is growing in time. Likewise, the mean area is also growing:

$$A = \pi b^2 \propto t^{\alpha/2} \tag{136}$$

This is the inverse cascade in the model—mergers are producing larger and larger vortices.

Interestingly, the vortex mergers do *not* conserve enstrophy. The enstrophy for a single vortex is:

$$Z = \frac{1}{L^2} \iint \zeta^2 \, dA = \frac{1}{L^2} \zeta_c^2 \pi b^2 \tag{137}$$

because the vorticity is constant inside and zero outside the patch. Again the total enstrophy is the sum over all the patches:

$$Z = \sum_i Z_i = \frac{1}{L^2} N \; \zeta_c^2 \, \pi \, b^2 \propto \rho \, \zeta_c^2 \, b^2 \tag{138}$$

Thus we have that:

$$Z \propto t^{-\alpha} \, t^0 \, t^{\alpha/2} = t^{-\alpha/2} \tag{139}$$

Given McWilliams' value for $\alpha = 0.7$, this implies the enstrophy decays as $t^{-0.35}$. This is remarkable, because except for the mergers, this vortex patch system has *no dissipation* at all. The prediction was supported by numerical simulations (Fig. 22).

Why does enstrophy decrease? During mergers, small *filaments* are cast off. These are then assumed to be dissipated by small scale damping. The mergers thus conserve energy, but they don't conserve vorticity.

The vortex view of 2-D turbulence is that the dynamics are determined by the vortices. Vortex mergers conserve energy, but enstrophy decreases in time, as filaments are cast off. This is basically the same conclusion that we reached in discussing the inertial ranges. But the vortex view is an appealing physical description which is easy to grasp. We'll return to the mean vortex model later on.

Exercise: *Enstrophy conservation*

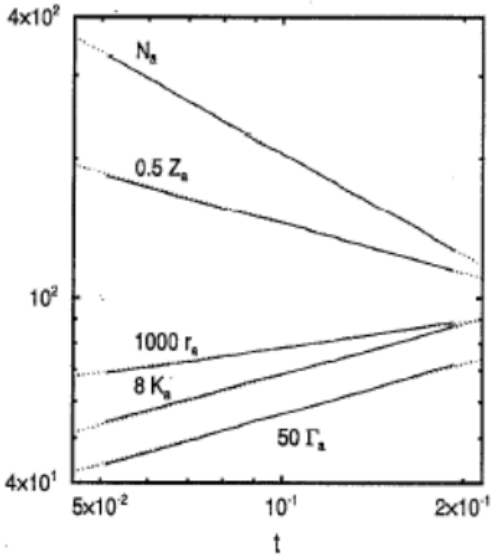

FIG. 10. A comparison of average vortex number $N_a(t)$, vortex radius $r_a(t)$, vortex circulation magnitude $\Gamma_a(t)$, enstrophy $Z_a(t)$, and kurtosis $K_a(t)$ from the modified point-vortex model (solid lines) and scaling theory (dotted lines). In the model, $t_0 \leq t \leq t_0 + t'_{end}$, where $t_0 = 0.050$ and $t'_{end} \approx 0.14$ is the earliest time for one of the 30 cycles to reach $N = 100$.

Figure 22: Vortex statistics from the simulations of from Weiss and McWilliams [49]. Here N, r and Γ are the vortex number and their mean radius and circulation. Z is the enstrophy and K is the vorticity kurtosis. The predictions from the mean vortex theory are indicated by lines.

What if vortex mergers conserved enstrophy instead of energy? Show that in this case, the total energy would *grow* in time. Thus the two quantities cannot be simultaneously conserved in this model.

7.7 Passive tracer spectra

Thus far, we have focused on vorticity, which is an *active* tracer. Advection of an active tracer changes the flow. Thus momentum, density and vorticity are active tracers. But we can also ask what happens to a *passive* tracer, which has no affect on the flow. Examples are smoke, ash from volcanic

plumes and spilled oil. Temperature is often considered to be a passive tracer, but since it affects the density, it is actually an active one.

The equation for a passive tracer can be written thus:

$$\frac{\partial}{\partial t}C + \vec{u} \cdot \nabla C = \kappa \nabla^2 C \tag{140}$$

where C is the tracer concentration. Changes in tracer concentration occur because of advection or by diffusion. The coefficient, κ, is the *diffusivity*. This is usually different from the viscosity, which dictates how molecular mixing affects the velocity. The tracer equation is very similar to the vorticity equation; the main difference is that the concentration is passive while the vorticity is active. An important consequence is that the advection term in the tracer equation is *linear*—u doesn't depend on C.

As with energy and vorticity, we can consider the spectrum of the tracer, or rather the tracer variance— the variation about the mean. If we Fourier transform C, we can determine the tracer fluctuations as a function of scale—exactly as we do with enstrophy (the vorticity variance) or energy (the velocity variance).

What would such a spectrum look like? Following our previous arguments, we might expect that in a turbulent inertial range, the flux of tracer variance across scales will be constant. Otherwise the tracer variance would pile up at a certain scale (e.g. we'd see filaments of a certain width emerging in the flow). The tracer flux has units of concentration squared per second. Let's call this χ.

Now the spectrum of tracer, $P(\kappa)$ will have units of tracer squared times length (so that the integral over all wavenumbers will yield tracer squared). So, on dimensional grounds, we expect:

$$P = \frac{\chi \tau}{\kappa} \tag{141}$$

where τ is the turbulent time scale.

Here is where the passive element comes in. The tracer doesn't affect the time scale, τ; that only depends on the active portion of the flow, the vorticity. So for τ, we use the time scales inferred for the turbulent ranges.

For the energy range, $\tau = \epsilon^{-1/3}\kappa^{-2/3}$. Substituting in, we get:

$$P(\kappa) = \chi\epsilon^{-1/3}\kappa^{-5/3} \tag{142}$$

So in the energy range, the tracer spectrum has the same slope as the energy spectrum.

For the enstrophy range, we have $\tau = \eta^{-1/3}$. As noted, the enstrophy range is "non-local" because the time scale is independent of scale and set by the largest eddies in the range. Substituting in, we get:

$$P(\kappa) = \chi\eta^{-1/3}\kappa^{-1} \tag{143}$$

So the spectra is shallower than the energy spectrum.

Interestingly though, the tracer spectrum is the *same* as the enstrophy spectrum (see the exercise below). This suggests that vorticity in the enstrophy range behaves like a passive tracer, even though it is an active one. The reason is that the enstrophy range is non-local; all fields are advected passively by the largest eddies in the range.

The spectra are summarized in Fig. (23). We assume that tracer is injected at the largest scales. Tracer variance then cascades *downscale*, through the energy and enstrophy ranges. The spectral slopes are $\kappa^{-5/3}$ and κ^{-1}.

Exercise: *Enstrophy spectrum*

Derive the enstrophy spectrum in the two inertial ranges for 2-D turbulence. Show then that the slope in the enstrophy range is the same as for a

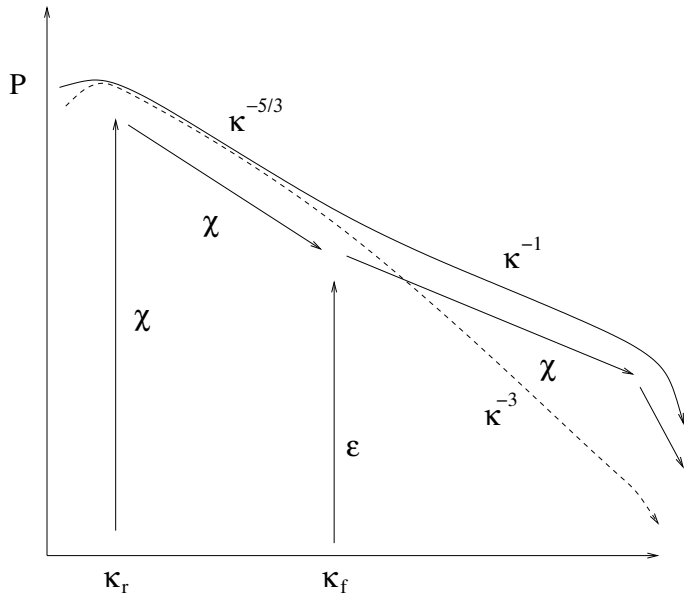

Figure 23: The passive energy spectrum in forced 2-D turbulence. The forcing is applied at κ_f, and the tracer is introduced at large scales, at κ_χ. Note the tracer variance cascades downscale at all scales.

passive tracer.

7.8 Predictability

Another interesting application of turbulence phenomenology is to predictability. Imagine the atmosphere was really just a 2-D turbulent fluid. Now consider that there was an error in the initial conditions at some small scale. We know the winds at large scales, from measurements, but we can't know them precisely at, say, the 1 m scale. Because the atmosphere is chaotic, slight differences between the modeled initial state and the actual state will grow, eventually disturbing the forecasts at large scales. But how quickly will this happen?

7.8.1 Lorenz Model

The usual point of reference for atmospheric predictability is Lorenz's (1963) [29] model. This model is essentially a *three mode truncation* of the equations describing a convective fluid system, under the influence of heating of the lower boundary. In other words, we Fourier transform the variables and retain only three terms. His equations can be written:

$$\begin{aligned} \frac{dx}{dt} &= \sigma(y - x) \\ \frac{dy}{dt} &= rx - y - xz \\ \frac{dz}{dt} &= xy - bz \end{aligned} \tag{144}$$

Here x, y, z are "state variables", representing temperature and velocity in the convective system, and where σ, r, b are various parameters (representing the aspect ratio, the Rayleigh number and the Prandtl number, three values which are important for buoyancy-driven convection). The equations are nonlinear, due to the xz and xy terms in the second and third equations. As with the logistic map (sec. 4), these terms are the source of the system's unpredictability.

The equations have three fixed points, found by setting the time derivatives in the equations above to zero:

$$(x, y, z) = (0, 0, 0), \quad (a, a, r - 1), \quad (-a, -a, r - 1) \tag{145}$$

Here

$$a = \sqrt{b(r - 1)}$$

The first solution is trivial, with no motion. The other two have convection, with opposing circulation.

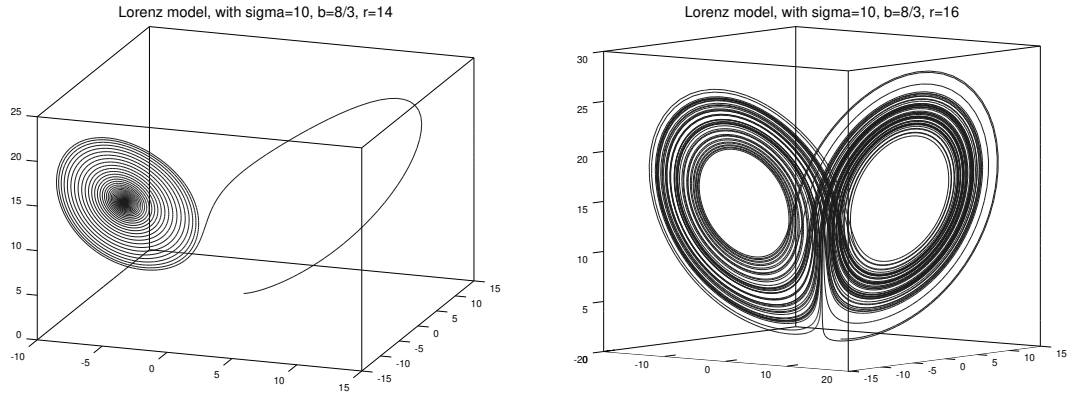

Figure 24: A phase space (x, y, z) portrait of the Lorenz model. The parameters are $\sigma = 10$, $b = 8/3$ and $r = 14$ (left) and $r = 16$ (right).

As with the logistic map in sec. (4), the system exhibits different behavior, dependent on the choice of parameters. We show two examples in Fig. (24). The parameters $\sigma = 10$ and $b = 8/3$ have been set to the same values used by Lorenz; this is equivalent to setting the aspect ratio (the ratio of the vertical to the horizontal length scales) and the ratio of the diffusivity and the viscosity. We will vary r, the Rayleigh number, which determines the type of convective behavior (laminar vs. turbulent). With $r = 14$, there are two non-trivial fixed points, at $(x, y, z) = (5.89, 5.89, 1.67)$ and at $(-5.89, -5.89, 1.67)$. We see that the system spirals in towards the latter fixed points, signalling a stable final state.

With $r = 16$ however, the system never settles into a steady state. Instead it orbits around the two non-trivial fixed points, at $(x, y, z) = (\pm 6.32, \pm 6.32, 1.67)$. It appears to approach one or the other, than abruptly jumps over to the other one. These transitions occur at random times.

The system in the latter case is chaotic and as such it exhibits a sensitive dependence on the initial condition. This is shown in Fig. (25), of the squared difference between two runs, one beginning at $(x, y, z) = (1, 2, 1)$

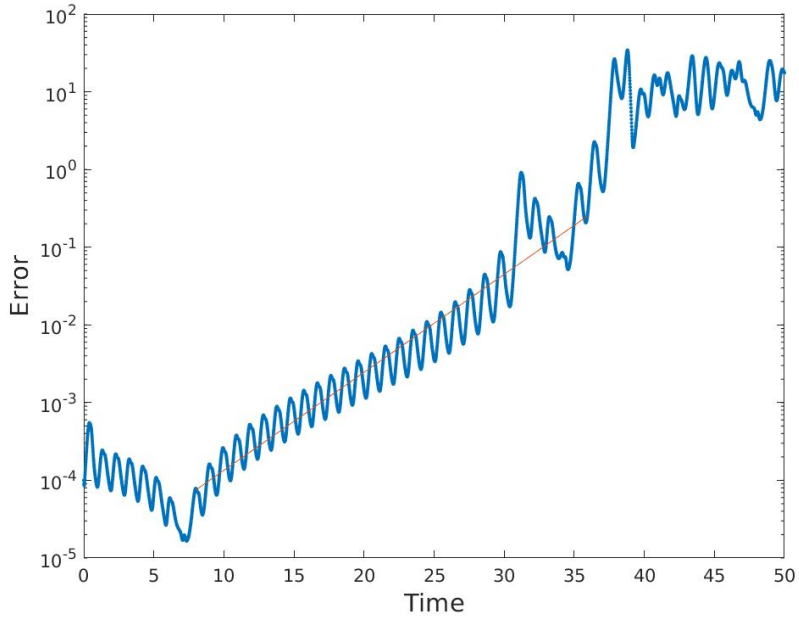

Figure 25: The absolute difference between two solutions to the Lorenz model, with parameters are $\sigma = 10$, $b = 8/3$ and $r = 16$. The log of the error is plotted as a function of time. Also shown is a exponential curve, with a growth rate of 0.3. This appears as a straight line on the semi-log plot.

and a second at $(x, y, z) = (1.0001, 2, 1)$. The plot shows that the difference is initially small, but then grows rapidly after roughly $t = 5$. Note that this is a semilogarithmic plot, so the difference is increasing by orders of magnitude. Also shown is a straight line, which indicates an *exponential* growth. The difference tracks this fairly well, until it saturates soon before $t = 20$.

Predictability is a measure of how quickly the system diverges under a change in the initial condition. In the Lorenz model, the error growth is exponential, as shown here. The magnitude of the error depends on the initial condition. The smaller the initial error, the longer it takes for the error to grow.

However, the Lorenz model isn't very realistic. Think if we truncated

a turbulence model with only three wavelengths. Energy could pass from to the other (assuming they made a triad), but it couldn't go any further. Energy would have to recycle between the three wavenumbers.

7.8.2 Predictability in 2-D turbulence

So how do errors propagate through in a fully turbulent system?[7] If the cascade is *local*, an error at one scale will affect the next largest scale. Then that scale affects the next scale, and so on up to the largest scales. The total time to reach the largest scale would then be an integral over all wavenumbers.

We can think of a "spectrum" of interaction times:

$$P = \frac{\tau(\kappa)}{\kappa} \tag{146}$$

Again we divide by κ so that the integral over all wavelengths will produce a quantity with units of time, i.e.:

$$T = \int_{\kappa 0}^{\kappa 1} \frac{\tau}{\kappa}\, d\kappa \tag{147}$$

Here κ_1 is the scale where the error is introduced, and κ_0 is our "weather scale", the large scale we're focused on.

Consider the enstrophy cascade first. Here $\tau = \eta^{-1/3}$, so:

$$T = \int_{\kappa 0}^{\kappa 1} \frac{\eta^{-1/3}}{\kappa}\, d\kappa = \eta^{-1/3}\, ln(\frac{\kappa_1}{\kappa_0}) \tag{148}$$

The predictability time depends on the scale of the error, so we can increase the predictability time by reducing the scale of the error (increasing κ_1). Rewriting the equation in terms of scales, $L \propto \kappa^{-1}$, we get:

$$L_0 = L_1\, e^{\eta^{1/3} T} \tag{149}$$

[7]The researcher C. Leith from the National Center for Atmospheric Research (NCAR) was an early proponent of using turbulence models to understand predictability. The following section is based on that of Vallis [46].

So errors grow exponentially in time, at a rate proportional to $\eta^{1/3}$. Thus the enstrophy range is in line with our expectations from the Lorenz model.

Now consider the energy inertial range. Then $\tau = \epsilon^{-1/3}\kappa^{-2/3}$. Substituting in, we get:

$$T = \int_{\kappa 0}^{\kappa 1} \epsilon^{-1/3}\kappa^{-5/3}\, d\kappa \propto \epsilon^{-1/3}\kappa^{-2/3}|_{\kappa 0}^{\kappa 1} \tag{150}$$

Now if the scale of the error is much smaller than the largest eddies, we have:

$$T \approx \epsilon^{-1/3}\kappa_0^{-2/3} \tag{151}$$

In an energy cascade, the predictability time is *independent* of the scale of the error! This is quite different from the Lorenz model. The reason is that in the energy cascade the interaction time decreases with increasing wavenumber. So error propagation depends on the largest scales, where the error transfer is the slowest.

7.8.3 Predictability in the atmosphere

Given these ideas, what would we infer about the atmosphere? To find out, we need to know what the energy spectra looks like. Nastrom and Gage [36] used velocity data collected from over 6000 commercial aircraft to calculate wavenumber spectra. The result is shown in Figure (26). This indicates a κ^{-3} range from 100-2000 km and a $\kappa^{-5/3}$ range at smaller scales.

The κ^{-3} range is thought to be en enstrophy cascade [28]. The dynamical basis of the $\kappa^{-5/3}$ range is still debated. If it is a 2-D energy cascade, it implies a source of energy at small scales, as the scales are too large to be a 3-D energy range. More recently, Buhler et al. (2016) have suggested the source is inertial gravity waves. Whatever the case, the small scale range, if turbulent, is *local*.

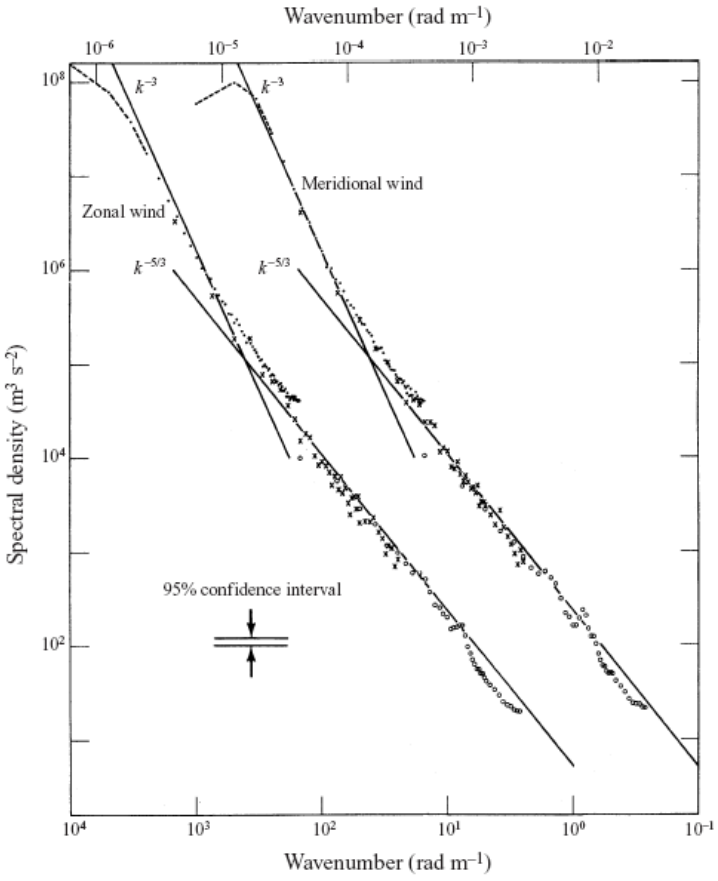

Figure 26: Kinetic energy spectra from data collected on commercial airplanes over the U.S. The zonal and meridional components are shown, with the latter shifted one decade to the right. Note the lower x-axis is mislabeled— it should say "wavelength". From [36].

Given what we now know about 2-D turbulence, we infer that predictability is limited by the local range at small scales, and by the transition scale, 100 km, which would determine κ_0 in the previous discussion. So regardless of how good our observations are, we could not improve the predictability time. Using approximate values for the dissipation rate, we obtain a value of T on the order of a week. We caution though that the dissipation rate is not well-known; indeed, even its *sign* is debated in the smaller scale range.

8 Geostrophic turbulence

Two-dimensional turbulence was first studied as an analogue to three-dimensional turbulence; two dimensions is less computationally intensive than three. But are the dynamics of two-dimensional flow actually relevant for the ocean and atmosphere?

In fact they are. At synoptic scales (the scale of weather systems in the atmosphere and of oceanic eddies), horizontal velocities greatly exceed the vertical ones. Consider the scaled incompressibility condition:

$$\begin{gathered}\frac{\partial}{\partial x}u + \frac{\partial}{\partial y}v + \frac{\partial}{\partial z}w = 0 \\ \frac{U}{L} \quad \frac{U}{L} \quad \frac{W}{H}\end{gathered} \tag{152}$$

If all three terms are of equal importance, the vertical velocity must scale as:

$$W \propto U\frac{H}{L} \equiv \delta U \tag{153}$$

where $\delta = H/L$ is the *aspect ratio of the flow*. This is typically of order 1/1000 at synoptic scales, so the vertical velocity is 1000 times smaller than the horizontal ones.

Second, when the Rossby number is small (sec. 1.2), the velocities are approximately geostrophic:

$$\begin{aligned} v \approx v_g &= \frac{1}{\rho_0 f}\frac{\partial}{\partial x}p \\ u \approx u_g &= -\frac{1}{\rho_0 f}\frac{\partial}{\partial y}p \end{aligned} \tag{154}$$

These are very reminiscent of 2D velocities, which can be expressed in terms of a streamfunction:

$$v = \frac{\partial}{\partial x}\psi, \qquad u = -\frac{\partial}{\partial y}\psi$$

However, the Coriolis parameter, f, in the denominator in (154) varies in the y-direction, so the relations are not quite equivalent.

But we can make them so if we make one additional approximation, the *β-plane approximation*. This involves a Taylor-expansion of the Coriolis parameter about a central latitude, θ_0:

$$f(\theta) = f(\theta_0) + \frac{df}{d\theta}(\theta_0)\ (\theta - \theta_0) + \frac{1}{2}\frac{d^2 f}{d\theta^2}(\theta_0)\ (\theta - \theta_0)^2 + ... \qquad (155)$$

We neglect the higher order terms, so that:

$$f \approx f(\theta_0) + \frac{df}{d\theta}(\theta_0)\ (\theta - \theta_0) \equiv f_0 + \beta y \qquad (156)$$

where

$$f_0 = 2\Omega sin(\theta_0)$$

$$\beta = \frac{1}{a}\frac{df}{d\theta}(\theta_0) = \frac{2\Omega}{a} cos(\theta_0)$$

and

$$y = R_e(\theta - \theta_0)$$

Here R_e is the radius of the earth.

The β-plane approximation is valid when the second term in the expansion, βy, is much less than the first, f_0. Scaling the two, we require:

$$\frac{\beta L}{f_0} \ll 1 \quad \rightarrow \quad L \ll \frac{f_0}{\beta} = R_e tan(\theta_0) \approx R_e$$

So the latitudinal extent of the doman, L, must be much less than the Earth's radius.

Under the β-plane approximation, we can replace f by f_0 in the geostrophic relations in (157):

$$v \approx v_g = \frac{1}{\rho_0 f_0}\frac{\partial}{\partial x} p = \frac{\partial}{\partial x}\psi$$

$$u \approx u_g = -\frac{1}{\rho_0 f_0}\frac{\partial}{\partial y}p = -\frac{\partial}{\partial y}\psi \tag{157}$$

where ψ is the "geostrophic streamfunction":

$$\psi \equiv \frac{p}{\rho_0 f_0} \tag{158}$$

Then the horizontal velocities are approximately non-divergent because:

$$\frac{\partial}{\partial x}u + \frac{\partial}{\partial y}v \approx \frac{\partial}{\partial x}u_g + \frac{\partial}{\partial y}v_g = 0$$

This implies that the concepts of 2-D turbulence should apply, as long as the flow is nearly geostrophic.

Figure (26) raises some interesting questions though. The 2D system we considered before is very idealized. Atmospheric and oceanic flows are affected by changes in planetary rotation, stratification and bottom topography, to name only a few complicating factors. Yet we see energy spectra which resemble those in pure 2-D turbulence. How can this be?

Geostrophic turbulence is what happens when we add geophysically relevant factors to 2D turbulence. The name orginates from an article where 2D turbulence was considered in a rotating fluid with continuous stratification [9]. But we also use the term to encompass variations in f and in topography. We'll consider these in turn. We begin with f.

8.1 The Beta-effect

What effect does rotation have on the flow? The vorticity equation (63) in two dimensions is given in (87):

$$\frac{\partial}{\partial t}\zeta + \vec{u}\cdot\nabla(\zeta + f) = 0 \tag{159}$$

We neglect forcing and dissipation for the moment. Thus if f is constant, it drops out of the vorticity equation completely. So a constant Coriolis parameter has *no effect* on 2D turbulence.

However, if f is variable f, the flow is affected. To see this, let's substitute $f_0 + \beta y$ for f in the equation:

$$\frac{\partial}{\partial t}\zeta + \vec{u} \cdot \nabla\zeta + \beta v = 0 \tag{160}$$

With β we pick up an additional term. Because of this, *meridional motion induces changes in the relative vorticity*. This can also be seen if we rewrite the equation in Lagrangian form:

$$\frac{d}{dt}\zeta + \beta\frac{d}{dt}y = \frac{d}{dt}(\zeta + \beta y) = 0 \tag{161}$$

So:

$$\zeta + \beta y = const. \tag{162}$$

If a fluid parcel moves north, to greater y, its vorticity must decrease.

The linear version of the vorticity equation is just:

$$\frac{\partial}{\partial t}\zeta + \beta v = 0 \tag{163}$$

Written in terms of the streamfunction, this is:

$$\frac{\partial}{\partial t}\nabla^2\psi + \beta\frac{\partial}{\partial x}\psi = 0 \tag{164}$$

We can solve this if we use a planar wave solution:

$$\psi = Re\{\hat{\psi}\, e^{ikx+ily-i\omega t}\} \tag{165}$$

where $Re\{\}$ signifies the real part. Then we obtain:

$$\omega = -\frac{\beta k}{k^2 + l^2} \tag{166}$$

This is the dispersion relation for *Rossby waves*. Rossby waves, discovered by C. G. Rossby [41] are fundamental to our understanding of large scale

variability in the atmosphere and ocean. Rossby waves have a zonal phase speed of:

$$c_x = \frac{\omega}{k} = -\frac{\beta}{k^2 + l^2} \tag{167}$$

So Rossby waves always propagate toward the west (in the absence of a mean flow), and larger waves move faster than smaller waves.

Now let's put advection back into the problem. Some scales will be turbulent and others will be wave-like. But which ones? We can get a rough idea by scaling the vorticity equation:

$$\frac{\partial}{\partial t}\zeta + \vec{u} \cdot \nabla\zeta + \beta v = 0$$

$$\frac{U}{LT} \qquad \frac{U^2}{L^2} \qquad \beta U$$

$$\frac{1}{\beta LT} \qquad \frac{U}{\beta L^2} \qquad 1 \tag{168}$$

In the last line, we've divided through by βU. Thus the advective term scales as $U(\beta L^2)^{-1}$.

This is like the Rossby number, except that f has been replaced by βL (which measures how much f changes over the length scale, L). If this parameter is small, the vorticity equation is approximately linear and the flow is dominated by Rossby waves. If large, the β term is unimportant and the dynamics are turbulent. We then anticipate a "boundary" between wave and turbulent dynamics. This is called the "Rhines scale" [39]:

$$L_\beta = \sqrt{\frac{U}{\beta}} \tag{169}$$

At L_β, all three terms in the vorticity equation are of equal importance.

Notice we haven't specified a time scale in the vorticity equation. This is because we assume the time scale adjusts to the dynamics. With Rossby

waves, the first term should balance the third, so that $T = (\beta L)^{-1}$. If turbulence, we would expect the advective time scale, $T = L/U$.

The above arguments apply to spin-down experiments, where energy is conserved. Then U and hence L_β are fixed over the experiment. But with forcing, the energy changes as the system spins up and the Rhines scale varies. How can we predict L_β in this case?

Assuming the turbulence reaches a steady state, we can think in terms of the energy dissipation rate, ϵ. Imagine turbulence forced at a small scale L_f (our "spoon", stirring the fluid). This generates a cascade to larger scales. At the largest scales, the dynamics are quasi-linear and turbulent transfers weak or non-existent. So the cascade should halt or *arrest* at the boundary between turbulence and waves.

We can deduce where the cascade stops by invoking time scales again. In the energy cascade range, the time scale is proportional to:

$$\tau \propto \epsilon^{-1/3} \kappa^{-2/3} \tag{170}$$

At the large scales, the relevant time is the Rossby wave period:

$$T \propto |\omega^{-1}| = \frac{k^2 + l^2}{\beta k} \tag{171}$$

If the flow is isotropic, then:

$$k = l \approx \kappa \tag{172}$$

So the wave time scale is just:

$$T \propto |\omega^{-1}| = \frac{\kappa}{\beta} \tag{173}$$

At the arrest scale, the two time scales are equal:

$$\epsilon^{-1/3} \kappa_\beta^{-2/3} = \frac{\kappa_\beta}{\beta} \tag{174}$$

or:

$$\kappa_\beta = \beta^{3/5}\epsilon^{-1/5} \tag{175}$$

This is the arrest wavenumber. We would expect the cascade to stop approximately here (assuming the dissipation is sufficiently strong to prevent the energy from building up here).

But an interesting thing happens when you try this numerically. An example is shown in Fig. (27), of numerical simulations with a barotropic[8] fluid on a sphere (which is periodic in the x direction). The simulations show the energy cascade does indeed arrest, but the arrest is *anisotropic*; the eddies are longer in the x direction than in y. The result is a banded structure, reminiscent of the Jovian atmosphere. So the arrest is not isotropic, and it's thus incorrect to assume that $k = l$ as we did above.

We can retain the anisotropy in the arrest wavenumber in the following way, following Vallis and Maltrud [47]. First we write:

$$k = \kappa cos(\theta), \quad l = \kappa sin(\theta) \tag{176}$$

where θ is the angle the wavenumber vector makes with the k-axis. Then the wave period is:

$$T \propto |\omega^{-1}| = \frac{\kappa^2}{\beta\kappa cos(\theta)} = \frac{\kappa}{\beta cos(\theta)} \tag{177}$$

Equating this to the turbulent time scale:

$$\epsilon^{-1/3}\kappa_\beta^{-2/3} = \frac{\kappa_\beta}{\beta cos(\theta)} \tag{178}$$

or:

$$\kappa_\beta = \beta^{3/5}\epsilon^{-1/5}cos^{3/5}(\theta) \tag{179}$$

[8] A barotropic flow has no vertical shear in the horizontal velocities, i.e. $\frac{\partial}{\partial z}u = \frac{\partial}{\partial z}v = 0$.

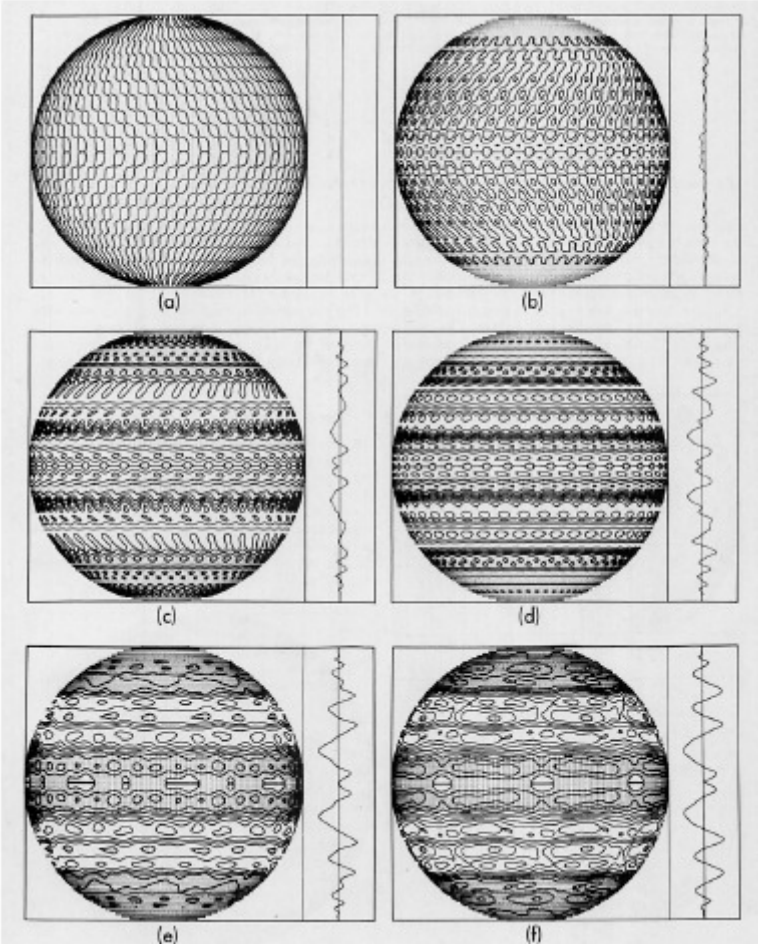

Figure 27: Numerical simulations of forced barotropic turbulence on a sphere. Note the formation of banded flow, superimposed over a field of eddies. The mean zonal velocities are indicated in the inserts. From [50].

This has two components:

$$(k_\beta, l_\beta) = [(\frac{\beta^3}{\epsilon})^{1/5} cos^{8/5}(\theta), (\frac{\beta^3}{\epsilon})^{1/5} cos^{3/5}(\theta) sin(\theta)] \tag{180}$$

The result is an arrest *boundary* in (k, l) space. The boundary is plotted in Fig. (28). It has two symmetric lobes. Outside the lobes, the wavenumbers transfer energy in triad interactions toward the lobes. Inside the lobes, the dynamics are essentially linear and the energy flux is weak.

Vallis and Maltrud tested this prediction numerically, in spin down ex-

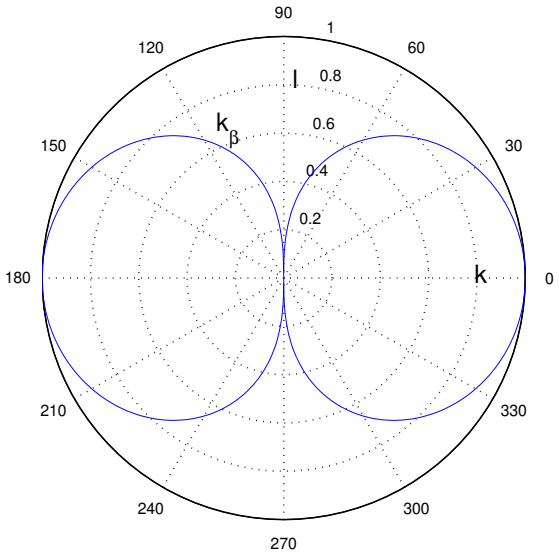

Figure 28: The boundary between turbulence and Rossby waves. For plotting, we assume $\beta^3/\epsilon = 1$.

periments from random initial conditions. The latter were isotropic and covered a specified band in wavenumber space (upper left panel of Fig. (29). The initial spectrum thus appears as a ring in (k, l) space. As time proceeds, energy shifts toward smaller wavenumbers, but it ceases at the lobe structures described above. Vallis and Maltrud called these "dumbbells".

The "dumbbell" shape explains the anisotropy observed in Fig. (27). Consider energy moving in along the axis where $l = 0$ (the x-axis in the figure). The energy cascade here would stop at $k = 1$. But energy moving along the y-axis, with $k = 0$, will proceed nearly to the center.

The reason for this is that if $k = 0$, the meridional velocity is zero and the β term drops out of the vorticity equation. So for zonal motion, it is as if the β effect were non-existent and the inverse cascade is not arrested by the waves.

So a forced cascade with β will produce structures with $k = 0$—zonal

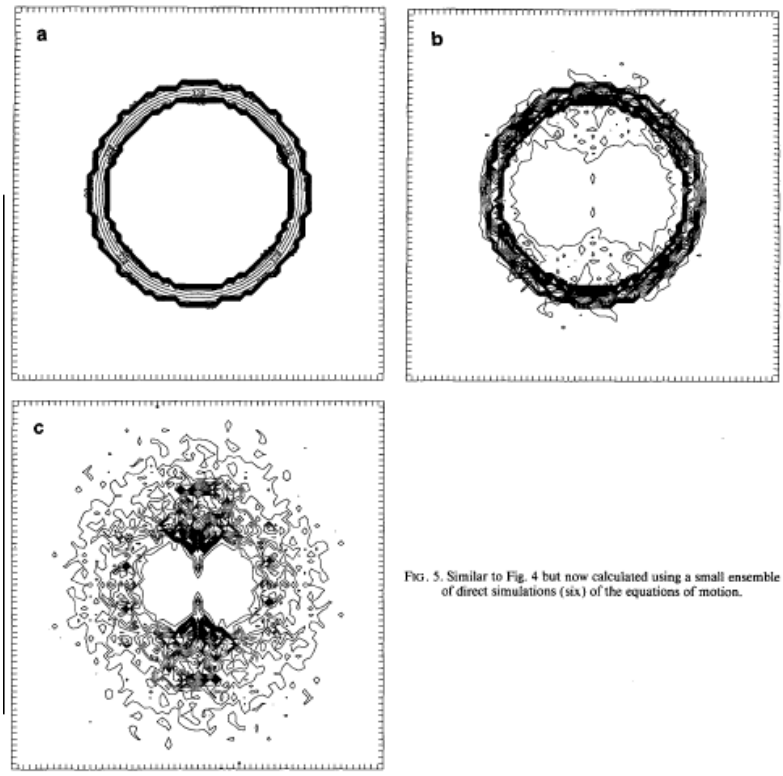

FIG. 5. Similar to Fig. 4 but now calculated using a small ensemble of direct simulations (six) of the equations of motion.

Figure 29: Spectra from a freely-evolving 2-D turbulence simulation, plotted in wavenumber space. From [47].

jets—as in Fig. (27). But there are also eddies superimposed on the bands; this is the turbulence at smaller scales. If you average the zonal velocities in time, you see that there are alternating eastward and westward flows associated with the bands. Those flows are in fact asymmetric; the eastward jets are sharper than the westward ones. This is a consequence of barotropic stability, which favors sharper eastward jets.[9]

Exercise: *Topographic arrest*

A bottom slope acts exactly like the β-effect in a barotropic fluid. The vorticity equation (see eq. 206 below) can be written:

[9] See [22].

$$\frac{\partial}{\partial t}\zeta + \vec{u} \cdot \nabla(\zeta + h) = 0 \tag{181}$$

where h is the topographic elevation. Say that $h = \alpha x$ (the bottom slopes up to the east). Find the dispersion relation for the waves (assume periodic boundary conditions in x and y). Now solve for the arrest wavenumber. Draw it in (k, l) space. What type of structures do you expect?

8.2 Beta turbulence in a closed basin

Zonal jets can exist in re-entrant domains, like the atmosphere. The Jet Stream is an example. But can zonal jets exist in the *ocean*, where there are lateral (continental) boundaries?

To see, we must consider Rossby waves in a closed basin. These have a slightly different structure and dispersion relation than the plane Rossby waves discussed above. The waves have a dual structure: a propagating wave superimposed upon a stationary "envelope". The latter ensures that there is no flow on the boundaries. For a rectangular basin, the streamfunction takes the form [38]:

$$\psi = Acos(kx - \omega t)sin(\frac{m\pi x}{L_x})sin(\frac{n\pi y}{L_y}) \tag{182}$$

Here L_x and L_y and the lengths of the domain in x and y. The two sine terms ensure that the streamfunction vanishes on the boundaries, and the wavelengths are quantized. This solution is referred to as a barotropic *basin mode*.

The dispersion relation for a basin mode is given by:

$$\omega = \omega_{mn} = -\frac{\beta}{2\pi(m^2/L_x^2 + n^2/L_y^2)^{1/2}} \tag{183}$$

This too is quantized, i.e. there are only discrete values of the frequency, corresponding to the discrete wavenumbers. The dispersion relation resembles the plane Rossby wave dispersion relation, except that there is no "k" in the numerator. This makes all the difference.

The basin mode period is proportional to the inverse of the frequency:

$$T \propto \frac{\kappa_{mn}}{\beta} \tag{184}$$

where $\kappa_{mn} = 2\pi(m^2/L_x^2 + n^2/L_y^2)^{1/2}$ is the (quantized) total wavenumber. Equating this to the turbulent time scale in the energy range:

$$\epsilon^{-1/3}\kappa_\beta^{-2/3} = \frac{\kappa_\beta}{\beta} \tag{185}$$

Assuming that the arrest wavenumber is also quantized. Then:

$$\kappa_\beta = \beta^{3/5}\epsilon^{-1/5} \tag{186}$$

[20]. So we obtain the *same arrest wavenumber that we did for the periodic domain when the flow was assumed isotropic*. Thus the wave-turbulence boundary in a basin is also isotropic. There is no reason to expect zonal jets.

Numerical simulations confirm this. Shown in Fig. (30) are the streamfunctions from two forced simulations, one in a periodic domain (left panel) and one with solid walls (right). The former shows zonally-elongated structures, spanning the domain. The closed basin simulation on the other hand has mostly isotropic eddies. The only place where the flow is zonally elongated is along the northern boundary (where in fact a stationary gyre develops [13]).

We quantify the arrest further, as follows. In the simulations shown, the damping was with Ekman friction, i.e. we have a linear damping term, $r\zeta$,

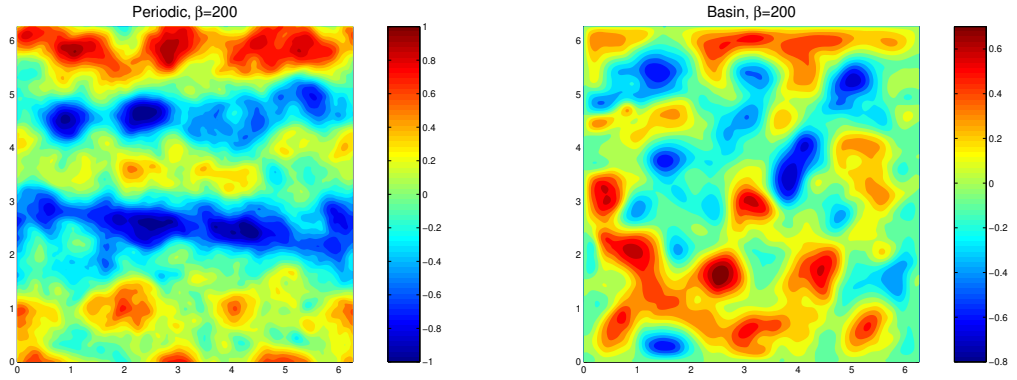

Figure 30: Streamfunctions from a forced 2-D turbulence simulations with periodic (left) and solid wall (right) boundary conditions.

in the vorticity equation. With this, the integrated energy equation (53) can be written:

$$\frac{d}{dt}E = \iint \vec{u} \cdot \vec{\mathcal{F}}\, dV - r \iint \vec{u} \cdot \vec{u}\, dV = \epsilon - 2rE \tag{187}$$

where E is the total kinetic energy. Notice that the forcing yields the energy flux, ϵ. When the flow obtains a statistically steady state, the change in energy on the LHS is approximately zero, leaving:

$$\epsilon = 2rE \tag{188}$$

Using this, we estimate the arrest scale as:

$$L_\beta \propto \kappa_\beta^{-1} = \beta^{-3/5}(2rE)^{1/5} \tag{189}$$

We compare this estimate to the simulations by calculating spatial correlations in the velocity field. In an eddy, the velocities are correlated (or anti-correlated) across the eddy. Outside the eddy, the velocities are uncorrelated with those in the eddy. So we can use velocity correlations to find the size of the eddies.

The correlations are plotted as ellipses in Fig. (31). The solid and dashed curves correspond to two different ways of calculating the correlation (either using parallel velocities along a line—the longitudinal velocities—or perpendicular velocities—the transverse velocities). Both yield the same result; the eddy scales are isotropic and are consistent with the length scale estimate in (189).

For comparison, the correlation ellipses from two simulations in a periodic domain are shown in Fig. (32). In this case, the longitudinal correlations (corresponding to the u velocities) are elongated in the x-direction, indicating coherent zonal flow. The transverse correlations on the other hand (corresponding to the v velocities in the x-direction) are more nearly isotropic. These reflect the small scale eddies superimposed on the zonal jets.

So the arrest in a rectangular basin is like that described by Rhines [39], but is isotropic. The isotropy stems from the fact that the wave time scale in a basin is also isotropic. So the boundaries prevent the formation of zonal jets.

However, this case is still quite unrealistic in terms of the ocean, as the bottom is entirely flat. The actual ocean of course has significant topography. We consider that next.

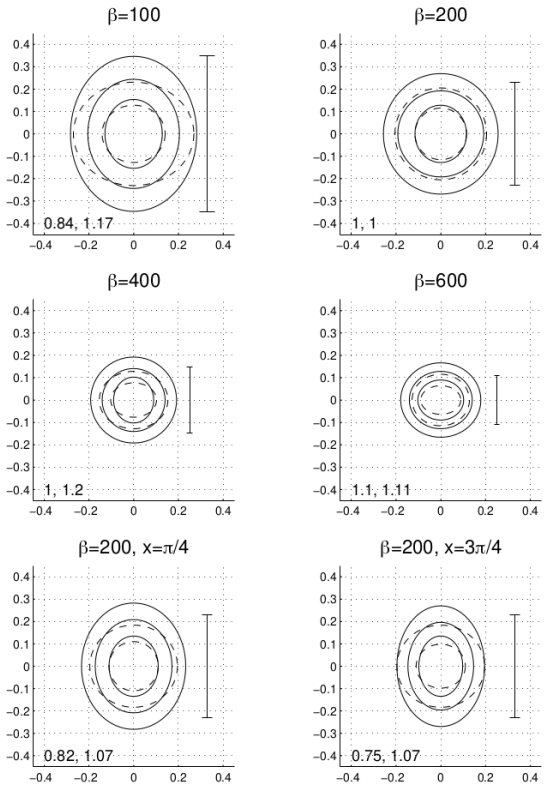

Figure 31: Velocity correlation ellipses from a series of experiments in a closed basin. The solid ellipses are from the longitudinal correlations (with values [0.8 0.6 0.4]); the dashed ellipses are transverse correlations (with values of [0.5 0]). The vertical lines indicate the arrest scale from (189). From [20].

8.3 Topography

As seen in the exercise in sec. (8.1), a bottom slope in a barotropic fluid acts like the β-effect. But instead of limiting N-S motion, topography inhibits motion *across the depth contours*. So an inverse cascade should generate jets over a topographic slope, as shown in [47].

But a major difference with topography is that it need not be a simple linear slope. We have mountains, ridges and closed basins. How do such features affect the inverse cascade?

This question was addressed in two independent, simultaneous papers,

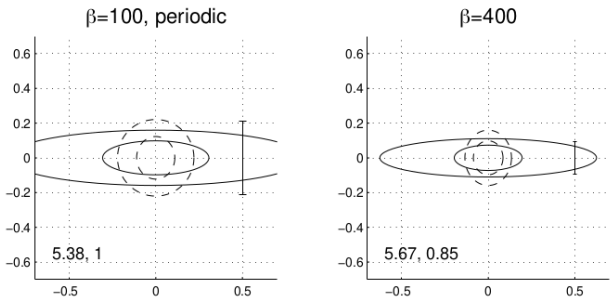

Figure 32: The velocity correlation ellipses from two simulations in a periodic domain. From [20].

one by Bretherton and Haidvogel [5] and the other by Salmon, Holloway and Hendershott [44]. Both considered freely-evolving (unforced) 2D turbulence over variable bottom topography. Salmon et al. used ideas from statistical mechanics to predict the most likely flow one would expect to find. Bretherton and Haidvogel used the calculus of variations. The two approaches in fact yield the same results, as demonstrated by [6].

8.3.1 The barotropic vorticity equation

First we need the vorticity equation with topography. Topography causes columns of fluid to compress or expand, thereby altering the vorticity. We can include this effect by using the full vorticity equation (63), without forcing or dissipation, applied to the 2D velocities:

$$\frac{\partial}{\partial t}\zeta + \vec{u}_2 \cdot \nabla(\zeta + f) + (\zeta + f)(\nabla \cdot \vec{u}_2) = 0 \tag{190}$$

where $\vec{u}_2 = (u, v, 0)$ and again ζ is the vertical component of the vorticity. The divergence term, the third, may be non-zero now because topography can induce convergence or divergence. Using the continuity equation, we

can rewrite this term:

$$\frac{\partial}{\partial t}\zeta + \vec{u}_2 \cdot \nabla(\zeta + f) - (\zeta + f)(\frac{\partial}{\partial z}w) = 0 \tag{191}$$

Assume the flow is barotropic, so that the horizontal velocities have no vertical shear. Then we can integrate the vorticity equation from the bottom of the fluid, say at $z = -H$, to the surface, at $z = 0$. Because the horizontal velocities, and hence ζ, have no shear, they pass through the integral:

$$\int_{-H}^{0} \frac{\partial}{\partial t}\zeta + \vec{u}_2 \cdot \nabla(\zeta + f) - (\zeta + f)(\frac{\partial}{\partial z}w)\, dz = 0$$

$$H\frac{\partial}{\partial t}\zeta + H\vec{u}_2 \cdot \nabla(\zeta + f) - (\zeta + f)[w(0) - w(-H)] = 0 \tag{192}$$

We'll assume the upper surface is flat (the *rigid lid assumption*) so that w vanishes there. At the bottom, the topography permits vertical flow, because a parcel resting on the bottom remains there. We can express this as:

$$\frac{d}{dt}(z + H)|_{z=-H} = 0 \tag{193}$$

This implies:

$$w(-H) = -\frac{d}{dt}H \tag{194}$$

Inserting this in the vorticity equation, we get:

$$H\frac{\partial}{\partial t}\zeta + H\vec{u}_2 \cdot \nabla(\zeta + f) - (\zeta + f)\frac{d}{dt}H = 0 \tag{195}$$

Because f doesn't vary in time, we can write this entirely in Lagrangian form:

$$H\frac{d}{dt}(\zeta + f) - (\zeta + f)\frac{d}{dt}H = 0 \tag{196}$$

Dividing through by H^2, this is simply:

$$\frac{d}{dt}\frac{\zeta + f}{H} = 0 \tag{197}$$

This is the *shallow water vorticity equation*. It states that the *potential vorticity*, $(\zeta + f)/H$, is conserved on fluid parcels without forcing or dissipation. The equation applies even in the presence of finite amplitude topography. This equation is the basis for global models for the barotropic tides.

However, the equation contains two unknowns (u, v), so it can't be solved without an additional equation. It's also awkward having the topographic term in the denominator. So we will work with a simplified equation, the *quasi-geostrophic* (QG) vorticity equation. This is based on three assumptions:

- The Rossby number, $\epsilon = U/(f_0 L)$, is small
- $|\beta y| \ll f_0$
- The bottom topography is weak

Consider the first condition. When the Rossby number, ϵ, is small, the horizontal velocities are approximately in geostrophic balance. Likewise, the vorticity is much less than f_0, because:

$$\frac{|\zeta|}{f_0} \propto \frac{U}{f_0 L} = \epsilon$$

The second condition is necessary if we are to make the β-plane approximation. If the β term weren't small compared to f_0, we'd have to retain all the higher order terms in the Taylor expansion of f. But we will further assume that:

$$\frac{|\beta y|}{|f_0|} \propto \epsilon$$

Of course we could demand the β term be even smaller, but then we would actually lose this term. Assuming a Rossby number scaling preserves the variation of f, as seen hereafter.

Lastly, we assume that we can write the depth as:

$$H = H_0 - h(x, y)$$

where:

$$\frac{|h|}{H_0} \propto \epsilon$$

So the topography is also of order Rossby number compared to the fluid depth. So we don't allow for mountains which extend from the bottom to the surface. The tallest mountains can only extend to, say, 10 % of the total depth (Fig. 33).

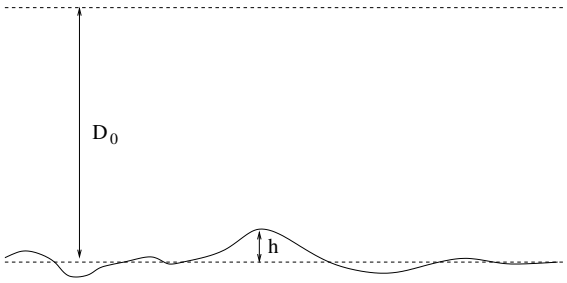

Figure 33: The geometry of our fluid layer. The topographic height, h, is much less than the depth of the layer.

We now use these assumptions to write a simpler version of the vorticity equation. First, we replace the horizontal velocities with their geostrophic equivalents in the Lagrangian derivative:

$$\frac{d}{dt} \rightarrow \frac{d_g}{dt} \equiv \frac{\partial}{\partial t} + u_g \frac{\partial}{\partial x} + v_g \frac{\partial}{\partial y} \tag{198}$$

Similarly, we replace the vorticity with its geostrophic version:

$$\zeta \rightarrow \zeta_g = \frac{\partial}{\partial x} v_g - \frac{\partial}{\partial y} u_g \tag{199}$$

We also replace f by it's β-plane approximation. So the PV equation is:

$$\frac{d_g}{dt}\frac{\zeta_g + f_0 + \beta y}{H_0 - h} = 0 \tag{200}$$

With the above assumptions, the PV can be simplified.

$$\begin{aligned}
\frac{\zeta_g + f_0 + \beta y}{H_0 - h} &= \frac{f_0}{H_0}\left(\frac{1 + \zeta/f_0 + \beta y/f_0}{1 - h/H_0}\right) && (201)\\
&\approx \frac{f_0}{H_0}\left(1 + \frac{\zeta}{f_0} + \frac{\beta y}{f_0}\right)\left(1 + \frac{h}{H_0}\right) && (202)\\
&\approx \frac{f_0}{H_0} + \frac{\zeta}{H_0} + \frac{\beta y}{H_0} + \frac{f_0 h}{H_0^2} && (203)
\end{aligned}$$

Each of the last three terms are of order Rossby number compared to the first term. The terms we've dropped involve the *products* of the small terms and are of order Rossby number squared. Substituting this into (200) yields:

$$\frac{d_g}{dt}(\zeta_g + \beta y + \frac{f_0}{H_0}h) = 0 \tag{204}$$

after multiplying through by the constant, H_0 and cancelling the constant first term, f_0/H_0. This the *quasi-geostrophic PV equation* without forcing or friction. Written in terms of the geostrophic streamfunction, this is:

$$(\frac{\partial}{\partial t} + u_g\frac{\partial}{\partial x} + v_g\frac{\partial}{\partial y})(\nabla^2\psi + \beta y + \frac{f_0}{H_0}h) = 0 \tag{205}$$

or:

$$\frac{\partial}{\partial t}\nabla^2\psi + \nabla\cdot[\vec{u}_g(\nabla^2\psi + \beta y + h)] = 0 \tag{206}$$

because the geostrophic velocities are horizontally non-divergent. Notice we absorbed the constant factor of f_0/H into the topographic term, h (so now the height has units of sec^{-1}, like the vorticity). This is a very useful equation for studying diverse phenomena, such as Rossby waves emanating from mountains and the barotropic Gulf Stream.

8.3.2 Conserved quantities

Hereafter we'll focus on the topographic term, and ignore the variation of the Coriolis parameter (and set $\beta = 0$). There are two conserved quantities in the absence of dissipation. One is the energy:

$$\frac{1}{2}\frac{\partial}{\partial t}\iint (u^2 + v^2)\, dxdy = 0 \tag{207}$$

The proof of this is left for an exercise. We also conserve "total enstrophy". First note that we can rewrite the vorticity equation (206) thus:

$$\frac{\partial}{\partial t} q + \nabla \cdot (\vec{u} q) = 0 \tag{208}$$

where

$$q \equiv \nabla^2 \psi + h \tag{209}$$

is the potential vorticity. If we multiply the equation by q and integrate over space, we get:

$$\frac{\partial}{\partial t}\frac{1}{2}\iint q^2\, dxdy + \iint \nabla \cdot (\vec{u}\, \frac{q^2}{2})\, dxdy = 0 \tag{210}$$

The second term on the LHS vanishes:

$$\iint \nabla \cdot (\vec{u}\, \frac{q^2}{2})\, dxdy = \oint \frac{q^2}{2}\, \vec{u} \cdot \hat{n}\, dl = 0 \tag{211}$$

So the total enstrophy, $q^2/2$, is also conserved. We will call this Q. Note though the enstrophy itself is *not* conserved; this is because the interaction with the topography itself can produce enstrophy.

Exercise: *Energy conservation*

Prove that the integrated kinetic energy is conserved, starting directly with the vorticity equation (206).

8.3.3 Minimum enstrophy

Under a dual cascade, we expect the energy to shift to large scales and the *total* enstrophy to move to smaller scales. If the dissipation is non-zero, the total enstrophy will then be dissipated. Bretherton and Haidvogel [5] suggested that the turbulence would thereby act to *minimize* the total enstrophy while conserving the energy.

To do this, we use the *calculus of variations*. Let Q be the total enstrophy. Its minimum occurs where its *variation* vanishes. This is exactly like when a function has an extremum where its first derivative vanishes. For example, the function $f(x) = x^2$ has an extremum at $x = 0$, because $f'(x) = 2x = 0$ at $x = 0$. To know that the extremum is a minimum, you have to evaluate the second variation at that point. We have $f''(0) = 2$, so the curvature is positive. That means the extremum is a minimum.

The first variation of Q is:

$$\delta Q = \delta \iint \frac{1}{2}(\nabla^2\psi + h)^2 \, dA =$$

$$\iint (\nabla^2\psi + h)\delta(\nabla^2\psi + h) \, dA = 0 \tag{212}$$

We assume the topography is fixed but that the streamfunction can vary. So the equation is:

$$\iint (\nabla^2\psi + h)\delta(\nabla^2\psi) \, dA = 0 \tag{213}$$

However, this only tells us where Q has an extremum; we haven't said anything about the energy. But we can impose energy conservation by using the method of *Lagrange multipliers*. In particular, we define a *functional*:

$$F = Q + \mu(E - E_0) \tag{214}$$

Here the constant μ is a Lagrange multiplier and E is the kinetic energy:

$$E = \frac{1}{2}\iint (u^2 + v^2)\, dA = \frac{1}{2}\iint |\nabla\psi|^2\, dA \tag{215}$$

E_0 is the kinetic energy of the system, assumed constant.

If we take the variation of F with respect to μ, we get:

$$\frac{\delta F}{\delta \mu} = E - E_0 = 0 \tag{216}$$

So this implies the solution will have an energy of E_0.

If, on the other hand, we keep μ constant and take the variation of F, we get:

$$\delta F = \delta(Q + \mu(E - E_0)) = \delta Q + \mu\delta E = 0 \tag{217}$$

The variation of E_0 is zero since it is a constant. Substituting in the expressions for Q and E, we have:

$$\delta Q + \mu\delta E = \iint (\nabla^2\psi + h)\delta(\nabla^2\psi)\, dA + \mu\iint \nabla\psi \cdot \delta\nabla\psi\, dA \tag{218}$$

Both integrals in (218) can be rewritten using integration by parts, assuming either periodic boundary conditions or that ψ vanishes on the boundaries. So for instance:

$$\iint \nabla\psi \cdot \delta\nabla\psi\, dA = -\iint \nabla^2\psi \cdot \delta\psi\, dA \tag{219}$$

Also:

$$\iint (\nabla^2\psi + h)\delta\nabla^2\psi\, dA = -\iint \nabla(\nabla^2\psi + h) \cdot \delta\nabla\psi\, dA =$$

$$\iint \nabla^2(\nabla^2\psi + h)\delta\psi\, dA \tag{220}$$

Combining the terms, we get:

$$\delta Q + \mu\delta E = \frac{1}{2}\iint \nabla^2(\nabla^2\psi + h - \mu\psi)\delta\psi\, dA = 0 \tag{221}$$

We require that the integral vanish for *all* variations $\delta\psi$. For this to happen, we must have:

$$\nabla^2\psi + h - \mu\psi = 0 \tag{222}$$

This is is known as the "Euler-Lagrange equation" for the problem. We can solve this by Fourier transforming both the streamfunction and the topography:

$$\psi = \sum_{k,l} \hat{\psi}(k,l) e^{ikx+ily}, \quad h = \sum_{k,l} \hat{h}(k,l) e^{ikx+ily} \tag{223}$$

Substituting both into the Euler-Lagrange equation, we can solve for $\hat{\psi}$ in terms of $\hat{h}$:

$$\hat{\psi} = \frac{\hat{h}}{\mu + k^2 + l^2} = \frac{\hat{h}}{\mu + \kappa^2} \tag{224}$$

This is the extremal solution for the streamfunction, i.e. the one with the minimum value of F. Of course, to find out whether this really is a minimum, we'd have to examine the second variation. We won't do that, but the solution is indeed a minimum.

The predicted streamfunction resembles the topography. If we know the transform of the topography, we have the transform of the streamfunction. Then we can inverse transform to obtain the actual streamfunction. The solution suggests that the flow is approximately parallel to the isobaths.

But the flow isn't entirely parallel to the isobaths. This is because the denominator in (224) filters the small scales. At large scales, so that $\kappa \ll \mu$, $\psi \approx \hat{h}/\mu$. But at small scales, $\psi \approx \hat{h}/\kappa^2$, which goes to zero as κ gets large. So the flow resembles a *low-pass filtered version of the topography*. In particular, there will be anticyclonic flow over seamounts and cyclonic flow in basins. This is often observed in the ocean.

To finish the solution, we have to impose the other condition, which

is that the energy is equal to the initial value, E_0. This determines μ, the Lagrange multiplier. We have that:

$$E = E_0 = \frac{1}{2}\sum_{k,l} \kappa^2 |\hat{\psi}|^2 = \frac{1}{2}\sum_{k,l} \frac{\kappa^2 |\hat{h}|^2}{(\mu + \kappa^2)^2} \tag{225}$$

It's not trivial to determine μ from this, given that the energy involves a sum over all wavenumbers, but it can be done numerically. The larger E is, the smaller μ will be. And the smaller μ is, the greater the low-pass filtering effect will be. Thus energetic flows will evolve to a smoother representation of the topography than weak flows.

The results from a numerical simulation by Bretherton and Haidvogel [5] are shown in Fig. (34). As noted, this was a freely-evolving experiment, i.e. one without forcing. The initial streamfunction is shown in the lower left panel and the topography in the upper left panel. After a period of time, the streamfunction settles down into the configuration shown in the lower right panel. The streamfunction strongly resembles the topography, and has the same signs. There is cyclonic flow in the depression in the upper part of the domain. But note too that the streamfunction has less small scale structure than the topography—evidence of the low pass filtering effect predicted by the variational solution.

Observations in the ocean show that mean flows are often correlated with bottom topography. The present theory is one possible explanation for this.

Exercise: *Minimum enstrophy with a free surface*

Consider the case of a barotropic flow with a free surface. It's possible

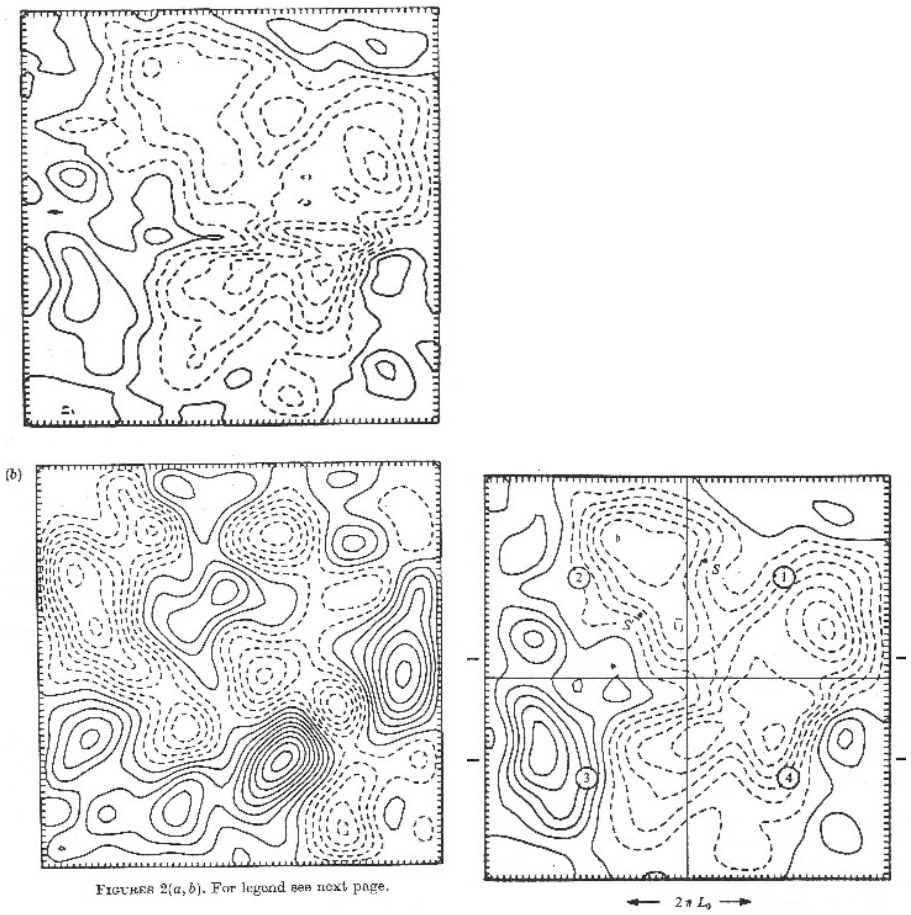

Figure 34: A numerical simulation from Bretherton and Haidvogel [5]. The topography is shown in the upper left panel and the initial streamfunction in the lower left panel. The final streamfunction is shown in the lower right panel. Notice that this is very similar to the topography.

to show that the potential vorticity then becomes:

$$q = \nabla^2\psi - \frac{1}{L_b^2}\psi + h \tag{226}$$

where L_b is the barotropic "deformation radius". Minimize the enstrophy, but neglect the conservation of energy. What is the solution for ψ? How does this differ from the solution in (224)?

8.4 Stratification

So far, we have looked only at barotropic flows. But the atmosphere and ocean are stratified, and many important dynamics are linked to stratification. Storms in the atmosphere derive from baroclinic instability, and the Gulf Stream is similarly unstable.

In barotropic turbulence, we speak of triad interactions among horizontal wavenumbers. But with stratification, we can have interactions between waves with different *vertical* structure. Thus the problem becomes three dimensional.

But we are interested in large scale turbulence, and the flow is still predominantly two dimensional at large scales, even with stratification. It will turn out that many of the concepts we have discussed will carry over to the stratified case.

The following is based on the stratified quasi-geostrophic potential vorticity (QGPV) equation. Derivations are given in [38] and [22]. We will use the Boussinesq form of the QGPV equation, which can be written:

$$\frac{\partial}{\partial t}q + \nabla \cdot (\vec{u}_g q) = 0 \tag{227}$$

where

$$q = \nabla^2 \psi + \frac{\partial}{\partial z}(\frac{f_0^2}{N^2}\frac{\partial \psi}{\partial z}) \tag{228}$$

This is the potential vorticity. It is comprised of two parts: the relative vorticity and the *stretching* vorticity. The latter depends on the vertial shear and N^2, the buoyancy frequency. Note too that the advecting velocities are the geostrophic and that the Laplacian is the horizontal Laplacian, not the three-dimensional one.

For concreteness, we'll assume we have a periodic domain in (x, y) and solid boundaries at $z = 0$ and $z = 1$. The boundary condition on

the vertical boundaries is that the vertical velocity vanishes. This can be shown to be satisfied if $\frac{\partial}{\partial z}\psi = 0$.

8.4.1 Conserved quantities

We can derive an energy equation if we multiply the PV equation by ψ and integrate over the volume:

$$\iiint \psi \frac{\partial}{\partial t}\nabla^2\psi \, dV + \iiint \psi \frac{\partial}{\partial t}\frac{\partial}{\partial z}(\frac{f_0^2}{N^2}\frac{\partial \psi}{\partial z}) \, dV + \iiint \psi \nabla \cdot (\vec{u}_g q) \, dV = 0 \tag{229}$$

The third term can be rewritten as before:

$$\iiint \psi \nabla \cdot (\vec{u}_g q) \, dV = \iiint \nabla \cdot (\psi \vec{u}_g q) \, dV = \oiint \psi q \, (\vec{u} \cdot \hat{n}) \, dS = 0 \tag{230}$$

This is zero because of periodicity in x and y and because the vertical velocity vanishes at the top and bottom.

Using integration by parts with the first term in (229), we get:

$$\iiint \psi \frac{\partial}{\partial t}\nabla^2\psi \, dV = -\frac{1}{2}\frac{\partial}{\partial t}\iiint |\nabla\psi|^2 \, dV = -\frac{1}{2}\frac{\partial}{\partial t}\iiint (u^2+v^2) \, dV \tag{231}$$

This is the time rate of change of the (horizontal) kinetic energy.

Then there's the other term. Now we apply integration by parts in the vertical:

$$\iiint \psi \frac{\partial}{\partial t}\frac{\partial}{\partial z}(\frac{f_0^2}{N^2}\frac{\partial \psi}{\partial z}) \, dV = \iint \psi \frac{\partial}{\partial t}\frac{f_0^2}{N^2}\frac{\partial \psi}{\partial z}|_0^1 \, dA - \frac{1}{2}\frac{\partial}{\partial t}\iiint \frac{f_0^2}{N^2}(\frac{\partial \psi}{\partial z})^2 \, dV \tag{232}$$

The first term on the RHS is zero because $\frac{\partial}{\partial z}\psi$ vanishes on the vertical boundaries. The second term on the RHS is the *potential energy* and is related to changes in the fluid density. Thus we have:

$$\frac{\partial}{\partial t}\,\frac{1}{2}\iiint (\frac{\partial \psi}{\partial x})^2 + (\frac{\partial \psi}{\partial y})^2 + \frac{f_0^2}{N^2}(\frac{\partial \psi}{\partial z})^2 \, dV = 0 \tag{233}$$

So the total energy—the horizontal kinetic plus potential—is conserved.

Now if we multiply the PV equation by q and integrate that over space, we get:

$$\frac{\partial}{\partial t}\frac{1}{2}\iiint q^2\, dV = 0 \tag{234}$$

So the second conserved quantity is the potential enstrophy (the square of the PV).

8.4.2 Energy cascade

With these two conserved quantities, Charney [9] demonstrated that the energy shifts to larger scales and the enstrophy to smaller scales, using an argument like Batchelor's [2].

Let's assume that the Brunt-Vaisala frequency, N, is also constant. Then we can redefine the vertical coordinate thus:

$$z^* = \frac{N}{f_0} z \tag{235}$$

Doing this, the PV is simply:

$$q = \nabla^2\psi + \frac{\partial^2}{\partial z^{*2}}\psi \equiv \nabla_3^2\psi \tag{236}$$

where ∇_3 is the three dimensional Laplacian, with the new vertical coordinate. Likewise, the energy is:

$$E = \frac{1}{2}\iiint |\nabla_3\psi|^2\, dV \tag{237}$$

and the potential enstrophy is:

$$Q = \frac{1}{2}\iiint (\nabla_3^2\psi)^2\, dV \tag{238}$$

We will Fourier transform the streamfunction as follows:

$$\psi(x,y,z) = \sum_{k,l,n} \hat{\psi} e^{ikx+ily} cos(n\pi z) \tag{239}$$

We use the cosine expansion in the vertical so that the vertical derivative of ψ vanishes on the vertical boundaries (at $z = 0$ and $z = 1$). With this, we have:

$$E = \frac{1}{2}\int \kappa^2 |\hat{\psi}|^2 \, d\kappa \tag{240}$$

and

$$Q = \frac{1}{2}\int \kappa^4 |\hat{\psi}|^2 \, d\kappa = \frac{1}{2}\int \kappa^2 E \, d\kappa \tag{241}$$

where now:

$$\kappa^2 = k^2 + l^2 + n^2\pi^2 \tag{242}$$

is the total wavenumber squared.

Now we can proceed exactly as in 2-D. Consider a spectrum peaked at some three-dimensional wavenumber, κ_1. We assume the peak will spread, so that:

$$\frac{d}{dt}\int (\kappa - \kappa_1)^2 E \, d\kappa > 0 \tag{243}$$

Expanding:

$$\frac{d}{dt}\int \kappa^2 E \, d\kappa - 2\kappa_1 \frac{d}{dt}\int \kappa E \, d\kappa + \kappa_1^2 \frac{d}{dt}\int E \, d\kappa > 0 \tag{244}$$

The first and third terms are zero, so;

$$\frac{d}{dt}\int \kappa E \, d\kappa < 0 \tag{245}$$

which implies the total energy shifts to smaller κ. There is an inverse cascade, as in 2-D turbulence.

However, the cascade is not only to larger horizontal scales—it is also to larger *vertical* scales. So an inverse cascade in a stratified flow favors the gravest baroclinic modes.

Exercise: *Fjørtoft's approach*

Consider Fjørtoft's single-triad problem, using the total energy and the potential enstrophy and the same three total wavenumbers: $\kappa/2$, κ and 2κ.

Assuming the energy is initially in the middle wavenumber, comment on how the vertical scale of motion is changing.

8.4.3 The vortex view

We can invoke a vortex view to obtain a physical impression of this process of increasing vertical extent. In geostrophic turbulence, the vortices are *potential vortices*, having both relative and stretching vorticity.

Consider a vortex, with potential vorticity q. We can scale the PV as follows:

$$\begin{gathered} q = \nabla^2\psi + \frac{f_0^2}{N^2}\frac{\partial^2}{\partial z^2}\psi \\ \frac{UL}{L^2} \qquad \frac{f_0^2 UL}{N^2H^2} \\ 1 \qquad \frac{f_0^2L^2}{N^2H^2} \end{gathered} \tag{246}$$

I've divided through by the scaling for the relative vorticity, and I'm taking N^2=const. We see that the relative scale of the stretching vorticity depends on the vortex size, L. We can rewrite this term as:

$$\frac{f_0^2L^2}{N^2H^2} = \frac{L^2}{L_d^2} \tag{247}$$

where

$$L_d = \frac{NH}{f_0} \tag{248}$$

is the *deformation radius*. If the vortex is much larger than the deformation radius, the stretching vorticity dominates and if the vortex is much smaller than L_d, the relative vorticity dominates.

Imagine we have a three-dimensional QG simulation, with random initial flow. The flow will organize itself into vortices, on different *levels* in the flow. These vortices will be smaller than the deformation radius and

dominated by relative vorticity. So they will behave just like vortices in 2-D turbulence. Like-sign vortices will merge, making larger vortices.

As the vortices become larger, the stretching vorticity is more important. We see, in particular, that the vortices have greater vertical extent. So they begin to interact with vortices on other levels. Occasionally, like-sign vortices will vertically *align* with one another. This is just like a merger, but between two vortices on different levels.

The flow thus evolves to a system of fewer and fewer vortices, with greater and greater vertical extent. This is the physical meaning of Charney's 3-D cascade.

The potential vorticity from such a simulation, from McWilliams et al. [33], is shown in Fig. (35). The flow started with a 3-D random initial condition. In the upper panel is the PV at an intermediate time. Already it is clear that like-sign vortices are congregating together. At a later time, shown in the lower panel, the vertical alignment is clear, and two large tornado-like structures have formed.

Thus the vortex view again illustrates the behavior that we have deduced from spectral considerations.

8.4.4 Enstrophy cascade

Another prediction of Charney's is that there will be an enstrophy cascade in quasi-geostrophic turbulence. This will have an energy spectrum given by:

$$E(\kappa) \propto \eta^{-2/3}\kappa^{-3} \tag{249}$$

where η is now the total enstrophy transfer rate, with units of sec^{-3}. The difference is that the wavenumber again is the full three-dimensional wavenumber given above. However, Charney assumes that the turbulence is *isotropic*

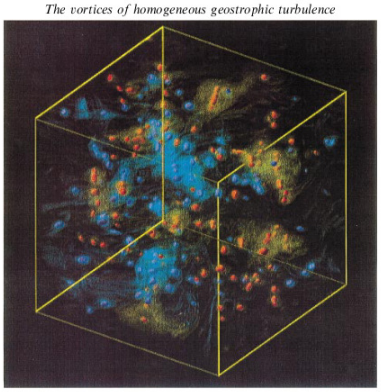

FIGURE 2. For caption see facing page.

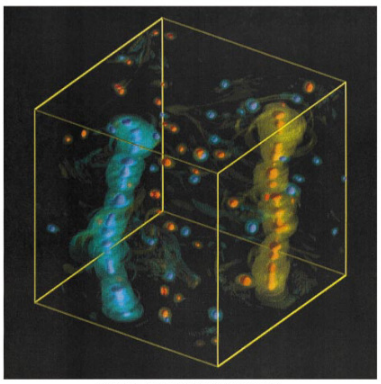

FIGURE 3. For caption see facing page.

Figure 35: Potential vorticity from a 3-D QG simulation from random initial conditions. The upper panel shows the PV at an intermediate time and the lower panel at a late time. Note the vertical alignment of the vortex structures.

in the three directions, (x, y, z^*). That implies that the energy spectrum will be the same for the horizontal kinetic energy, or indeed even one component, i.e. for u^2.

This is a possible explanation for the κ^{-3} range below 2000 km in the Nastrom and Gage spectra in Fig. (26). The atmosphere is not a 2-D fluid, but at large scales it is quasi-geostrophic. The Brunt-Vaisala frequency is approximately constant in the troposphere too, so Charney's stretched vertical coordinate is a reasonable choice. Further analysis has shown that the enstrophy flux in this range is downscale, as expected for an enstrophy cascade [28].

There are *also* indications of an enstrophy cascade in the ocean. Wang et al. [48] calculated energy spectra from current measurements collected from a ferry steaming between the U.S. and Bermuda, across the Gulf Stream. The results (Fig. 36) also show a clear κ^{-3} range. The peak of the scale corresponds to roughly the 50 km scale. In addition, the kinetic and potential energy show the same slope, consistent with Charney's assumption of an energy flow which is isotropic in the three dimensional wavenumber.

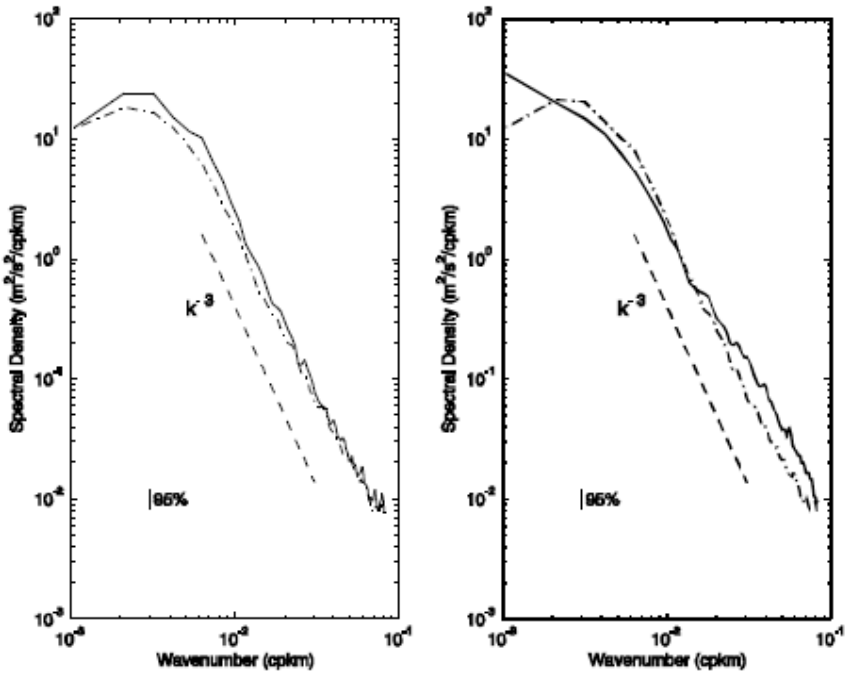

Figure 36: Kinetic energy spectra from ADCP data collected from a ferry steaming between the U.S. and Bermuda. The left panel shows the u and v components, and the right panel the kinetic and potential energies. From [48].

Thus the addition of stratification hasn't changed the situation greatly. However, as the vertical extent of the flow increases, the boundaries become important. So it is likely that Charney's construction works better at small scales, i.e. in the enstrophy range.

Where does baroclinic instability fit in? Instability implies a conversion of large scale potential energy to kinetic energy at the deformation radius. How do we reconcile this with an inverse cascade? The answer can be found in detailed consideration of the triad interactions occurring in a baroclinic system.

Exercise: *Enstrophy conservation*

Show that *any* function of the potential vorticity q is also conserved in the QG system.

8.4.5 Cascades in a two mode system

Triad interactions become very complicated when we have vertical modes in addition to the horizontal wavenumbers. However, we can get a good idea of how the system behaves when we consider only two vertical modes.[10]

Consider again the PV equation, which we write thus:

$$\frac{\partial}{\partial t}q + u\frac{\partial}{\partial x}q + v\frac{\partial}{\partial y}q = \frac{\partial}{\partial t}q - \frac{\partial \psi}{\partial y}\frac{\partial}{\partial x}q + \frac{\partial \psi}{\partial x}\frac{\partial}{\partial y}q = 0 \tag{250}$$

We can write this in shorthand form thus:

$$\frac{\partial}{\partial t}q + J(\psi, q) = 0 \tag{251}$$

The $J(,)$ function is called the *Jacobian*. It is defined as:

$$J(a, b) = \frac{\partial a}{\partial x}\frac{\partial b}{\partial y} - \frac{\partial b}{\partial x}\frac{\partial a}{\partial y} \tag{252}$$

We'll take $N = const.$, so the PV is:

$$q = \nabla^2 \psi + \frac{f_0^2}{N^2}\frac{\partial^2}{\partial z^2}\psi \tag{253}$$

[10]The following is based on Salmon's [42].

Assuming the fluid depth is such that $0 \leq z \leq H$, we can express the streamfunction in terms of *vertical modes*, thus:

$$\psi(x, y, z, t) = \sum_n \psi_n(x, y, t) cos(\frac{n\pi z}{H}) \tag{254}$$

We will only consider the first two terms:

$$\psi(x, y, z, t) = \psi_B(x, y, t) + \psi_T(x, y, t)\, cos(\frac{n\pi z}{H}) \tag{255}$$

Here ψ_B is the *barotropic* streamfunction; it does not vary in the vertical. ψ_T is the *first baroclinic* mode. It is the gravest of the cosine modes; if we integrate it in the vertical, it vanishes. We will exploit this below.

The PV also has two components:

$$q = \nabla^2\psi_B + (\nabla^2 - F)\psi_T\, cos(\frac{n\pi z}{H}) \tag{256}$$

where

$$F = \frac{\pi^2 f_0^2}{N^2 H^2} \tag{257}$$

Notice that this parameter has units of L^{-2}. Thus the square root of F is like a wavenumber. This corresponds to the inverse of the deformation radius.

Plugging the streamfunction and PV into the PV equation, we get:

$$\begin{aligned} &\frac{\partial}{\partial t}\nabla^2\psi_B + \frac{\partial}{\partial t}(\nabla^2 - F)\psi_T cos(\frac{n\pi z}{H}) + J(\psi_B, \nabla^2\psi_B) + \\ &J(\psi_B, (\nabla^2 - F)\psi_T) cos(\frac{n\pi z}{H}) + J(\psi_T, \nabla^2\psi_B) cos(\frac{n\pi z}{H}) + \\ &J(\psi_T, (\nabla^2 - F)\psi_T) cos^2(\frac{n\pi z}{H}) = 0 \end{aligned} \tag{258}$$

We can isolate the time derivative of the barotropic streamfunction if we integrate this equation in z over the depth of the fluid, and then divide by the depth H:

$$\frac{\partial}{\partial t}\nabla^2\psi_B + J(\psi_B, \nabla^2\psi_B) + \frac{1}{2}J(\psi_T, (\nabla^2 - F)\psi_T) = 0 \tag{259}$$

The terms multiplied by cosine vanish, and the cosine squared term integrates to one half. This is the vorticity equation for the barotropic mode. Notice that the barotropic vorticity can change by two terms. The first involves the barotropic velocity advecting the barotropic vorticity, and the second the baroclinic velocity advecting the baroclinic vorticity.

Similarly, we can obtain an equation for the baroclinic vorticity if we multiply the equation by $cos(n\pi z/H)$ and integrate over the depth. Then we get:

$$\frac{\partial}{\partial t}(\nabla^2 - F)\psi_T + J(\psi_B, (\nabla^2 - F)\psi_T) + J(\psi_T, \nabla^2\psi_B) = 0 \qquad (260)$$

after canceling a common factor of 1/2. This is the baroclinic vorticity equation. This states the baroclinic PV changes when the barotropic velocity advects baroclinic PV, and vice versa.

Each PV equation has an energy relation associated with it. If we multiply (259) by ψ_B and integrate over the area of the domain, we get:

$$\frac{d}{dt}\iint \frac{1}{2}|\nabla\psi_B|^2\, dA - \iint \psi_B J(\psi_T, (\nabla^2 - F)\psi_T)\, dA = 0 \qquad (261)$$

after integrating by parts. Note the barotropic advection term vanishes when integrated over the area. The first term is the barotropic energy, which is purely kinetic. This is *not* conserved, because of the interaction with the baroclinic mode.

Likewise, multiplying (260) by ψ_T and integrating over area, we get:

$$\frac{d}{dt}\iint \frac{1}{2}[|\nabla\psi_T|^2 + F|\psi_T|^2]\, dA - \iint \psi_T J(\psi_B, (\nabla^2 - F)\psi_T)\, dA = 0 \quad (262)$$

again, after integration by parts. The first term is the change in the total baroclinic energy, which has both kinetic and potential parts. The baroclinic energy isn't conserved either, due to the interaction with the barotropic mode.

However, if we integrate by parts again, we can show that:

$$-\iint \psi_B J(\psi_T, (\nabla^2 - F)\psi_T)\, dA = \iint \psi_T J(\psi_B, (\nabla^2 - F)\psi_T)\, dA \quad (263)$$

So adding the two equation energy equations together, we get:

$$\frac{d}{dt}\frac{1}{2}\iint |\nabla\psi_B|^2 + |\nabla\psi_T|^2 + F|\psi_T|^2\, dA = 0 \quad (264)$$

So the total energy, barotropic plus baroclinic, is conserved.

After a similar derivation, you can show that:

$$\frac{d}{dt}\frac{1}{2}\iint (\nabla^2\psi_B)^2 + ((\nabla^2 + F)\psi_T)^2\, dA = 0 \quad (265)$$

So the total enstrophy is also conserved.

Now, how energy is transferred in the two mode system depends on the triad interactions. To see how these work, we'll focus on the barotropic PV equation (259). We write this for Fourier components, and we leave out the summations for simplicity. The equation then looks like this:

$$-\frac{\partial}{\partial t}(k_x^2 + k_y^2)\psi_{B1}e^{ik\cdot x} + J(\psi_{B2}, -(m_x^2 + m_y^2)\psi_{B3})e^{im\cdot x + in\cdot x}$$
$$+J(\psi_{T1}, -(q_x^2 + q_y^2 + F)\psi_{T2})e^{ip\cdot x + iq\cdot x} = 0 \quad (266)$$

Note that I'm using n now as a horizontal wavenumber (not the vertical mode number). To extract an equation for the barotropic streamfunction with wavenumbers (k_x, k_y), we multiply by $\psi_{B1}e^{-ik\cdot x}$ and integrate over the area. The result is:

$$-\frac{\partial}{\partial t}(k_x^2 + k_y^2)|\psi_{B1}|^2 + Re\{\psi_{B1}^* J(\psi_{B2}, -(m_x^2 + m_y^2)\psi_{B3})\}\delta(m + n - k)$$
$$+Re\{\psi_{B1}^* J(\psi_{T1}, -(q_x^2 + q_y^2 + F)\psi_{T2})\}\delta(p + q - k) = 0 \quad (267)$$

This equation accounts for the change in barotropic energy at wavenumber (k_x, k_y). Remember that the two advection terms involve sums over

many wavenumbers. Interactions between wavenumber triads can transfer energy.

We see though that there are two types of triad. The first involves interactions between three barotropic waves. This corresponds to the triads we considered previously. The second though is something new, and involves the barotropic wave (at (k_X, k_y)) and two baroclinic waves.

Consider a triad of barotropic waves first. These conserve barotropic energy and enstrophy:

$$\frac{d}{dt}(E_1 + E_2 + E_3) = 0$$
$$\frac{d}{dt}(Z_1 + Z_2 + Z_3) = 0 \tag{268}$$

We can rewrite the enstrophy relation thus:

$$\frac{d}{dt}(\kappa_1^2 E_1 + \kappa_2^2 E_2 + \kappa_3^2 E_3) = 0 \tag{269}$$

This is exactly like Fjørtoft's barotropic example. We expect then that energy will shift to larger scales and enstrophy to smaller scales.

Now consider the barotropic/baroclinic triads. The enstrophy relations are:

$$\frac{d}{dt}(\kappa_1^2 E_1 + (\kappa_2^2 + F)E_2 + (\kappa_3^2 + F)E_3) = 0 \tag{270}$$

This is more complicated than the barotropic case because of the F terms (which also affect the baroclinic energies). Consider first that all three members of the triad have scales well below the deformation radius, so that $(\kappa_1, \kappa_2, \kappa_3) \gg F$. Then the enstrophy equation is, approximately:

$$\frac{d}{dt}(\kappa_1^2 E_1 + \kappa_2^2 E_2 + \kappa_3^2 E_3) = 0 \tag{271}$$

This is the same as with the barotropic triad. Thus we expect energy to be transferred to the triad member with the largest scale (regardless of whether this is barotropic or baroclinic). Energy would thus shift toward the deformation radius.

Now consider that we have a large scale triad, so that $(\kappa_1, \kappa_2, \kappa_3) \ll F$. Then we have, approximately:

$$\frac{d}{dt}(FE_2 + FE_3) = 0 \tag{272}$$

This simply states that energy will pass between the two baroclinic waves. But the direction of transfer is undetermined—we can't say whether energy is moving up or downscale.

Does this mean that baroclinic energy at large scales can't transition to smaller scales? It would seem so. But what about baroclinic instability? In that, energy is transferred from a baroclinic mean shear to barotropic eddies. This would seem to contradict the present finding. In fact the problem here is the assumption of *local* interactions. What about a non-local interaction, between a large scale baroclinic mode and smaller scale barotropic and baroclinic waves?

The usual models of baroclinic instability (the Eady model, the Charney model and the Philips model) all involve a baroclinic shear with no lateral shear. So we could express this as a baroclinic mode in which:

$$(\kappa_2^2 + F)\psi_{T1} = F\psi_{T1} \tag{273}$$

(the Laplacian is zero because the mode is constant in x and y). Making no other assumptions about scales, we have:

$$\frac{d}{dt}(E_1 + E_2 + E_3) = 0$$

$$\frac{d}{dt}(\kappa_1^2 E_1 + F E_2 + (\kappa_3^2 + F) E_3) = 0 \tag{274}$$

Using the first equation, we can eliminate dE_2/dt from the enstrophy equation. This yields:

$$\frac{d}{dt}(\kappa_1^2 E_1 - F E_1 - F E_3 + (\kappa_3^2 + F) E_3) = 0 \tag{275}$$

or:

$$\frac{d}{dt}\kappa_3^2 E_3 = \frac{d}{dt}((F - \kappa_1^2) E_1) \tag{276}$$

This implies that the energy in both the other modes can increase in time if:

$$\kappa_1^2 < F \tag{277}$$

In other words, if the barotropic wave is larger than the deformation radius, it can take energy from the primary baroclinic wave. This is precisely the short-wave cut-off that we found when we studied the Eady model—only the long waves can be unstable.

But more than that, the barotropic wave can be much smaller than the primary baroclinic wave. Recall that the most unstable wave in the Eady problem has a scale somewhat larger than the deformation radius. Such a triad is *non-local*, because there is a large separation in scales between the triad members.

We can summarize the results by using a schematic diagram (Fig. 37), based on a figure of Salmon's [42]. The energy at small scales cascades to larger scales in both the baroclinic and barotropic modes via local interactions. Baroclinic modes with scales larger than the deformation radius are unstable and transfer energy non-locally to the barotropic modes. Then energy eventually cascades locally to large scales in the barotropic mode.

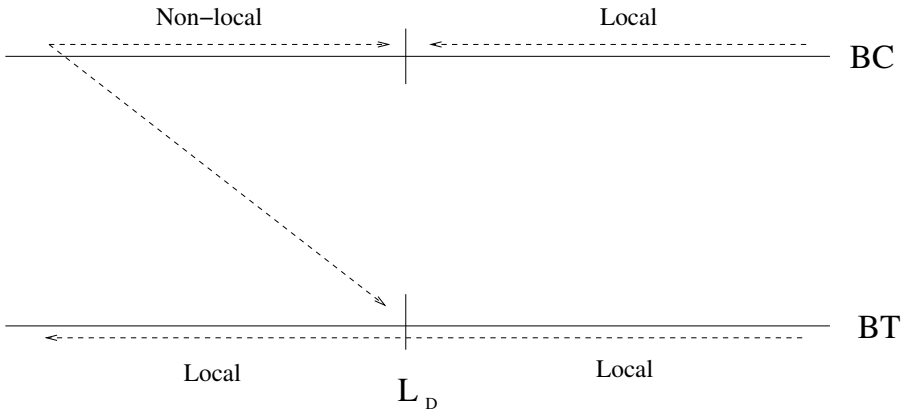

Figure 37: A idealized diagram indicating the tendencies for energetic transfer in the two layer model. The upper line represents the baroclinic mode and the lower line the barotropic mode. Adapted from [42].

An important point here is that baroclinic instability in this turbulence context is simply a non-local triad interaction. This means that the transfer to the barotropic mode is *generic* for large scale baroclinic modes. Thus, for example, a large scale baroclinic Rossby wave can be unstable too [24, 16]. It is not necessary to have a mean flow.

9 Turbulent Diffusion

We will examine how turbulent flows advect passive tracers, and in particular what happens with particles and pairs of particles. In section (7.7), we examined how the spectrum of passive tracer variance would look in a given turbulent inertial range. In that case, we treated the tracer as a continuous Eulerian field, like vorticity. Now we take a more Lagrangian view.

9.1 Single particle dispersion

9.1.1 Random walk

The essence of single particle motion is captured in the *random walk* or "drunkard's walk" problem. This is the basis of "Brownian motion", as studied by Einstein [10]. Einstein's theoretical work was motivated by Brown's earlier observations of the random motion of dust grains on the surface of a fluid in a dish.

Consider an idealized drunk person. Imagine he takes uniform steps, of length s. But because he is drunk, each step is randomly oriented and uncorrelated with the previous step. We can write his position as:

$$\vec{D}_n = \vec{D}_{n-1} + \vec{s} \tag{278}$$

where $\vec{s}$ is the random displacement. So the squared displacement of the drunk is:

$$|\vec{D}_n|^2 = |\vec{D}_{n-1}|^2 + s^2 + 2\vec{D}_{n-1} \cdot \vec{s} \tag{279}$$

where s is the magnitude of $\vec{s}$. Now, if we have a party of drunks, each moving in this way, we can average the mean square displacement for the whole group. If you think of a "cloud" of drunks, the root mean square displacement is proportional to the cloud's radius. Averaging, we get:

$$< |\vec{D}_n|^2 >=< |\vec{D}_{n-1}|^2 > +s^2 \tag{280}$$

where the brackets indicate an average over all the drunks. The averaged cross correlation term:

$$< \vec{D}_{n-1} \cdot \vec{s} >= 0$$

This is because the drunks' steps are uncorrelated with their previous steps. Assuming all the drunks start at the pub, at zero displacement, we have:

$$< |\vec{D}_1|^2 >= 0 + s^2 \tag{281}$$

and

$$< |\vec{D}_2|^2 >= 2s^2 \tag{282}$$

so

$$< |\vec{D}_n|^2 >= ns^2 \tag{283}$$

Thus the root mean square displacement is:

$$(< |\vec{D}_n|^2 >)^{1/2} = \sqrt{n}s \tag{284}$$

If the drunks take steps with a uniform rate, e.g. one step per second, the rms displacement grows as $t^{1/2}$ power. This is a characteristic feature of Brownian motion. We will see later that single particle dispersion behaves the same way, when the particle motion is uncorrelated.

9.1.2 Diffusion

Now we show that a diffusing cloud, with a constant diffusivity, has a radius which also increases as $t^{1/2}$ power. The equation for a passive tracer was given in (140). Without advection, this is a simple diffusion equation:

$$\frac{\partial}{\partial t}C = \kappa \nabla^2 C \tag{285}$$

We define the variance of the cloud as:

$$< r^2 >= \frac{\iint r^2 C \, dA}{\iint C \, dA} \tag{286}$$

This is essentially the mean square radius of the tracer cloud. We are interested in how this changes in time, i.e. $\frac{d}{dt} < r^2 >$. We can obtain an equation for this by multiplying equation (285) by r^2 and integrating over space. Assuming the spreading is isotropic, we have (using cylindrical coordinates):

$$\frac{d}{dt}\int_0^\infty r^2 C \, r dr = \int_0^\infty r^2 \, \kappa \, \frac{1}{r}\frac{\partial}{\partial r}(r\frac{\partial}{\partial r}C) \, r dr$$

$$= -2\kappa \int_0^\infty r^2 \frac{\partial}{\partial r} C \, dr = 4\kappa \int_0^\infty C \, r dr \tag{287}$$

after integration by parts. Thus:

$$\frac{d}{dt} < r^2 >= \frac{d}{dt} \frac{\iint r^2 C \, dA}{\iint C \, dA} = 4\kappa \tag{288}$$

Integrating this in time, we get:

$$< r^2 >= 4\kappa t \quad \rightarrow \quad < r^2 >^{1/2} = 2\sqrt{\kappa t} \tag{289}$$

The rms cloud radius increases as $t^{1/2}$, just as in a random walk. This imples a random walk is a *diffusive process*. Drunks stumbling from a pub behave as a passive tracer, diffusing with a constant diffusivity. We call the time rate of change of the variance the "diffusivity" when dealing with particles.

An alternate way of deriving the same result is to use the exact solution to (285). Assume that the initial tracer distribution is a delta function at the origin (all the the drunks are initially at the pub at $r = 0$). One can show that the solution to (285) is given by:

$$C = \frac{1}{2\pi\kappa t} exp(-\frac{r^2}{4\kappa t}) \tag{290}$$

The prefactor guarantees that:

$$\int_0^{2\pi} \int_0^\infty C \, r \, dr d\theta = 1 \tag{291}$$

We can use this solution to find the variance of the cloud, i.e.:

$$< r^2 >= \frac{1}{\kappa t} \int_0^\infty r^3 exp(-\frac{r^2}{4\kappa t}) \, dr \tag{292}$$

The result turns out to be:

$$< r^2 >= 4\kappa t \tag{293}$$

9.1.3 Einstein's diffusion relation

You may wonder how realistic the random walk is, given that the particles (drunks) take a uniform step every second. But a similar result obtains even with a variable step size. This can be shown using an argument due to Einstein [10].

Say that particles at every time step take a step of variable length, call it $\triangle$. The distribution of step lengths can be represented by a PDF, $p(\triangle)$. We assume this PDF isn't changing in time, i.e. that the process is *stationary*. Then we can write a PDF for the particles' positions at time $t + 1$:

$$p(x, t + 1) = \int_{-\infty}^{\infty} p(x + \triangle, t)p(\triangle)\ d\triangle \tag{294}$$

This states that particles at x have a range of step sizes and integrating over all step sizes yields the distribution at the new time. Note that in multiplying the probabilities on the RHS, we are assuming that the position and step probabilities are uncorrelated.

Taylor-expanding the LHS of (294) to first order yields:

$$p(x, t + 1) = p(x, t) + \frac{\partial p}{\partial t}$$

Expanding the RHS, to second order, yields:

$$p(x,t) \int_{-\infty}^{\infty} p(\triangle)\ d\triangle + \frac{\partial p}{\partial x} \int_{-\infty}^{\infty} \triangle p(\triangle)\ d\triangle$$
$$+ \frac{1}{2} \frac{\partial^2 p}{\partial x^2} \int_{-\infty}^{\infty} \triangle^2 p(\triangle)\ d\triangle \tag{295}$$

The first integral is one, as the sum over all possible outcomes must be:

$$\int_{-\infty}^{\infty} p(\triangle)\ d\triangle = 1 \tag{296}$$

If we assume the probability distribution, $p(\triangle)$, is symmetric about zero, then the second integral is also zero:

$$\int_{-\infty}^{\infty} \triangle p(\triangle)\ d\triangle = 0 \tag{297}$$

The last integral is the variance of step distribution:

$$D \equiv \int_{-\infty}^{\infty} \triangle^2 p(\triangle)\, d\triangle \tag{298}$$

Collecting terms and canceling $p(x,t)$ from both sides, we have:

$$\frac{\partial p}{\partial t} = \frac{D}{2}\frac{\partial^2 p}{\partial x^2} \tag{299}$$

Thus the probability obeys a diffusion equation, meaning the variance will again grow linearly in time. So this is true even if the steps are non-uniform.

9.1.4 Single particle dispersion

As noted, Einstein studied random molecular motion. His purpose, actually, was to deduce Avogadro's number (the number of molecules in a mole of substance). But the same ideas apply to the turbulent advection of particles, even if the advecting eddies are much larger [45].

Imagine we have a collection of particles. We can define the diffusivity (in the x-direction) of the cloud by:

$$K \equiv \frac{1}{2}\frac{d}{dt} < X^2 > \tag{300}$$

where $X(t)$ is the particle displacement in the x-direction from its starting position. The brackets denote an ensemble average (e.g. over all the particles). As this average is over a fixed number of particles, the time derivative can be moved through the brackets. Thus we can also write:

$$K =< u(t)X(t) > \tag{301}$$

i.e. the diffusivity is the correlation between the particle velocities and their displacements. Furthermore, realizing that the displacement is just

the integral of the velocity, we can rewrite this as:

$$K =< u(t) \int_0^t u(t')dt' >= \int_0^t < u(t)\, u(t') > \, dt' \tag{302}$$

If the velocity field is stationary, we can rewrite this as:

$$K = \nu^2 \int_0^t R(t') \, dt' \tag{303}$$

where

$$R(t) \equiv \frac{1}{\nu^2} < u(0)\, u(t') > \tag{304}$$

Here ν^2 is the velocity variance for the particles and $R(t)$ is the normalized velocity *autocorrelation*. Notice that we have exchanged $u(t)$ for $u(0)$; this follows from stationarity.

Thus the diffusivity is the integral of the velocity autocorrelation. For a random walk, the velocity is uncorrelated at each step. So the autocorrelation is a delta function. But usually the velocity is correlated over some period.

Taylor [45] considered the behavior of the diffusivity in the limits of short and long times. At short times, the autocorrelation can be expanded in a Taylor[11] series:

$$R(t) = 1 + \frac{dR}{dt}t + ... \tag{305}$$

As $t \to 0$ then, $R \to 1$; the limit is one because we normalized by the velocity variance, ν^2. Thus we have:

$$lim_{t\to 0} \, K = \nu^2 t \tag{306}$$

So the dispersion, $< X^2 >$, increases as t^2 initially.

[11]Not the same Taylor. The Taylor series was invented by mathematician James Gregory and was first published in a book by Brook Taylor—no relation to G. I. Taylor, the great fluid dynamicist discussed here.

At long times, the behavior is also predictable. Assuming the velocity eventually becomes decorrelated, the integral of the autocorrelation will converge:

$$T_L = \int_0^\infty R(t')\, dt' = const. \tag{307}$$

This integral has units of time, and is known as the *Lagrangian integral time*. T_L indicates how long the velocity is correlated with itself and is a basic measure of predictability. Thus the diffusivity is:

$$lim_{t\to\infty}\, K = \nu^2 T_L \tag{308}$$

and this is constant.

The system is therefore diffusive and hence can be modeled using a diffusion-type equation. However the diffusivity is not the molecular diffusivity, but one related to the eddies; it is often called the "eddy diffusivity". Typical values for the eddy diffusivity at synoptic scales in the ocean are on the order of 1000 m^2/sec, roughly 8 orders of magnitude larger than the molecular diffusivity in water.

An implication of Taylor's work is that we can represent many particle dispersion problems as a random walk. We can, for instance, model ash spreading from a volcano as a mixture of advection (left out here, but important) and a random walk. This opens the possibility for *stochastic models* for pollution spreading.

But there is a downside as well. Since single particle motion has such generic limits, it is not so useful when one is trying to distinguish different types of turbulence. Say for example you would like to know whether an energy or enstrophy cascade is occurring. In both cases, the single particle diffusivity should simply asymptote to a constant. To study turbulent dispersion, it is better to use pairs of particles, as seen hereafter.

9.1.5 The vortex merger problem

In section (7.6), we showed that freely evolving 2-D turbulence can be viewed as a merger process between discrete vortices. Carnevale [7] constructed a theory in which the important flow statistics, like the enstrophy, could be deduced from the vortex population. The only unknown in their theory was the decay rate of the vortex density, ρ. Here we show that can be accounted in terms of the dispersion of the vortices [21].

The numerical experiment in this case was a freely-evolving, 2-D turbulence simulation in a periodic domain, from random initial conditions. Vortices emerge at the early times and begin merging. At some point, particles were deployed in the flow, and the dispersion of the particles and vortices was compared (left panel of Fig. 38). We see that after a short time, the dispersion for vortices and particles is statistically indistinguishable. That implies that the vortices are dispersing exactly like the passive particles. Note too that the dispersion is increasing *faster* that diffusively. A best fit of the data suggests:

$$< X^2 > \propto t^{1.3} \tag{309}$$

This implies that the diffusivity increases as $t^{0.3}$. Such dispersion is called "super-diffusive", since the spreading is greater than in a random walk.

As the vortex dispersion matches the particles', we can think of a diffusivity to characterize the vortex spreading. We can scale the diffusivity thus:

$$D = \frac{1}{2}\frac{d}{dt} < X^2 > = < uX > \propto UL \tag{310}$$

where U is the mean vortex velocity and L is the typical spacing between

vortices. Now if we have a vortex density of ρ, then the typical spacing is:

$$L \propto \rho^{-1/2} \tag{311}$$

The velocity on the other hand scales as the square root of the total energy, given in (132):

$$U \propto E^{1/2} \propto \rho^{1/2} \zeta_c \, b^2 \tag{312}$$

So the diffusivity scales as:

$$D \propto UL \propto \rho^{1/2} \zeta_c \, b^2 \rho^{-1/2} \propto \Gamma \tag{313}$$

where

$$\Gamma = \zeta_c \, \pi b^2 \tag{314}$$

is the mean vortex *circulation*. So the diffusivity and the circulation should behave the same way. In the experiment shown in the left panel of Fig. (38), the diffusivity scales as:

$$D = \frac{1}{2} \frac{d}{dt} < X^2 > \propto t^{0.3} \tag{315}$$

So the circulation, if this argument is correct, should scale the same way.

Shown in the right panel of Fig. (38) are the exponents, α, obtained from a suite of experiments with different initial conditions and different types of small scale damping. We see that the exponents tend to be between 0.2-0.4, for both the diffusivity and circulation, for most of the experiments. The average value for the exponent is roughly $\alpha = 1/3$.

If we know the scaling for the circulation, we can find the decay rate for the density, because the total energy is conserved. So:

$$E = \rho \zeta_c^2 b^4 = \rho \Gamma^2 = const. \tag{316}$$

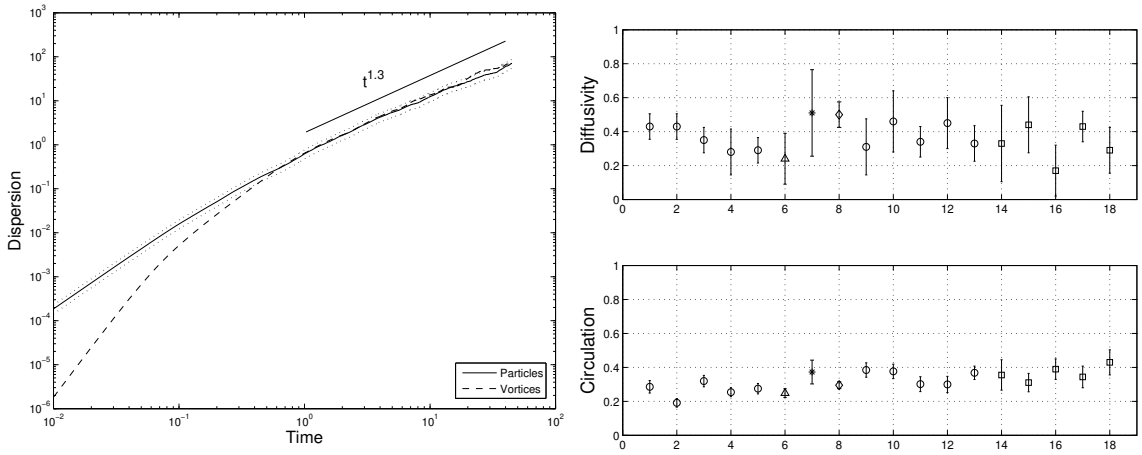

Figure 38: The dispersion for vortices (solid curve) and passive particles (dashed line) in a 2-D turbulence simulation (left panel). Shown in the right panel are the growth exponents, α, from various runs for the vortex diffusivity and the mean vortex circulation. The value is usually between 0.2-0.4. From [21].

Thus:

$$\rho \propto \Gamma^{-2} \propto t^{-2/3} \tag{317}$$

This is close to the value, 0.7, inferred by McWilliams [32] and Weiss and McWilliams [49] (sec. 7.6). In other simulations, we find a value of $2/3$ (Fig. 39), using a range of different initial conditions.

The results shown in Fig. (38) are from numerical experiments with very weak lateral damping. Increasing the damping accelerates the vortex decay, because lateral diffusion causes the vortices to spread out, hence increasing their chance for collisions. But nevertheless, it is fruitful to think of vortex merger as a dispersion problem.

Note though that this problem is not completely solved! All we've done is to change the unknown. Previously, we didn't know what set the density decay. Now we know that, but we don't know what determines the dispersion exponent. So there's still work to be done.

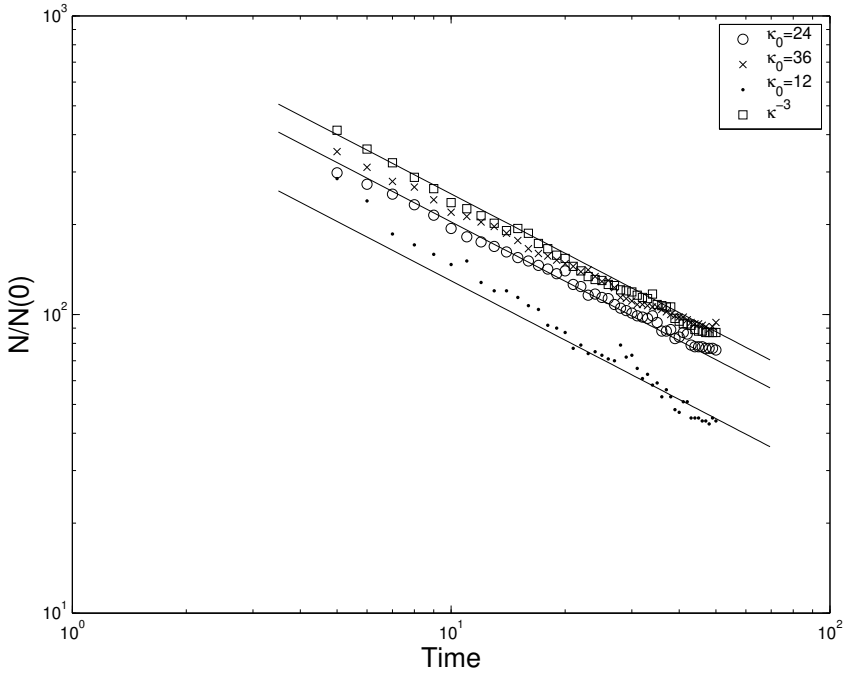

Figure 39: Vortex density from 4 experiments with different initial conditions. The lines indicate a decay of $t^{-2/3}$. From [21].

9.2 Two particle dispersion

As noted, the single particle dispersion exhibits generic behavior and so is not terribly useful for differentiating different types of flow. Better in this regard is the dispersion between *two* particles, called "relative dispersion". Rather than study how a particle drifts from its starting location, we see how two particles separate in time. An advantage is that two particle dispersion is unaffected by a constant background flow, U (it is "Galilean invariant").

Say the velocities of the two particles are $\vec{u}_1$ and $\vec{u}_2$. Then the mean square difference between the velocities, averaged over a large number of pairs, is:

$$< |\vec{u}_i - \vec{u}_j|^2 >=< |\vec{u}_i|^2 > + < |\vec{u}_j|^2 > -2 < \vec{u}_i \cdot \vec{u}_j > \qquad (318)$$

If the flow is homogeneous, then:

$$< |\vec{u}_i|^2 >=< |\vec{u}_j|^2 >= \nu^2 \tag{319}$$

where ν^2 is the single particle velocity variance, introduced previously. So:

$$< |\vec{u}_i - \vec{u}_j|^2 >= 2\nu^2 - 2 < \vec{u}_i \cdot \vec{u}_j > \tag{320}$$

If the two particles are moving independently, i.e. if their velocities are uncorrelated, the cross correlation term will be zero. This is what happens when the particles are far apart. Then the mean square relative velocity is just twice the mean square single particle velocity and relative dispersion is just like single particle dispersion. Similarly if we define a two particle diffusivity, then in this limit:

$$\begin{aligned} K_{2x} &\equiv \int_0^t < (u_i(0) - u_j(0))(u_i(t') - u_j(t')) > \; dt' \\ &= \int_0^t < u_i(0)u_i(t') > + < u_j(0)u_j(t') > - < u_i(0)u_j(t') > \\ &- < u_j(0)u_i(t') > \; dt' \\ &\rightarrow 2\int_0^t < u_i(0)u_i(t') > \; dt' \\ &= 2K_{1x} \end{aligned} \tag{321}$$

again from homogeneity. Thus the two particle diffusivity asymptotes to twice the single particle diffusivity when the particle velocitiess are uncorrelated.

But what happens when the particle motion *is* correlated? This is where relative dispersion is interesting. Two particles are effectively measuring the velocities at the points in space and time where the particles are (Fig. 40). Thus the difference between the particle velocities is equal to the difference in Eulerian velocities at that time and location. Now if the flow is

homogeneous and isotropic, the mean square velocity difference for particles with a separation r is the same as the mean square velocity difference for any two points in the flow also with a separation r.

The mean square velocity difference is the second order structure function (see the exercise after sec. 6.3). In the turbulent inertial ranges, this scales with energy or enstrophy transfer rate, just as the spectrum does. So in the energy cascade, we have:

$$< |\vec{u}_1 - \vec{u}_2|^2 > \propto \epsilon^{2/3} r^{2/3} \tag{322}$$

The two thirds can be deduced from dimensional grounds: ϵ has units of m^2/sec^3 and the square velocity difference has units of m^2/sec^2. This relation is known as "Kolmogorov's 2/3 Law".

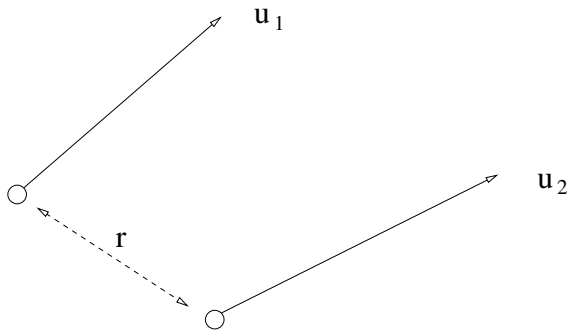

Figure 40: Two particles moving in a flow.

In the enstrophy range on the other hand, we have:

$$< |\vec{u}_1 - \vec{u}_2|^2 > \propto \eta^{2/3} r^2 \tag{323}$$

So the velocity difference increases more rapidly with separation in the enstrophy range.

We can deduce corresponding relations for the relative diffusivity. In the energy range, the diffusivity scales as:

$$K_2 \propto \epsilon^{1/3} r^{4/3} \tag{324}$$

because the diffusivity has units of m^2/sec. This dependence was first deduced by Richardson [40], from observations of smoke plumes. The connection to Kolmogorov's theory was made by Obukhov [37] and Batchelor [1]. This implies:

$$\frac{d}{dt} < (x_1 - x_2)^2 >= \frac{d}{dt} < r^2 > \propto \epsilon^{1/3} r^{4/3} \tag{325}$$

If we integrate this, we find that:

$$< r^2 > \propto \epsilon t^3 \tag{326}$$

Integrating (325) is not strictly correct, because the LHS involves the mean square separation, not the separation. But from a scaling perspective, this is reasonable. The cubic growth is now known as "Richardson's Law".

In the enstrophy range, dimensional arguments suggest:

$$\frac{d}{dt} < r^2 > \propto \eta^{1/3} r^2 \tag{327}$$

Integrating this in time, we get:

$$< r^2 > \propto exp(\eta^{1/3} t) \tag{328}$$

This is sometimes called "Lin's Law" [27]. So separations in the enstrophy range grow exponentially in time.

These results can be compared with those that we derived for predictability, in sec. (7.8). In the enstrophy range, the scale of the error was found to increase as $exp(\eta^{1/3}t)$—exactly as the separation in particles increases here. Similarly, in the energy range we found:

$$T = \int_{\kappa 0}^{\kappa 1} \epsilon^{-1/3} \kappa^{-5/3} \, d\kappa \approx \epsilon^{-1/3} \kappa^{-2/3} |_{\kappa 0}^{\kappa 1} \approx \epsilon^{-1/3} \kappa_0^{-2/3} \tag{329}$$

This implies that the length scale scales as:

$$L_0^{2/3} \propto \epsilon^{1/3} T \tag{330}$$

as $L_0 = 2\pi/\kappa_0$. Thus:

$$L_0^2 \propto \epsilon T^3 \tag{331}$$

The predictability relations are thus identical in form to the two particle dispersion relations. This is not coincidental; two particle dispersion is actually a measure of Lagrangian predictability. If we change the initial condition of a particle slightly, the growth of the error is determined by relative dispersion.

How do these predictions compare to observations? Morel and Larcheveque [35] calculated pair statistics for pairs of balloons deployed in the lower stratosphere in the Southern Hemisphere, during the French EOLE experiment. The dispersion was found to grow exponentially in time during the first 6 days, up to separations of 1000-2000 km. Thereafter, the two particle dispersion increased linearly in time. From the turbulence perspective, we would interpret this as evidence of an enstrophy cascade at scales below 2000 km, and random, uncorrelated motion at larger scales.

Compare this with the Nastrom and Gage energy spectrum, shown in Fig. (26). The spectrum exhibits a κ^{-3} spectrum at scales below roughly 2000 km. So the exponential growth seen here is consistent. However, the energy spectrum also shows a $\kappa^{-5/3}$ range at smaller scales. This would produce a t^3 growth in the dispersion, which we don't see. However, this occurs below 100 km, the smallest separation of the balloons. So we wouldn't expect to resolve the smaller scale dispersion. Er-El and Peskin [11] examined another set of balloons, also from the Southern Hemisphere, and obtained exponential growth at scales below 1000 km.

Two results from the ocean are shown in Fig. (42). These come from surface buoy pairs, deployed in the Gulf of Mexico during the SCULP experiment and in the Nordic Seas during the POLEWARD experiment.

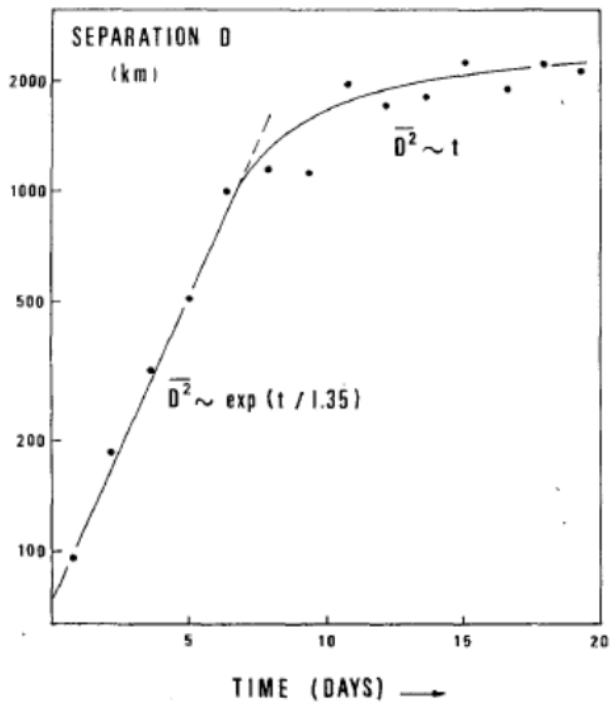

Figure 41: Relative dispersion for pairs of balloons from the EOLE experiment in the Southern Hemisphere. From [35].

In both cases, we see exponential dispersion at early times. In the Gulf, the growth occurs below scales of $\sqrt{2000} = 45$ km, and in the Nordic Seas below the 10 km scale. In the Gulf case, the dispersion at large scales is super-diffusive. In the Nordic Seas case, the dispersion increases more rapidly, perhaps as t^3, up to 100 km; it grows diffusively thereafter. So it is possible there is an inverse cascade happening between 10-100 km in the eastern Nordic Seas.

An interesting point is that 1000 km is comparable to the deformation radius (sec. 8.4.3) in the atmosphere. Furthermore, the deformation radius is close to 45 km in the Gulf of Mexico and 10 km in the Nordic Seas. So these studies all suggest exponential growth below the deformation radius. This is what one would expect if there was an enstrophy cascade,

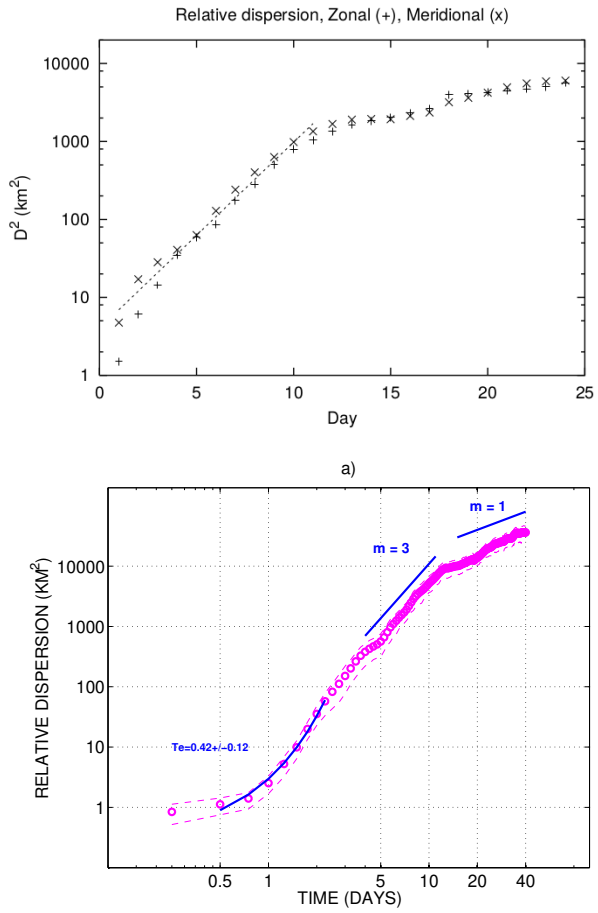

Figure 42: Relative dispersion for pairs of surface drifters in the Gulf of Mexico deployed during the SCULP experiment (upper panel) and in the Nordic Seas during the POLEWARD campaign (lower panel). Note the dispersion in the first is plotted on a semi-logarithmic plot and that in the second is on a logarithmic plot. From [23] and [18].

suggesting a source of enstrophy at the deformation scale.

Following Richardson [40], one can also write an equation for the probability of pair separations. It is possible to solve this equation and then compare the predicted probabilities with the observed distributions of pair separations for balloons or drifters. Details can be found in [25].

10 PV fluxes

The potential vorticity (PV) is conserved in the absence of forcing. It is useful then to think about how PV can be redistributed by the motion of fluid parcels. As shown by Bretherton [4], such thinking can shed light on baroclinic stability.

Consider flow in a channel, bounded by northern and southern walls and also by flat surfaces at the bottom and at some upper height. Assuming there are no temperature gradients on the vertical boundaries and that these are flat, we have:

$$\frac{\partial}{\partial z}\psi = 0 \quad at \quad z = 0, H \tag{332}$$

In addition, the meridional flow vanishes at the northern and southern walls:

$$\frac{\partial}{\partial y}\psi = 0 \quad at \quad y = 0, M \tag{333}$$

With these conditions *alone*, we can show:

$$\int_0^H \int_O^M \overline{vq}\, dydz = 0 \tag{334}$$

where now q is the full potential vorticity (relative plus stretching plus planetary):

$$q = \nabla^2\psi + \frac{\partial}{\partial z}(\frac{f_0^2}{N^2}\frac{\partial}{\partial z})\psi + \beta y \tag{335}$$

and where:

$$\overline{C} = \int_0^L C\, dx \tag{336}$$

is a zonal average. Equation (334) implies that the net meridional PV flux, $\overline{vq}$, must vanish when integrated over the domain.

We can see this by expanding the PV flux:

$$\overline{vq} = \overline{\psi_x q} = \overline{\psi_x \psi_{xx}} + \overline{\psi_x \psi_{yy}} + \overline{\psi_x(\frac{f_0^2}{N^2}\psi_z)_z} + \overline{\psi_x \beta y}$$

$$= (\overline{\psi_y \psi_x})_y + (\overline{\frac{f_0^2}{N^2}\psi_z \psi_x})_z + \overline{(\beta y \psi + \frac{1}{2}\psi_x^2 - \frac{1}{2}\psi_y^2 + \frac{1}{2}\frac{f_0^2}{N^2}\psi_z^2)_x}$$

$$= \frac{\partial}{\partial y}\overline{\psi_y \psi_x} + \frac{\partial}{\partial z}\overline{\frac{f_0^2}{N^2}\psi_z \psi_x} \tag{337}$$

The last term in the second line is zero because the domain is x-periodic. So integrating:

$$\int_0^H \int_O^M \overline{vq}\, dydz = \overline{\psi_y \psi_x}|_0^M + \frac{f_0^2}{N^2}\overline{\psi_z \psi_x}|_0^H = 0 \tag{338}$$

because ψ_x vanishes on the meridional boundaries and ψ_z on the vertical boundaries. Note we didn't have to invoke the conservation of PV—the integral vanishes because of the choice of boundary conditions.

Now say we have a mean flow, which has an associated PV field, $q_s(y, z)$. Then we can write:

$$q(x, y, z, t) = q_s(y, z) + q'(x, y, z, t) \tag{339}$$

where $q'(x, y, z, t)$ is the perturbation about the mean. If an air parcel is initially at a latitude $y = y_0$, its perturbation PV must change if it is displaced from that latitude, in order to conserve the total PV. Define the displacement to be $\eta = y - y_0$. If η is small, then we can write:

$$q'(x, y_0 + \eta, z, t) = q_s(y_0, z) - q_s(y_0 + \eta, z) \approx -(\frac{\partial}{\partial y} q_S)\eta \tag{340}$$

(ignoring terms in η^2 and higher).

Now the parcel's meridional velocity is just:

$$v = \frac{d}{dt}\eta \tag{341}$$

So the meridional flux of perturbation PV is:

$$\overline{vq'} = -(\frac{\partial}{\partial y} q_S)\overline{\eta \frac{d}{dt}\eta}$$

$$= -(\frac{\partial}{\partial y} q_S) \frac{d}{dt} \frac{1}{2} \overline{\eta^2} \tag{342}$$

From section (9.1), we recognize that:

$$\frac{d}{dt} \frac{1}{2} \overline{\eta^2} = \kappa_y \tag{343}$$

is the *diffusivity in the meridional direction*. So we can represent the PV flux as a meridional diffusion. The diffusivity is thus defined:

$$\kappa_y = -\frac{\overline{vq'}}{\frac{\partial}{\partial y} q_S} \tag{344}$$

If the RHS side is constant, so is the diffusivity. And if the diffusivity is *positive*, the mixing is *down the mean PV gradient*. So mixing tends to weaken the mean PV gradient.

From equation (334), we have:

$$\int_0^H \int_O^M \overline{vq}\, dydz = \int_0^H \int_O^M \overline{vq_s}\, dydz + \int_0^H \int_O^M \overline{vq'}\, dydz = 0 \tag{345}$$

It's easy to show that the integral of the mean PV vanishes on its own, so we have:

$$\int_0^H \int_O^M \overline{vq'}\, dydz = 0 \tag{346}$$

Thus:

$$\int_0^H \int_O^M (\frac{\partial}{\partial y} q_S) \frac{d}{dt} \frac{1}{2} \overline{\eta^2}\, dydz = 0 \tag{347}$$

Now, we can substitute in for η if we know what the velocity looks like. The full Lagrangian equation for η is:

$$\frac{d}{dt} \eta = v \tag{348}$$

We can linearize this about the mean by writing:

$$(\frac{\partial}{\partial t} + U \frac{\partial}{\partial x}) \eta = v \tag{349}$$

The velocity on the RHS derives from the Eulerian field, which itself is a solution to the PV equation, like in (227). Let's write that as a streamfunction:

$$\psi(x, y, z, t) = Re[\phi(z, t)e^{ik(x-ct)}sin(\frac{n\pi y}{M})] \tag{350}$$

where $Re[]$ denotes the real part. This is the type of solution we use when studying Rossby waves, for example. Note the sine factor ensures that the streamfunction vanishes at the northern and southern walls. Given this, the meridional velocity is:

$$v = \frac{\partial}{\partial x}\psi = Re[ik\psi] = Re[ik\phi(z, t)e^{ik(x-ct)}sin(\frac{n\pi y}{M})] \tag{351}$$

Now if the meridional velocity depends on $e^{ik(x-ct)}$, then so does η. So:

$$(\frac{\partial}{\partial t} + U\frac{\partial}{\partial x})\eta = (-ikc + ikU)\eta e^{ik(x-ct)} \tag{352}$$

Combining:

$$\eta = Re[\frac{\phi}{U - c}e^{ik(x-ct)}] \tag{353}$$

Note that c can be complex:

$$c = c_r + ic_i$$

If the imaginary component, c_i, is greater than zero, the solution grows exponentially in time:

$$e^{ik(x-ct)} = e^{ik(x-c_r t)+c_i t} \tag{354}$$

Then the solution is *unstable*.

Using this, we can write:

$$\kappa_y = \frac{1}{2}\frac{d}{dt}\eta^2 = -\frac{1}{2}Re[ikc|\eta|^2 e^{2kc_i t}] = \frac{1}{2}\frac{|\phi|^2 kc_i}{|U - c|^2}e^{2kc_i t} \tag{355}$$

The diffusivity is positive if $c_i > 0$, i.e. *if there is unstable growth*. So there is a (remarkable) connection between lateral mixing and instability.

Substituting into (347), we get:

$$\int_0^H \int_O^M \frac{1}{2}(\frac{\partial}{\partial y} q_S) \frac{|\phi|^2 k c_i}{|U-c|^2} e^{2kc_i t}\, dy\, dz = 0 \tag{356}$$

If $c_i > 0$, then the only way this integral can be zero is if $\frac{\partial}{\partial y} q_s$ *changes sign somewhere in the interior of the fluid*. This is the Charney-Stern criterion for instability [38, 22]. Normally when deriving this, one has to do numerous integration by parts. Here it comes out naturally in terms of particle diffusion.

So our notions about Lagrangian diffusion are also useful when talking about an active tracer, like potential vorticity. Mixing tends to happen down the mean gradient, reducing that gradient. And the diffusivity emerges as a natural measure. Note though that the above development is *linear*—in this way, the results are consistent with linear stability theory. But the actual mixing in the atmosphere and ocean need not be small in amplitude—then models are required to diagnose the mixing.

References

[1] G. K. Batchelor. Diffusion in a field of homogeneous turbulence ii; the relative motion of particles. *Proc. Cambridge Phil. Soc.*, 48:345–362, 1952.

[2] G. K. Batchelor. *The theory of homogeneous turbulence*. Cambridge University Press, 1953.

[3] G. K. Batchelor. Computation of the energy spectrum in homogeneous two dimensional turbulence. *Phys. Fluids*, 12:233–237, 1969.

[4] F. P. Bretherton. Critical layer instability in baroclinic flows. *Quart. J. Roy. Meteor. Soc.*, 92:325–334, 1966.

[5] F. P. Bretherton and D. B. Haidvogel. Two-dimensional turbulence above topography. *J. Fluid Mech.*, 78:129–154, 1976.

[6] G. F. Carnevale and J.S. Frederiksen. Nonlinear stability and statistical mechanics of flow over topography. *J. Fluid Mech.*, 175:157–181, 1987.

[7] G. F. Carnevale, J.C. McWilliams, Y. Pomeau, J. B. Weiss, and W. R. Young. Evolution of vortex statistics in two-dimensional turbulence. *Phys. Rev. Lett.*, 66:2735–2737, 1991.

[8] F. H. Champagne. The fine-scale structure of the turbulent velocity field. *J. Fluid Mech.*, 86:67–108, 1978.

[9] J. G. Charney. Geostrophic turbulence. *J. Atmos. Sci.*, 28:1087–1095, 1971.

[10] A. Einstein. The theory of the brownian movement. *Ann. der Physik*, 17:549, 1905.

[11] J. Er-el and R. Peskin. Relative diffusion of constant-level balloons in the southern hemisphere. *J. Atmos. Sci.*, 38:2264–2274, 1981.

[12] R. Fjørtoft. On the changes in the spectral distribution of kinetic energy for twodimensional, nondivergent flow. *Tellus*, 5:225–230, 1953.

[13] N. P. Fofonoff. Steady flow in a frictionless homogeneous ocean. *J. Mar. Res.*, 13:254–262, 1954.

[14] U. Frisch. *Turbulence*. Cambridge University Press, Cambridge, UK, 1996.

[15] H. L. Grant, R. W. Stewart, and A. Moilliet. Turbulence spectra from a tidal channel. *J. Fluid Mech.*, 12:241–268, 1962.

[16] P. E. Isachsen, J. H. LaCasce, and J. Pedlosky. Rossby wave instability and apparent phase speeds in large ocean basins. *J. Phys. Oceanogr.*, 37:1177–1191, 2007.

[17] A. N. Kolmogorov. The local structure of turbulence in incompressible viscous fluid for very large reynolds numbers. *Dokl. Akad. Nauk SSSR*, 30:299–303, 1941.

[18] I. Koszalka, J. H. LaCasce, and K. A. Orvik. Relative dispersion in the Nordic Seas. *J. Mar. Res.*, in press, 2009.

[19] R. H. Kraichnan. Inertial ranges in two-dimensional turbulence. *Phys. Fluids*, 10:1417–1423, 1967.

[20] J. H. LaCasce. On turbulence and normal modes in a basin. *J. Mar. Res.*, 60:431–460, 2002.

[21] J. H. LaCasce. The vortex merger rate in freely-decaying, 2-d turbulence. *Phys. Fluids*, 20:085102, 2008.

[22] J. H. LaCasce. *Introduction to Atmosphere-Ocean Dynamics*. UiO Press, 2012.

[23] J. H. LaCasce and C. Ohlmann. Relative dispersion at the surface of the Gulf of Mexico. *J. Mar. Res.*, 61:285–312, 2003.

[24] J. H. LaCasce and J. Pedlosky. The instability of rossby basin modes and the oceanic eddy field. *J. Phys. Oceanogr.*, 34:2027–2041, 2004.

[25] J.H. LaCasce. Relative displacement probability distribution functions from balloons and drifters. *Journal of Marine Research*, 68:433–457, 2010.

[26] C. E. Leith. Diffusion approximation for two dimensional turbulence. *Phys. Fluids*, 11:671–673, 1968.

[27] J.-T. Lin. Relative dispersion in the enstrophy-cascading inertial range of homogeneous two-dimensional turbulence. *J. Atmos. Sci.*, 29:394–395, 1972.

[28] E. Lindborg. Can the atmospheric kinetic energy spectrum be explained by two-dimensional turbulence? *J. Fluid Mech.*, 388:259–288, 1999.

[29] E. N. Lorenz. Deterministic nonperiodic flow. *J. Atmos. Sci.*, 20:130–141, 1963.

[30] R. M. May. Simple mathematical models with very complicated dynamics. In B. R. Hunt, T.-Y. Li, J. A. Kennedy, and H. E. Nusse, editors, *The Theory of Chaotic Attractors*, pages 85–93. Springer, 2004.

[31] J. C. McWilliams. The emergence of isolated coherent vortices in turbulent flow. *J. Fluid Mech.*, 146:21–43, 1984.

[32] J. C. McWilliams. The vortices of two dimensional turbulence. *J. Fluid Mech.*, 219:361–385, 1990.

[33] J. C. McWilliams, J. B. Weiss, and I. Yavneh. The vortices of homogeneous geostrophic turbulence. *J. Fluid Mech.*, 401:1–26, 1999.

[34] P. E. Merilees and H. Warn. On energy and enstrophy exchanges in two-dimensional non-divergent flow. *J. Fluid Mech.*, 69:625–630, 1975.

[35] P. Morel and M. Larcheveque. Relative dispersion of constant-level balloons in the 200 mb general circulation. *J. Atmos. Sci.*, 31:2189–2196, 1974.

[36] G. D. Nastrom and K. S. Gage. A climatology of atmospheric wavenumber spectra of wind and temperature observed by commerical aircraft. *J. Atmos. Sci.*, 42:959–960, 1985.

[37] A. M. Obukhov. On the distribution of energy in the spectrum of turbulent flow. *Dokl. Akad. Nauk SSSR*, 32:22–24, 1941.

[38] J. Pedlosky. *Geophysical fluid dynamics*. Springer-Verlag, 1987.

[39] P. B. Rhines. Waves and turbulence on a beta-plane. *J. Fluid Mech.*, 69:417–443, 1975.

[40] L. F. Richardson. Atmospheric diffusion on a distance-neighbour graph. *Proc. R. Soc. Lond. A*, 110:709–737, 1926.

[41] C. G. Rossby. Dynamics of steady ocean currents in the light of experimental fluid mechanics. *Papers Phys. Oceanogr. Meteor.*, 5:1–43, 1936.

[42] R. Salmon. Baroclinic instability and geostrophic turbulence. *Geophys. Astrophys. Fluid Dyn.*, 15:167–211, 1980.

[43] R. Salmon. *Lectures on geophysical fluid dynamics*. Oxford University Press, 1998.

[44] R. Salmon, G. Holloway, and M. Hendershott. The equilibrium statistical mechanics of simple quasi-geostrophic models. *J. Fluid Mech.*, 75:691–703, 1976.

[45] G. I. Taylor. Diffusion by continuous movements. *Proc. Lond. Math. Soc.*, 20:196–212, 1921.

[46] G. K. Vallis. *Atmospheric and oceanic fluid dynamics: fundamentals and large-scale circulation*. Cambridge University Press, 2006.

[47] G. K. Vallis and M. E. Maltrud. Generation of mean flows and jets on a beta plane and over topography. *J. Phys. Oceanogr.*, 23:1346–1362, 1993.

[48] D.-P. Wang, C. N. Flagg, K. Donohue, and H. T. Rossby. Wavenumber spectrum in the gulf stream from shipboard adcp observations and comparison with altimetry measurements. *J. Phys. Oceanogr.*, 40:840–844, 2010.

[49] J. B. Weiss and J. C. McWilliams. Temporal scaling behavior of decaying two dimensional turbulence. *Physica A*, 5:608–621, 1993.

[50] G. P. Williams. Planetary circulations: 1. barotropic representation of jovian and terrestrial turbulence. *J. Atmos. Sci.*, 35:1399–1426, 1978.